AD-A051 535 AKRON UNIV OH DEPT OF MECHANICAL ENGINEERING F/G 20/4
DEVELOPMENT OF A METHOD FOR PREDICTING SUBSONIC TURBULENT SEPAR--ETC(U)
FEB 78 P M GERHART, R V CHIMA DAHC04-75-G-0026

UNCLASSIFIED ARO-12437.1-E NL

1 OF 2
AD
A051535

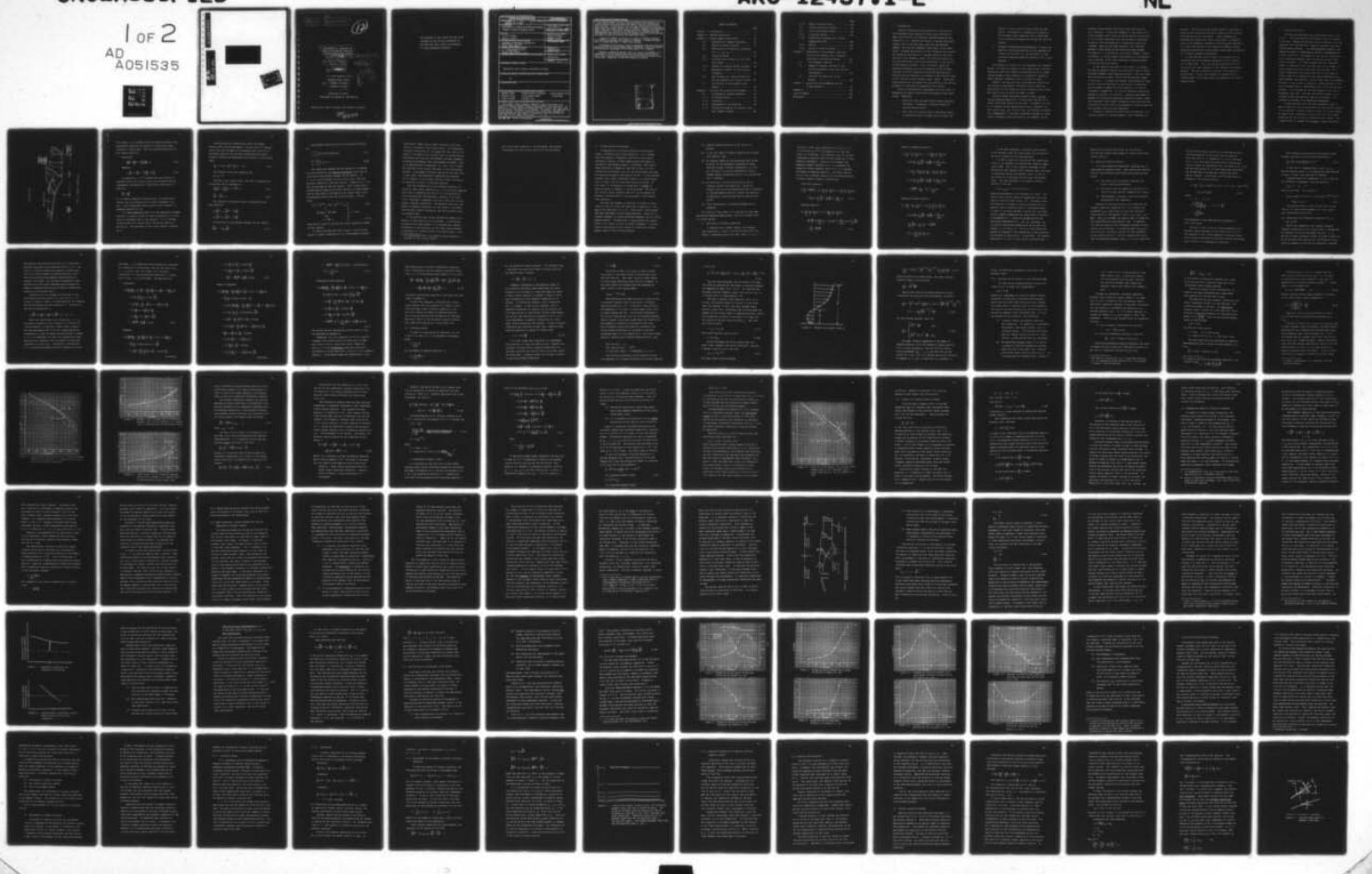

(18) ARO

(19) 12437.1-E

(12)

(6) DEVELOPMENT OF A METHOD FOR PREDICTING SUBSONIC TURBULENT SEPARATING BOUNDARY LAYERS.

(9) Final Report. 1 Sep 74 - 31 Dec 77,

by

(10) Philip M. Gerhart
Rodrick V. Chima

(12) 171 p.

(11) Feb [redacted] 1978

U. S. Army Research Office

Prepared Under Grants

(15) DAHC04-75-G-0026,
DAAG29-77-G-0030

University of Akron
Department of Mechanical Engineering

Approved for public release; distribution unlimited.

New 410608

THE FINDINGS IN THIS REPORT ARE NOT TO BE CONSTRUED AS AN OFFICIAL DEPARTMENT OF THE ARMY POSITION, UNLESS SO DESIGNATED BY OTHER AUTHORIZED DOCUMENTS.

SECURITY CLASSIFICATION OF THIS PAGE (When Data Entered)

REPORT DOCUMENTATION PAGE		READ INSTRUCTIONS BEFORE COMPLETING FORM
1. REPORT NUMBER 12437.1-E	2. GOVT ACCESSION NO.	3. RECIPIENT'S CATALOG NUMBER
4. TITLE (and Subtitle) DEVELOPMENT OF A METHOD FOR PREDICTING SUBSONIC TURBULENT SEPARATING BOUNDARY LAYERS		5. TYPE OF REPORT & PERIOD COVERED Final Report 1 Sept 1974 - 31 Dec 1977
		6. PERFORMING ORG. REPORT NUMBER
7. AUTHOR(s) Philip M. Gerhart Rodrick V. Chima		8. CONTRACT OR GRANT NUMBER(s) DAHC04-75-G-0026 DAAG29-77-G-0030
9. PERFORMING ORGANIZATION NAME AND ADDRESS Department of Mechanical Engineering The University of Akron Akron, Ohio 44325		10. PROGRAM ELEMENT, PROJECT, TASK AREA & WORK UNIT NUMBERS
11. CONTROLLING OFFICE NAME AND ADDRESS U. S. Army Research Office Box CM, Duke Station Durham, North Carolina 27706		12. REPORT DATE February 1978
		13. NUMBER OF PAGES
14. MONITORING AGENCY NAME & ADDRESS(if different from Controlling Office)		15. SECURITY CLASS. (of this report) Unclassified
		15a. DECLASSIFICATION/DOWNGRADING SCHEDULE NA

16. DISTRIBUTION STATEMENT (of this Report)

Approved for public release; distribution unlimited.

17. DISTRIBUTION STATEMENT (of the abstract entered in Block 20, if different from Report)

NA

18. SUPPLEMENTARY NOTES

19. KEY WORDS (Continue on reverse side if necessary and identify by block number)

Boundary layers	Viscous-inviscid interaction	Inverse potential flow
Separated flows	Finite element method	calculations
Integral methods	Turbulent flow	

20. ABSTRACT (Continue on reverse side if necessary and identify by block number)

An attempt is made to develop a method for predicting subsonic flows exhibiting pressure gradient induced turbulent boundary layer separation. The concept of a strong interaction between rotational (viscous) layer near a body and an external irrotational flow is adopted. The boundary layer approximations to the equations of motion are retained in the viscous layer; mathematical coupling between the flow regions is introduced by requiring continuity of flow speed (or Mach number) and direction.

Over

DD FORM 1 JAN 73 1473 EDITION OF 1 NOV 65 IS OBSOLETE

Unclassified

SECURITY CLASSIFICATION OF THIS PAGE (When Data Entered)

An integral method is used to solve the boundary layer equations; the equations are set up so that either flow speed or angle can be calculated, given the other. A modification of the wall-wake velocity profile valid for compressible flow is used together with an algebraic non-equilibrium turbulence model. Equations solved are the integral continuity, momentum, and moment of momentum equations. Predictions for compressible and incompressible plane two-dimensional separating and reattaching boundary layers are quite good when edge speed or angle are available from experimental data.

A method of "inverse" calculations for subsonic axisymetric potential flow, based on the surface source method is presented. Although the method works for simple test cases, it seems highly unstable.

A formulation for calculating inviscid compressible flows over axisymetric geometries using the finite element method is presented. Direct calculations are satisfactory, development of the inverse mode is still underway.

Attempts to combine the boundary layer and inviscid flow methods into a comprehensive a priori separated flow prediction method met with failure, this is felt to be due to the sensitivity of the inviscid flow method in the inverse mode. Suggestions for possible remedies are offered.

TABLE OF CONTENTS

1. Introduction

Practical engineering calculations of flow fields in which boundary layer separation occurs have historically been very difficult with realistic methods appearing only recently [1 - 7]. The main difficulty in making such calculations lies in the fact that, even for high Reynolds numbers, the classical boundary layer theory is not applicable. Although the effects of fluid viscosity and rotation may indeed be confined to a (limited) region of the flow, typically such "boundary layers" are thick and induce significant deflection of the flow streamlines in the vicinity of the boundary surfaces. This, of course, causes the pressure distribution on solid boundaries to be different from the "inviscid" pressure distribution and hence the pressure must be treated as an unknown in both the main body of the flow and in the "boundary layer" region. Additional complications are introduced into the problem by the possible presence of turbulence and compressibility effects.

There are three possible approaches one might adopt in attempting to predict flows exhibiting boundary layer separation. These are:

1. Solve the (time averaged) Navier-Stokes equations including, if necessary, turbulence models of varying sophistication.

2. Use a form of viscous-inviscid interaction theory in which the flow is divided into (at least) two

regions, in one of which viscous forces are neglected. The pressure is treated as an unknown in the "boundary layer" equations and is determined via an interaction between the viscous and inviscid regions.

3. Introduce "engineering approximations" in which the details of the separated flow are not computed but "forced" on the flow, e.g. by specifying a fixed dividing streamline shape and treating it as a solid boundary.

Each method, of course, has its advantages and drawbacks. Method 1 has been the subject of much research but solutions obtained to date have tended to concentrate mainly on shock-induced boundary layer separation or separation induced by abrupt changes in geometry such as cavities or steps.

Method 3 has seen much use in engineering practice but the necessary experimental information always restricts application of this method to those situations which closely duplicate the one on which the model is based.

Method 2 adopts the middle ground in that, although lacking complete generality, it should have the ability to reveal significant details of the flow. In method 2 (as well as 3) research can be concentrated on basic "modules" (e.g. the viscous layer, the inviscid flow, the interaction mechanism) independently. Previously obtained knowledge and experience in boundary layer calculations, for example, can be

brought to bear because the viscous layer equations are still parabolic. Within the framework of the strong interaction approach, many levels of sophistication are possible. It is of utmost importance that the problem be formulated correctly, with the mechanism of interaction clearly delineated. Once this has been achieved, the analysis methods in each region can be chosen with some freedom. For example, it is possible to use either integral, finite difference, or finite element formulations for the boundary layer equations, while using completely different methods for the inviscid flow region.

In the research described in this report, an attempt was made to develop a method for calculating flows in which turbulent boundary layer separation occurs. The flow fields were restricted to those in which the maximum Mach number is less than 1. Although the methods investigated have many portions that are applicable to both plane 2-dimensional and axisymmetric geometries, major emphasis is placed on axisymmetric geometries. The strong interaction method was adopted as the basis for the work. Separate development of methods for calculating separating turbulent boundary layers with necessary "free stream" information input given and for calculating inviscid flows with appropriate strong interaction type boundary conditions was undertaken.

Although a complete calculation was not obtained, significant success in the development of each component was

achieved. The failure of the overall method is believed to be due to the lack of the ability to make an initial "guess" close enough to the final answer. (Each component was developed and tested with "exact" experimental information input as the necessary information from the other component.) It is felt that the use of an interactive computer system (presently unavailable to the authors) would open the possibility of making complete calculations.

In the remainder of this report, the problem will be formulated and the approaches considered in this research will be described. First the problem formulation will be discussed, with major emphasis on the interactive mechanism adopted. Then the calculations for each flow region will be described. Finally the attempts at integration of a complete model will be described and suggestions for future research made.

2. Problem Formulation

Consider the separated flow configuration shown in Figure 2.1. For some portion, the boundary layer is attached to the body. Because of adverse pressure gradients, the flow separates from the body and a region of reversed flow (separation bubble) develops. At some downstream location, the separation bubble is terminated by either a reattachment to a solid surface or a realignment of the flow via interaction with a separated boundary layer originating on the "lower" side of the body. It is here assumed that this separated region is relatively "thin" and that the flow is steady i.e. vortex shedding and bluff body flows are excluded. This type of separation often occurs near the trailing edge of airfoils and off of boattailed after bodies employed on jet engine nacelles and missiles. In the latter case, the reattachment may in fact be onto a propulsive plume, although in the work considered herein, reattachment onto a solid surface was assumed. It is assumed that the Mach number of the flow is everywhere less than 1 and that the Reynolds number is sufficiently large that boundary layers are turbulent. All surfaces are assumed to be smooth and impermeable.

In analyzing this flow, the major assumption that is made is that the flow can be divided into two distinct regions: (1) a rotational "viscous" region in which all of the effects of shear stress, turbulence, reverse flow, etc. are concentrated and (2) an inviscid, irrotational outer region. The viscous region is assumed to be <u>finite</u> in extent and within

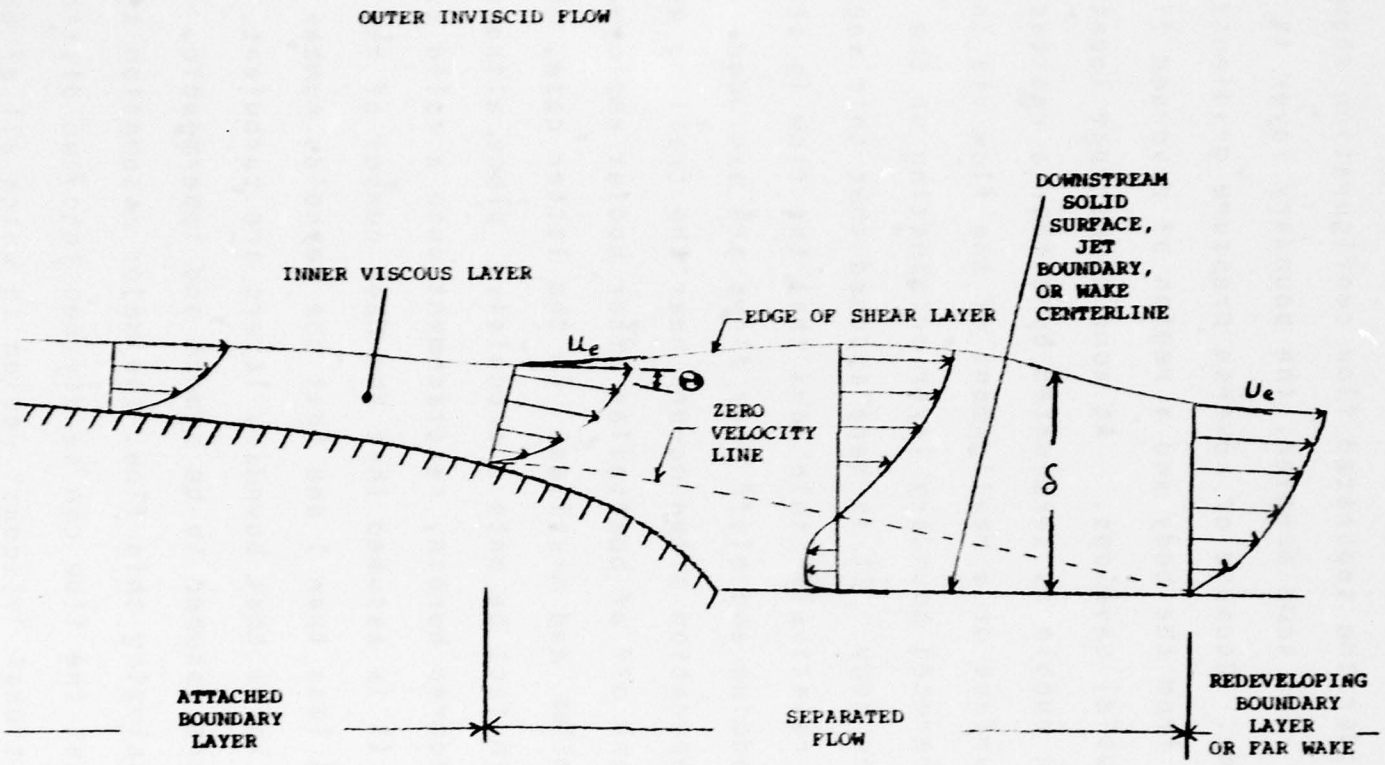

FIGURE 2.1 SCHEMATIC OF SEPARATED FLOW

this region, it is assumed that the standard boundary layer assumptions regarding the neglect of stream-wise stress gradients is applicable. Thus the governing equations for the viscous layer are

Continuity

$$\frac{\partial \rho u}{\partial x} + \frac{\partial \rho v}{\partial y} + j \frac{\rho u}{R} \frac{dR}{dx} = 0 \qquad (2.1)$$

Momentum

$$u \frac{\partial u}{\partial x} + v \frac{\partial u}{\partial y} = - \frac{1}{\rho} \frac{dP}{dx} + \frac{1}{\rho} \frac{\partial \tau}{\partial y} \qquad (2.2)$$

In equation 2.2, it is assumed that the pressure is constant across the viscous layer; this assumption may be subsequently replaced with a "centrifugal correction" of the form:

$$\frac{\partial P}{\partial y} \simeq \frac{\rho u^2}{\mathcal{R}}$$

or in integral methods of solution with an assured polynominal P(y) distribution with a typical parameter (say $P(\delta) - P(o)$) determined from solution of the (integral) y-momentum equation [8 - 9].

It is here emphasized that it is not necessarily assumed that P(x) is known a priori for use in equation 2.2; at this point it represents one of the unknowns. If P is assumed uniform across the viscous layer, then we may replace it with $P_e(x)$. The thickness of the viscous region is denoted by δ.

When dealing with compressible flows, the energy equation must also be considered. In this work, all compressible flows were assumed to be adiabatic and a solution to the energy equation was provided by employing the Crocco integral relating the temperature and velocity in the viscous layer.

$$\frac{T}{T_e} = 1 + RF \left(\frac{\gamma-1}{2} \right) M_e^2 (1 - \phi^2) \tag{2.3}$$

The recovery factor was computed from

$$RF = Pr^{.33}$$

Outside of the viscous layer, the flow is assumed to be irrotational and is governed by

$$\frac{\partial(\rho v_z)}{\partial z} + \frac{\partial(\rho v_r)}{\partial r} + j \frac{\rho v_r}{r} = 0 \tag{2.4}$$

$$\frac{\partial v_r}{\partial z} - \frac{\partial v_z}{\partial r} = 0 \tag{2.5}$$

The pressure in the outer region is governed by the Euler equations

$$v_z \frac{\partial v_z}{\partial z} + v_r \frac{\partial v_z}{\partial r} = - \frac{1}{\rho} \frac{dP}{\partial z}$$

$$v_z \frac{\partial v_r}{\partial z} + v_r \frac{\partial v_r}{\partial r} = - \frac{1}{\rho} \frac{\partial P}{\partial r}$$

In particular at the boundary between the two regions:

$$\frac{dP_e}{dx} \simeq - \rho_e u_e \frac{du_e}{dx} \tag{2.6}$$

The boundary conditions which can be applied directly are

$$\left.\begin{aligned} u &= 0 \\ v &= 0 \end{aligned}\right\} \text{ at solid boundaries} \tag{2.7}$$

$$\left.\begin{aligned} v_z &\to V_\infty \\ v_r &\to 0 \end{aligned}\right\} \; r,z \to \infty \tag{2.8}$$

The interaction between the two regions is introduced into the problem via the <u>matching conditions</u> which must be satisfied at the boundary between the two regions. If $y = \delta(x)$ is the thickness of the viscous layer, then the matching condition is that the velocity (vector) at $y = \delta(x)$ must be the same for the two regions. This is most easily accomplished by equating the total velocity (or Mach number) and the flow angle at the edge of the viscous layer to the corresponding values from the inviscid region. Thus we write

$$\left.\begin{aligned} (v_r^2 + v_z^2)^{1/2} &= (u_e^2 + v_e^2)^{1/2} \simeq u_e \\ &\text{or} \\ M_e|_{outer} &= M_e|_{inner} \\ &\text{and} \\ \theta &= \Theta + \alpha \end{aligned}\right\} \; y = \delta(x) \tag{2.9, 2.10}$$

Equations 2.9 and 2.10 provide the formal connection between the two regions.

It should be noted here that viscous - inviscid interaction is usually accounted for via "displacement thickness

interaction" rather than a formal matching of the flow fields at the edge of the viscous layer. In displacement thickness interaction, it is assumed that the velocity (or angle) at the edge of the viscous layer can be obtained by calculating the flow over the boundary surfaces augmented by adding the boundary layer displacement thickness. This is an approximation to equations 2.9 and 2.10 in that the angle Θ is very closely the angle of the displacement surface. Displacement thickness interaction has been used in most other (non-supersonic) separated flow analyses [1-5]; however, in this study, the more formal interaction of equations 2.9 and 2.10 has been retained.

With the introduction of the customary equations of state for ideal gases, equations 2.1 - 2.10 provide a closed set sufficient to determine the flow.* It is not possible to solve the equations simultaneously, however, so an interitive technique is employed, with the viscous and inviscid regions computed alternately. The matching conditions then appear as boundary conditions for one region or the other, with the most current information from the alternate calculation being used.

In the sections that follow, methods for making calculations in each region will be discussed. In developing the analysis for each region, it is assumed that complete information on the conditions at the inner-region boundary is available i.e. either or both of M_e, Θ are known. First

---

* For compressible flow, the adiabatic energy equation is included in the inviscid region.

the viscous layer method will be considered, then methods investigated for the inviscid region will be considered.

3. Viscous Region Calculations

In developing a calculation method for the viscous region ("boundary layer") with separation, it is assumed that the necessary information from the inviscid region (pressure, velocity, or Mach number and/or flow angle at the edge of the boundary layer) is available. Only one of these variables is needed as input and in fact in a full interaction calculation, only one can be provided; the other one being calculated by the analysis itself. In the attached boundary layer (weak interaction) region it is the pressure that is input, with the flow angle being calculated. At this point it is necessary to assume that if either of these variables is needed, it can be provided. The task of the inviscid region analysis then will be to compute the necessary variable which is not calculated in the boundary layer analysis.

The task then becomes to construct a solution to equations 2.1 and 2.2, given the conditions of equation 2.7 and one of the conditions 2.9, 2.10. Historically, three methods have been developed to solve these equations. These are (1) integral methods, (2) finite difference methods, and (3) finite element methods. Although each of these methods has several points in its favor, as well as several drawbacks, it was decided at the outset of this research to develop an integral method, based on the following reasons:

(1) Integral methods were felt to be simpler to program,

(2) It was felt that an integral method should consume less computer time,

(3) An integral method can be formulated which solves directly for the parameters necessary to formulate the viscous - inviscid interaction i.e. $\delta(x)$, M_e, Θ, while in a finite-difference or finite element method, parameters such as $\delta(x)$ and hence Θ are ill-defined,

(4) By selecting a velocity profile which has an inherent reverse flow capability, regions of reverse flow can be calculated while still "marching" in the downstream direction, without the necessity of employing a special algorithm for reverse flow points,

(5) Local inaccuracies in turbulence models may be smoothed.

As a result of this study, it is possible to draw some conclusions regarding these points; this will be dealt with in a later section.

3.1 Derivation of Integral Equations

In employing the integral method, the boundary layer equations 2.1 and 2.2 are multiplied by $u^m y^n$ and formally integrated across the layer from $y = 0$ to $y = \delta$

(actually, rather than integration of 2.2 as is, 2.1 is multiplied by $u^{m+1}y^n$ and added to 2.2, then the result is integrated). This produces a set of (usually independent) equations which can be solved for a finite number of parameters. Using $m = n = 0$ produces the momentum integral equation, $m = 1$, $n = 0$ produces the mechanical energy equation, while $m = 0$, $n = 1$ produces the moment of momentum equation. The formal application of this procedure leads to the following equations following lengthy algebraic manipulations

Continuity Equation:

$$\frac{1}{\delta}\frac{v_e}{u_e} = \frac{\tan\Theta}{\delta} = -\left[\int_0^1 \frac{\rho}{\rho_e}\frac{\partial}{\partial x}\left(\frac{u}{u_e}\right)d\xi + \int_0^1 \frac{u}{u_e}\frac{\partial}{\partial x}\left(\frac{\rho}{\rho_e}\right)d\xi\right]$$

$$+ \left[(M_e^2-1)\frac{1}{u_e}\frac{du_e}{d_x} - \frac{j}{R}\frac{dR}{dx}\right]\int_0^1 \frac{\rho u}{\rho_e u_e}\,d\xi \qquad (3.1)$$

Momentum Equation:

$$\left[\int_0^1 \frac{u^2}{u_e^2}\frac{\partial}{\partial x}\left(\frac{\rho}{\rho_e}\right)d\xi + 2\int_0^1 \frac{\rho u}{\rho_e u_e}\frac{\partial}{\partial x}\left(\frac{u}{u_e}\right)d\xi\right]$$

$$+ \frac{j\delta}{R}\frac{dR}{dx}\int_0^1 \frac{\rho u^2}{\rho_e u_e^2}\,d\xi + \left[(2-M_e^2)\int_0^1 \frac{\rho u^2}{\rho_e u_e^2}\,d\xi - 1\right]\frac{1}{u_e}\frac{du_e}{dx}$$

$$= -\frac{C_f}{2\delta} - \frac{\tan\Theta}{\delta} \qquad (3.2)$$

Moment of Momentum Equation:

$$\int_0^1 \left(\frac{u}{u_e}\right)^2 \frac{\partial}{\partial x}\left(\frac{\rho}{\rho_e}\right)\xi d\xi + 2\int_0^1 \frac{\rho u}{\rho_e u_e}\frac{\partial}{\partial x}\left(\frac{u}{u_e}\right)\xi d\xi$$

$$+ \left[(2-M_e^2)\frac{1}{u_e}\frac{du_e}{dx} + \frac{j}{R}\frac{dR}{dx}\right]\int_0^1 \frac{\rho u^2}{\rho_e u_e^2}\xi d\xi$$

$$+ \int_0^1 \frac{u}{u_e}\left[\int_0^\xi \left(\frac{\rho}{\rho_e}\frac{\partial}{\partial x}\left(\frac{u}{u_e}\right) + \frac{u}{u_e}\frac{\partial}{\partial x}\left(\frac{\rho}{\rho_e}\right)\right)d\zeta\right.$$

$$\left. + \left(\left[1-M_e^2\right]\frac{1}{u_e}\frac{du_e}{dx} + \frac{j}{R}\frac{dR}{dx}\right)\int_0^\xi \frac{\rho u}{\rho_e u_e}d\zeta\right]d\xi$$

$$= -\frac{\tan\Theta}{\delta} + \frac{1}{2u_e} - \frac{1}{\delta}\int_0^1 \frac{\tau}{\rho_e u_e^2}d\xi \qquad (3.3)$$

Mechanical Energy Equation:

$$\left[\int_0^1 \left(\frac{u}{u_e}\right)^3 \frac{\partial}{\partial x}\left(\frac{\rho}{\rho_e}\right)d\xi + 3\int_0^1 \frac{\rho}{\rho_e}\frac{u^2}{u_e^2}\frac{\partial}{\partial x}\left(\frac{u}{u_e}\right)d\xi\right]$$

$$+ \left[\left(\{3-M_e^2\}\frac{1}{u_e}\frac{du_e}{dx} + \frac{j}{R}\frac{dR}{dx}\right)\int_0^1 \frac{\rho u^3}{\rho_e u_e^3}d\xi\right.$$

$$\left. - \frac{2}{u_e}\frac{du_e}{dx}\int_0^1 \frac{u}{u_e}d\xi\right] = -\frac{\tan\Theta}{\delta}$$

$$- \frac{1}{\delta}\int_0^1 \frac{2\tau}{\rho_e u_e^2}\frac{\partial}{\partial\xi}\left(\frac{u}{u_e}\right)d\xi \qquad (3.4)$$

In the above equations, isentropic flow external to the boundary layer has been assumed and the approximation of equation 2.6 has been employed.

In order to make any calculations with these equations, it is necessary to evaluate the integrals appearing in them. This in turn requires knowledge of the variation of the velocity ratio, density ratio, and their x - derivatives across the boundary layer, as well as the variation of the shear stress across the boundary layer. The usual approach is to assume a velocity profile of the form

$$u(x,y)/u_e(x) = f(y,a_1(x),a_2(x)\ldots)$$

where the parameters a_i are functions of x only. The density ratio can be related to temperature ratio and hence to velocity ratio via eq. 2.3. The shear stress distribution is related to velocity distribution via Newton's law of viscosity and/or a "turbulence model". In some (if not most) methods in actual use, the shear stress integrals themselves are postulated as functions of parameters of x. Using the assumed profile the indicated integrations on ξ can be performed and the partial derivatives become total derivatives with respect to x of the $a_i(x)$. The $a_i(x)$ thus effectively become the unknowns of the problem and as many equations are required as there are a_i to calculate. The boundary conditions 2.7, 2.9, 2.10 are usually satisfied auto-

matically by the function chosen for the velocity profile; the problem then becomes an initial value problem for the a_i's.

3.2 Choice of Velocity Profile

It is here noted that henceforth, consideration is restricted to turbulent flows. When chosing the velocity profile, the following restrictions and guidelines must be met

(1) The profile must accurately represent the actual velocity distribution,

(2) The profile must be capable of exhibiting reverse flow near the wall (negative wall shear),

(3) The parameters involved in the profile should be meaningful and convenient.

Relevant to the third point, it is noted that the integral equations themselves (3.1 - 3.4) contain the parameters $u_e(x)$ (equivalent to $M_e(x)$ for isentropic flow external to the boundary layer), $\delta(x)$, $C_f(x)$, and $\Theta(x)$. Now $u_e(x)$ and $\Theta(x)$ are exactly what is needed for the interaction with the external flow. In addition, $\delta(x)$ must be known so that the boundary between the two regions may be located. It therefore seems that $u_e(x)$, $\delta(x)$ and $C_f(x)$ are logical choices for the parameters of the velocity profile. Now for incompressible turbulent non-separated boundary layers, it is well known that

the wall-wake velocity profile [10] provides an excellent approximation to the actual velocity profile. Alber and Coats [11], Mathews et al. [12], and Alber et al. [13] have shown that this profile can be modified to account for compressibility, and Alber et al. [13] and Kuhn and Nielsen [2 - 3] have shown that the profile can be modified to include both reverse flow and a laminar sublayer. Accordingly, the following form is adopted for the velocity profile

$$\phi = \frac{u}{u_e} = \frac{1}{a} \sin \{a\lambda[\frac{1}{k} \ln (1+y^+) + B - (1.5y^+ + B)e^{-.18y^+}] + au_\beta \sin^2(\frac{\pi}{2} \frac{y}{\delta})\} \qquad (3.5)$$

where

$$k = .41 \quad , \quad B = 5.0$$

$$a = \frac{RF(\frac{\gamma-1}{2})M_e^2}{1 + R(\frac{\gamma-1}{2})M_e^2} \quad , \quad y^+ = |\lambda| \frac{yu_e}{\nu_w}$$

$$\lambda = \frac{C_f/2}{|C_f/2|^{1/2}}$$

The parameters in this equation are $u_e(x)[M_e(x)]$, $\delta(x)$, $\lambda(x)$, $u_\beta(x)$.

The unit in the ln and the linear-exponential term provide a smooth decrease to zero velocity at $y = y^+ = 0$. The constants in the linear-exponential term were selected to provide an optimum fit with the Spalding - Kleindienst law of the wall, as presented by White [15].

With constant pressure across the boundary layer assumed, the density ratio can be calculated by

$$\frac{\rho}{\rho_e} = \frac{T_e}{T} = [1+RF(\tfrac{\gamma-1}{2})M_e^2(1-\phi^2)]^{-1} \qquad (3.6)$$

If the flow is incompressible, $\rho/\rho_e \equiv 1$, $\nu_w = \nu_e$ and the velocity ratio, ϕ, is given by the term enclosed in the {} in Eqn. 3.5, with the "a" removed.

Although there are 4 parameters in (3.5), they are not completely independent since the condition

$$u/u_e = 1 \quad \text{at} \quad y = \delta$$

must be satisfied. This results in

$$\frac{1}{a}\sin\{a\lambda[\frac{1}{k}\ln(1+\delta^+) + B - (1.5\delta^+ + B)e^{-.18\delta^+}] + au_\beta\} \equiv$$

$$F(M_e,\lambda,\delta,u_\beta) = 1 \qquad (3.7)$$

This may be called a "skin friction law", at any rate it is a relationship between $\lambda(x)$, $\delta(x)$, $M_e(x)$, $u_\beta(x)$ which must be satisfied.

3.3 Formulation of Differential Equations for λ, δ, M_e, u_β, Θ

Within the framework of the integral approach, complete information on the viscous layer is represented by knowledge of the five parameters M_e, Θ, λ, δ, u_β. Now one of these parameters (either M_e or Θ) is specified by the inviscid flow coupling so 4 (differential) equations are needed to solve for the remaining 4 unknowns.

One equation that must be satisfied is 3.7, the other 3 necessary equations can be selected from 3.1 - 3.4. The choice is actually between the mechanical energy equation (3.4) and the moment of momentum equation (3.3), with the continuity and momentum equation being retained in all cases. For the sake of generality, both equations will be further developed here although the moment of momentum equation was ultimately selected for reasons to be discussed later.

Substitution of the assumed velocity profile and the resulting density profile 3.5, 3.6 into 3.1 - 3.4 allows (at least in theory) the performing of the integrals and the differentiation with respect to x. The form of the resulting equations is

$$A_1 \frac{dM_e}{dx} + A_2 \frac{d\lambda}{dx} + A_3 \frac{d\delta}{dx} + A_4 \frac{du_\beta}{dx} = A_5 + A_6 + A_7$$

Where the coefficients $A_1 \rightarrow A_5$ involve M_e, λ, δ, u_β and require evaluation of an integral on y from $0 \rightarrow \delta$, A_6 involves Θ and A_7 is possibly a shear stress integral. Now the complicated form of 3.5 for ϕ makes analytical integration of ϕ and its powers and derivatives as needed in 3.1 - 3.4 impossible (at least for compressible flow), therefore the integration must in general be performed numerically to find $A_1 \rightarrow A_5$. Accordingly, the equations 3.1 - 3.4 are here presented with the integrals yet to be

evaluated. It is emphasized that although the integrands are algebraically complicated, they are functions of M_e, λ, δ, u_β and ξ only and hence the indicated integration on ξ can be performed (numerically if necessary) if M_e, λ, δ, u_β are known. The equations are

Continuity:

$$\left\{\int_0^1 \left[\frac{\partial\phi}{\partial a}\frac{\partial a}{\partial M_e}(r+\phi\frac{\partial r}{\partial\phi}) + \frac{\partial\phi}{\partial y^+}\frac{\partial y^+}{\partial M_e}(r+\phi\frac{\partial r}{\partial\phi}) + \phi\frac{\partial r}{\partial M_e}\right]d\xi\right.$$

$$\left. + (1-M_e^2)\frac{T_e}{T_o}\frac{1}{M_e}\int_0^1 r\phi\,d\xi\right\}\frac{dM_e}{dx}$$

$$+ \left\{\int_0^1\left[\left(\frac{\partial\phi}{\partial\lambda} + \frac{\partial\phi}{\partial y^+}\frac{\partial y^+}{\partial\lambda}\right)\left(r + \phi\frac{\partial r}{\partial\phi}\right)\right]d\xi\right\}\frac{d\lambda}{dx}$$

$$+ \left\{\int_0^1 \frac{\partial\phi}{\partial\delta}\left(r+\phi\frac{\partial r}{\partial\phi}\right)d\xi\right\}\frac{d\delta}{dx}$$

$$+ \left\{\int_0^1 \frac{\partial\phi}{\partial u_\beta}\left(r+\phi\frac{\partial r}{\partial\phi}\right)d\xi\right\}\frac{du_\beta}{dx}$$

$$= -\frac{\tan\Theta}{\delta} - \frac{j}{R}\frac{dR}{dx}\int_0^1 r\phi\,d\xi \qquad (3.8)$$

Momentum:

$$\left\{\int_0^1\left(\left[\frac{\partial\phi}{\partial a}\frac{\partial a}{\partial M_e} + \frac{\partial\phi}{\partial y^+}\frac{\partial y^+}{\partial M_e}\right]\left[\phi^2\frac{\partial r}{\partial\phi} + 2r\phi\right] + \phi^2\frac{\partial r}{\partial M_e}\right)d\xi\right.$$

$$\left. + \frac{T_e}{T_o}\frac{1}{M_e}\left[(2-M_e^2)\int_0^1 r\phi^2 d\xi - 1\right]\right\}\frac{dM_e}{dx}$$

$$+ \left\{\int_0^1\left[\frac{\partial\phi}{\partial\lambda} + \frac{\partial\phi}{\partial y^+}\frac{\partial\lambda}{\partial y^+}\right]\left[\phi^2\frac{\partial r}{\partial\phi} + 2r\phi\right]d\xi\right\}\frac{d\lambda}{dx}$$

(continued)

$$+ \{\int_0^1 \frac{\partial\phi}{\partial\delta}\,[\phi^2\,\frac{\partial r}{\partial\phi} + 2r\phi]d\xi\}\,\frac{d\delta}{dx}$$

$$+ \{\int_0^1 \frac{\partial\phi}{\partial u_\beta}\,[\phi^2\,\frac{\partial r}{\partial\phi} + 2r\phi]d\xi\}\,\frac{du_\beta}{dx}$$

$$= -\frac{\lambda|\lambda|}{\delta} - \frac{\tan\Theta}{\delta} - \frac{j}{R}\,\frac{dR}{dx}\int_0^1 r\phi^2 d\xi \qquad (3.9)$$

Moment of Momentum:

$$\{\int_0^1 ([\frac{\partial\phi}{\partial a}\,\frac{\partial a}{\partial M_e} + \frac{\partial\phi}{\partial y^+}\,\frac{\partial y^+}{\partial M_e}][\phi^2\,\frac{\partial r}{\partial\phi} + 2r\phi] + \phi^2\,\frac{\partial r}{\partial M_e})\xi d\xi$$

$$+ \frac{T_e}{T_o}\,\frac{1}{M_e}\,[(2-M_e^2)\int_0^1 r\phi^2\xi d\xi - \frac{1}{2}]$$

$$+ \int_0^1 \phi[\int_0^\xi ([\frac{\partial\phi}{\partial a}\,\frac{\partial a}{\partial M_e} + \frac{\partial\phi}{\partial y^+}\,\frac{\partial y^+}{\partial M_e}][r + \phi\,\frac{\partial r}{\partial\phi}] + \phi\,\frac{\partial r}{\partial M_e})d\zeta]d\xi$$

$$+ [(1-M_e^2)\,\frac{T}{T_o}\,\frac{1}{M_e}\int_0^1 [\phi\int_0^\xi r\phi d\zeta]d\xi\}\,\frac{dM_e}{dx}$$

$$+ \{\int_0^1 [\frac{\partial\phi}{\partial\lambda} + \frac{\partial\phi}{\partial y^+}\,\frac{\partial y^+}{\partial\lambda}][\phi^2\,\frac{\partial r}{\partial\phi} + 2r\phi]\xi d\xi$$

$$+ \int_0^1 (\phi\int_0^\xi [\frac{\partial\phi}{\partial\lambda} + \frac{\partial\phi}{\partial y^+}\,\frac{\partial y^+}{\partial\lambda}][r + \phi\,\frac{\partial r}{\partial\phi}]d\zeta)d\xi\}\,\frac{d\lambda}{dx}$$

$$+ \frac{d\delta}{dx}\,\{\int_0^1 \frac{\partial\phi}{\partial\delta}\,[\phi^2\,\frac{\partial r}{\partial\phi} + 2r\phi]\xi d\xi$$

$$+ \int_0^1 (\phi\int_0^\xi \frac{\partial\phi}{\partial\delta}\,(r + \phi\,\frac{\partial r}{\partial\phi})d\zeta)d\xi\}$$

$$+ \{\int_0^1 \frac{\partial\phi}{\partial u_\beta}[\phi^2\,\frac{\partial r}{\partial\delta} + 2r\phi]\xi d\xi$$

$$+ \int_0^1 (\phi\int_0^\xi \frac{\partial\phi}{\partial u_\beta}\,(r + \phi\,\frac{\partial r}{\partial\phi})d\zeta)d\xi\}\,\frac{du_\beta}{dx}$$

(continued)

$$= -\frac{\tan\Theta}{\delta} - \frac{j}{R}\frac{dR}{dx}\left[\int_0^1 r\phi^2\xi d\xi + \int_0^1 \phi\left(\int_0^\xi r\phi d\zeta\right)d\xi\right]$$

$$- \frac{1}{\delta}\int_0^1 \frac{\tau}{\rho_e u_e^2}\, d\xi \qquad (3.10)$$

Mechanical Energy Equation

$$\left\{\int_0^1\left(\left[\frac{\partial\phi}{\partial a}\frac{\partial a}{\partial M_e} + \frac{\partial\phi}{\partial y^+}\frac{\partial y^+}{\partial M_e}\right]\left[\phi^3\frac{\partial r}{\partial\phi} + 3r\phi^2\right] + \phi^3\frac{\partial r}{\partial M_e}\right)d\xi\right.$$

$$\left. + \left[(3-M_e^2)\int_0^1 r\phi^3 d\xi - 2\int_0^1\phi d\xi\right]\frac{T_e}{T_o}\frac{1}{M_e}\right\}\frac{dM_e}{dx}$$

$$+ \left\{\int_0^1\left[\frac{\partial\phi}{\partial\lambda} + \frac{\partial\phi}{\partial y^+}\frac{\partial y^+}{\partial\lambda}\right]\left[\phi^3\frac{\partial r}{\partial\phi} + 3r\phi^2\right]d\xi\right\}\frac{d\lambda}{dx}$$

$$+ \left\{\int_0^1\frac{\partial\phi}{\partial\delta}\left[\phi^3\frac{\partial r}{\partial\phi} + 3r\phi^2\right]d\xi\right\}\frac{d\delta}{dx}$$

$$+ \left\{\int_0^1\frac{\partial\phi}{\partial u_\beta}\left[\phi^3\frac{\partial r}{\partial\phi} + 3r\phi^2\right]d\xi\right\}\frac{du_\beta}{dx}$$

$$= -\frac{\tan\Theta}{\delta} - \frac{2}{\delta}\int_0^1\frac{\tau}{\rho_e u_e^2}\frac{\partial\phi}{\partial\xi}\,d\xi - \frac{j}{R}\frac{dR}{dx}\int_0^1 r\phi^3 d\xi$$

(3.11)

The various partial derivatives of the ϕ and $r(=\rho/\rho_e)$ are tabulated in Appendix A.

Equations 3.8, 3.9, either of 3.10 or 3.11 and 3.7, together with a specification of either $M_e(x)$ or $\Theta(x)$ and a set of initial values thus form a closed set. Now 3.8 - 3.11 are <u>differential</u> equations, which will ultimately be solved numerically, while 3.7 is an algebraic equation. In performing numerical computations, it has

been found easier to solve 4 differential equations than 3 differential and one algebraic equation; therefore, 3.7 is differentiated with respect to x to yield:

$$\frac{dF}{dx} = \left[\frac{\partial F}{\partial a}\frac{\partial a}{\partial M_e} + \frac{\partial F}{\partial \delta^+}\frac{\partial \delta^+}{\partial M_e}\right]\frac{dM_e}{dx} + \left[\frac{\partial F}{\partial \lambda} + \frac{\partial F}{\partial \delta^+}\frac{\partial \delta^+}{\partial \lambda}\right]\frac{d\lambda}{dx}$$

$$+ \left[\frac{\partial F}{\partial \delta^+}\frac{\partial \delta^+}{\partial \delta}\right]\frac{d\delta}{dx} + \frac{\partial F}{\partial u_\beta}\frac{du_\beta}{dx} = 0 \qquad (3.12)$$

The partial derivatives appearing in the above are tabulated in Appendix A.

We have thus completely formulated the viscous layer problem, with the exception of a means of evaluating the shear stress integrals appearing in the mechanical energy and moment of momentum equations. This of course requires the introduction of some semi-empirical "model" of the turbulent transport process; this complicated subject will now be dealt with.

3.4 Turbulence Models

In order to close the set of equations 3.8, 3.9, 3.10 or 3.11, and 3.12, it is necessary to evaluate either

$$\int_0^1 \frac{\tau}{\rho_e u_e^2}\, d\xi$$

for the moment of momentum equation, or

$$\int_0^1 \frac{\tau}{\rho_e u_e^2}\frac{\partial \phi}{\partial \xi}\, d\xi$$

for the mechanical energy equation. For turbulent flow, τ represents the sum of the laminar viscous shear and the Reynolds shear stresses.

$$\tau = \mu \frac{\partial u}{\partial y} - \rho \overline{u'v'} = \tau_L + \tau_t$$

Complete information on the Reynolds stress is not currently available, hence these terms (or their integrals) are evaluated via some semi-emperical model. In many integral methods, an attempt is made to introduce information on the integrals themselves [14]; however, in differential methods a local formulation for τ is needed. In the current research, since a numerical evaluation of integrals of the velocity profile function and its derivatives (typical terms appearing on the right hand sides of equations 3.8 - 3.11) is to be undertaken, a numerical integration of a local shear stress formulation was selected. An eddy viscosity formulation was selected in order that a negative shear would be predicted in regions of reverse flow.

$$\tau = (\mu + \rho\varepsilon) \frac{\partial u}{\partial y} \qquad (3.13)$$

It is well known that turbulence is a phenomenon which exhibits at least two length scales, therefore for turbulent flow near walls, separate formulations for the eddy viscosity near the wall and in the outer region are often used. A popular choice for the eddy viscosity is the mixing length formulation

$$\varepsilon = \ell^2 \left|\frac{\partial u}{\partial y}\right| \qquad (3.14)$$

The mixing length is at least an order of magnitude larger in the outer region of the boundary layer than near the wall. Most eddy viscosity models employ a mixing length formulation near the wall; however, in the outer region an alternate form may sometimes be used, typical is the Clauser model

$$\varepsilon_{outer} = .016\, u_e \delta_k^* \qquad (3.15)$$

Both approaches have been applied to a wide variety of turbulent boundary layer calculations, including separating flows [2 - 4]; in the basic ("equilibrium") form embodied in 3.14 and 3.15 there seems to be little to choose between the two. Calculations undertaken in the current research bear this out for attached boundary layers; however, the mixing length model was found to be more ameable to extension to non-equilibrium flows and to boundary layers with backflow; therefore, the mixing length formulation was selected as the basic turbulence model for the present work. The mixing length typically exhibits the following characteristics [15]

Near the wall: $\ell \sim y$

Very near the wall: $\ell \sim y^{3/2}$

In the outer region: $\ell \sim$ independent of y, $\ell \sim \delta$

The following (continous) mixing length distribution embodies all of these characteristics and was employed

in this work

$$\frac{\ell}{\delta} = \frac{\ell_\infty}{\delta} \tanh\left[\frac{k}{\ell_\infty/\delta}\,\frac{Y}{\delta}\right]\left(1 - \exp\left[-\frac{Y}{26\nu}\left(\frac{\tau_w}{\rho} + \frac{1}{\rho}\frac{dP}{dx}\,y\right)^{1/2}\right]\right) \tag{3.16}$$

The last term represents the van Driest [16] damping factor as modified for the effect of pressure gradient as suggested by Cebeci et al. [17]. For "equilibrium" attached turbulent boundary layers, the value of ℓ_∞/δ is a constant equal to approximately 0.09.

Now when a boundary layer separates from a solid surface, the damping effects of the wall on the turbulence are removed; in fact, the layer becomes almost entirely "wake like", accordingly the following model was adopted for the mixing length in separated boundary layers. With reference to Figure 3.1, the layer is divided into two regions at the zero velocity point y_0. Above the zero velocity point

$$\ell = \ell_\infty = (\ell_\infty/\delta)\delta \tag{3.17}$$

while below the zero velocity point

$$\ell = \ell_\infty\, y/y_0. \tag{3.19}$$

Having introduced the mixing length model the shear stress integrals may now be formulated. Assuming a laminar viscosity law of the form

$$\mu/\mu_0 = (T/T_0)^{3/4} \tag{3.20}$$

the shear stress function becomes

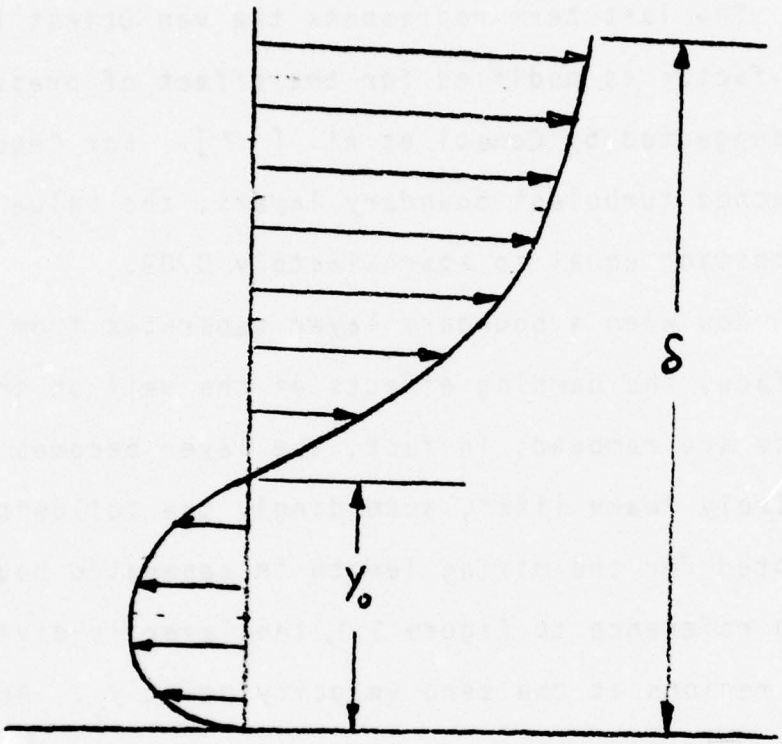

FIGURE 3.1 REVERSE FLOW VELOCITY PROFILE

$$\frac{\tau}{\rho_e u_e^2} = \left[(M_e R_\delta)^{-1} \left(\frac{T_e}{T_o}\right)^{-9/4} \left(\frac{\rho}{\rho_e}\right)^{-3/4} + \frac{\rho}{\rho_e} \frac{\varepsilon}{u_e \delta}\right] \frac{\partial \phi}{\partial \xi} \quad (3.21)$$

Employing the mixing length model, the "eddy viscosity Reynolds number" can be written

$$\frac{\varepsilon}{u_e \delta} = \left(\frac{\ell}{\delta}\right)^2 \left|\frac{\partial \phi}{\partial \xi}\right|$$

Substituting the mixing length equation 3.16 and introducing the velocity profile parameters, we obtain

$$\frac{\varepsilon}{u_e \delta} = \left(\frac{\ell_\infty}{\delta}\right)^2 \tanh^2 \left[\frac{k}{\ell_\infty/\delta} \xi\right] \{1 - \exp\left[-\frac{R_\delta M_e}{26} \left(\frac{T_e}{T_o}\right)^{9/4} \left(\frac{\rho}{\rho_e}\right)^{7/4} \xi \right.$$

$$\left. (\lambda|\lambda| - \xi \frac{\delta}{M_e} \frac{dM_e}{dx})^{1/2}{}^2 \right]\} \left|\frac{\partial \phi}{\partial \xi}\right| \quad (3.22)$$

for the attached boundary layer and

$$\frac{\varepsilon}{u_e \delta} = \begin{cases} \left(\frac{\ell_\infty}{\delta}\right)^2 \left|\frac{\partial \phi}{\partial \xi}\right| & \xi \geq \xi_o \\ \left(\frac{\ell_\infty}{\delta}\right)^2 \left(\xi/\xi_o\right)^2 \left|\frac{\partial \phi}{\partial \xi}\right| & \xi < \xi_o \end{cases} \quad (3.23)$$

The shear integrals appearing in the moment of momentum equation (3.10) and mechanical energy equation (3.11) can be evaluated as functions of the velocity profile parameters M_e, λ, δ, u_β and their derivatives using 3.21, 3.22, 3.23, 3.5, and the derivatives relations of Appendix A, if ℓ_∞/δ is specified (ℓ_∞/δ becomes, in

effect, an additional parameter of the flow in the boundary layer).

3.4.1 Non-Equilibrium Effects in the Turbulence Model

For equilibrium attached boundary layers, the value of ℓ_∞/δ is rather well determined as

$$\ell_\infty/\delta \simeq 0.09$$

essentially independent of pressure gradient effects. Successful calculations of non-equilibrium boundary layers have also been made using this value; however, the simple use of a constant value for this parameter was found to be unsatisfactory for calculations of the separating boundary layers considered here. At least two reasons for this behavior may be offered:

(1) "History" effects are present, especially near separation. As separation is approached, the boundary layer grows rapidly, that is δ increases rapidly. The turbulence structure does not respond rapidly so that as δ grows rapidly, ℓ_∞ does not and thus ℓ_∞/δ decreases,

(2) The separating boundary layer is in reality a process of transition between an attached shear flow and a free shear flow. Even for equilibrium layers, while a value of $\ell_\infty/\delta \simeq .09$ is appropriate for attached flows, a value of

ℓ_∞/δ = 0.05 to 0.07 is appropriate for free shear layers [18]. A calculation method for both attached and free shear flows and the transition between them (separating boundary layers) must reflect this change in ℓ_∞/δ.

In order to successfully calculate separating boundary layers using the current method, it is necessary for ℓ_∞/δ to change as the flow develops toward separation, separates, develops a free shear-like character, and (possibly) reattaches and redevelops as an attached boundary layer. It is of course necessary to connect the change of ℓ_∞/δ with changes in their flow parameters. There are two* possibilities for accomplishing this:

(1) Use an algebraic formulation of the form

$$\ell_\infty/\delta = f(M_e, \lambda, \delta, u_\beta)$$

(2) Solve a differential equation of the form

$$\frac{d}{dx}\ (\ell_\infty/\delta) = f(M_e, \lambda, \delta, u_\beta, \ell_\infty/\delta, x)$$

Within the differential equation approach, the choice is between solving an empirical differential equation of the "lag" or "departure from equilibrium" type

---

* The idea of a formulation ℓ_∞/δ = prescribed function of x is rejected as being possible only if the answer is known in the first place!

$$\frac{d(\ell_\infty)}{dx} \sim [\ell_\infty)_{eq} - \ell_\infty]$$

or of solving a differential equation with a more solid physical basis, typically some form of the "turbulence kinetic energy equation".

During the course of this investigation, all three of the above approaches were investigated. Each approach will be described in turn.

Considering first the algebraic formulation, the overall approach of Alber [19] was employed. The reasoning proceeds as follows. For <u>equilibrium</u> boundary layers, Clauser [20] has shown that the appropriate correlating parameter for turbulence parameters is $\beta(\equiv \frac{\delta_k^*}{\tau_w}\frac{dP}{dx})$ * thus for equilibrium boundary layers we would assume

$$\ell_\infty/\delta = f(\beta)$$

The function f must satisfy

$f = 0.09 \quad \beta = 0$ (flat plate)

$f \to 0.05$ to 0.07 as $\beta \to \infty$ (free shear layer)

The form chosen here was determined by numerical experimentation and is typical of other methods [2]; it is

$$\frac{\ell_\infty}{\delta} = 0.055 + 0.035 \exp(-\beta/5) \qquad (3.24)$$

---

* In terms of the principal parameters employed in the present study $\beta = -\delta_k^* \frac{2}{\lambda|\lambda|}\frac{T_e}{T_o}\frac{1}{M_e}\frac{dM_e}{dx}$

Following Alber [19] it is assumed that the equilibrium correlation can be used if β is related to the equilibrium shape parameters rather than its definition as a pressure gradient parameter*. Accordingly, β is calculated from

$$G = 6.1\sqrt{\beta + 1.81} - 1.7 \tag{3.25}$$

where G (the equilibrium shape parameter) is related to the local velocity shape parameters by

$$G \equiv \frac{\int_0^1 \left(\frac{u_e - u}{u^*}\right)^2 d\xi}{\int_0^1 \left(\frac{u_e - u}{u^*}\right) d\xi} = \frac{H_k - 1}{\lambda H_k} \tag{3.26}$$

Equations 3.24 - 3.26 are sufficient to relate ℓ_∞/δ to the local velocity profile parameters $M_e, \lambda, \delta, u_\beta$.

Plotted in Figures 3.2 - 3.4 are skin friction coefficients, boundary layer thicknesses, and shape factors predicted for the incompressible two dimensional separating boundary layer flow of Simpson et al. [21]. For reasons that will become clear later, only the results up to $C_f = 0.0005$ are shown. Clearly, the predictions with the constant (equilibrium) value of ℓ_∞/δ are unsatisfactory (in fact it is not even possible to predict separation using this model). In fact, predictions with the algebraic correlation are good enough

---

* In Alber's terminology, β is "unhooked" from the pressure gradient.

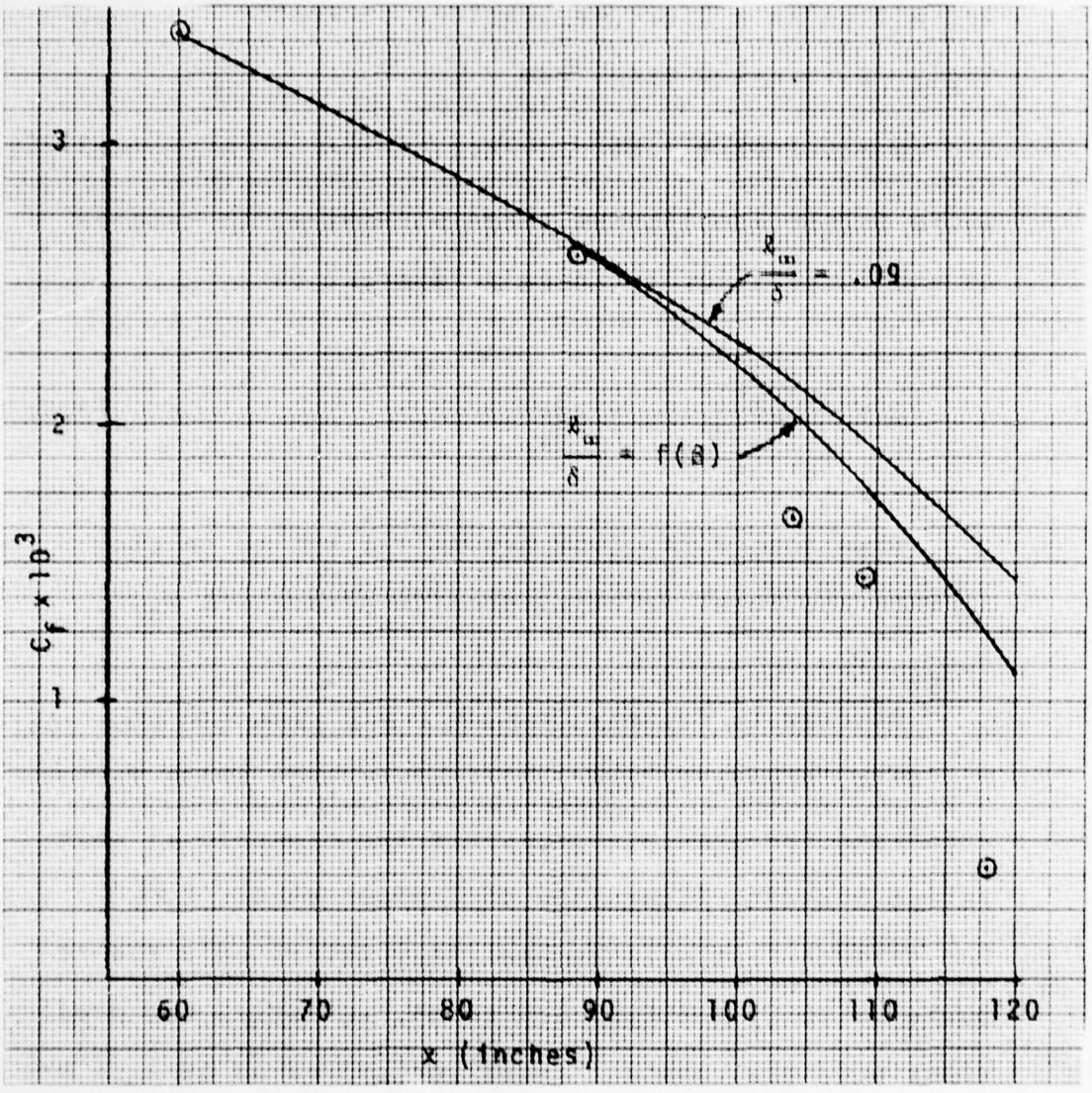

FIGURE 3.2 SKIN FRICTION COEFFICIENT FOR THE SEPARATING BOUNDARY LAYER FLOW OF SIMPSON ET AL. SHOWING EFFECT OF NON-EQUILIBRIUM MIXING LENGTH MODEL

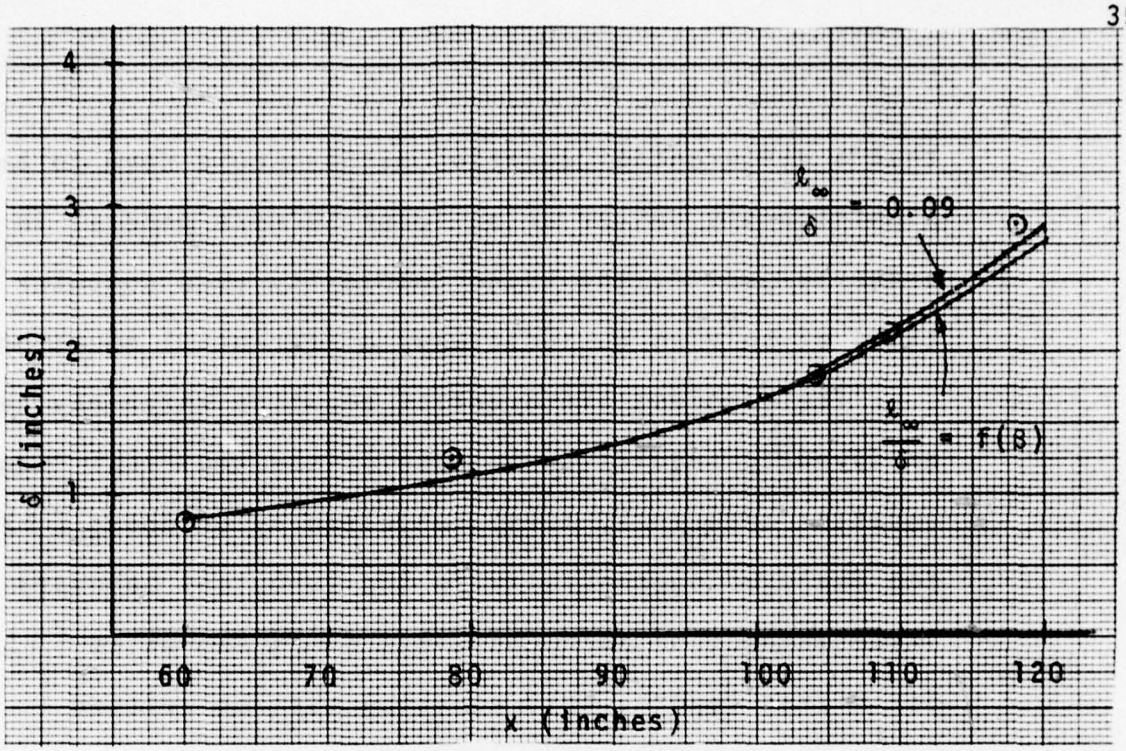

FIGURE 3.3 BOUNDARY LAYER THICKNESS FOR THE SEPARATING BOUNDARY LAYER FLOW OF SIMPSON ET AL. SHOWING EFFECT OF NON-EQUILIBRIUM MIXING LENGTH MODEL

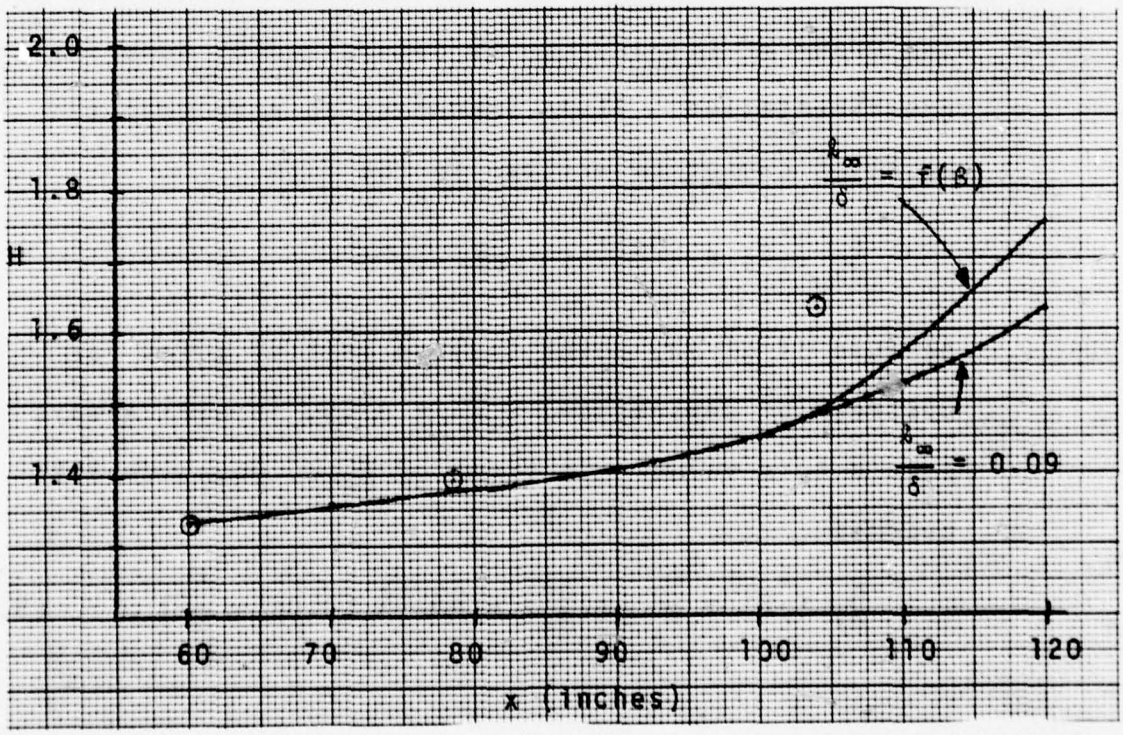

FIGURE 3.4 SHAPE FACTOR FOR THE SEPARATING BOUNDARY LAYER FLOW OF SIMPSON ET AL. SHOWING EFFECT OF NON-EQUILIBRIUM MIXING LENGTH MODEL

that a differential equation method would have to be significantly better or at least be more general in order to justify the added complexity (and computer time) of solving an additional differential equation.

The simplest differential equation which may be employed to predict turbulence is the empirical "lag" equation apparently first suggested by Goldberg [22] and employed successfully in the turbulent boundary layer methods of Nash and Hicks [23] and White [15]. For mixing length, this equation must be written

$$\frac{d\ell_\infty}{dx} = \frac{\text{const}}{\delta} \left(\ell_\infty)_{eq} - \ell_\infty\right) \tag{3.27}$$

where $\ell_\infty)_{eq} = 0.09\ \delta$.

The value of the constant in the equation is on the order of 0.1 and can be determined by numerical experimentation. It is important to note that the equation <u>cannot</u> be written in the form

$$\frac{d}{dx}\left(\frac{\ell_\infty}{\delta}\right) = \frac{\text{const}}{\delta}\left(0.09 - \frac{\ell_\infty}{\delta}\right)$$

because if at any point (say an initial point far upstream of separation) $\ell_\infty/\delta = 0.09$, it will always retain this value! In terms of ℓ_∞/δ, equation 3.27 becomes

$$\frac{d}{dx}\left(\frac{\ell_\infty}{\delta}\right) + \frac{\ell_\infty}{\delta}\left(\frac{1}{\delta}\frac{d\delta}{dx}\right) = \frac{\text{const}}{\delta}\left[0.09 - \frac{\ell_\infty}{\delta}\right] \tag{3.28}$$

Calculations for the Simpson et al. [21] flow and for the two dimensional transonic separating flow of Alber et al. [13] were preformed using 3.28 and were not significantly different from those using 3.24 - 3.26.

The differential equation that has been used most extensively to represent turbulence is the "turbulence kinetic energy equation". This equation has been employed in differential [24] and integral [25,26] forms and has been used with differential [24,26] and integral [25] methods of boundary layer predictions. In the current research, the basic approach of McDonald et al. [25,26] was employed to convert the turbulence kinetic energy equation into a differential equation for ℓ_∞/δ. The development is as follows. The partial differential equation governing the turbulence kinetic energy is

$$\frac{1}{2}\left(\rho u \frac{\partial q^2}{\partial x} + \rho v \frac{\partial q^2}{\partial y}\right) = \tau_t \frac{\partial u}{\partial y} - (\underset{\sim}{u}^2 - \underset{\sim}{v}^2) \frac{\partial u}{\partial x}$$

$$- \frac{\partial}{\partial y}\left[\underset{\sim}{v}\left(P + \frac{\rho q^2}{2}\right)\right] - \rho\Phi \qquad (3.28)$$

where Φ is a collection of many fluctuating terms and may be found elsewhere [15]. The terms in the equation are usually given names of the following form:

Advection = shear stress turbulence production + normal stress turbulence production - pressure - strain diffusion - viscous dissipation (of turbulence)

Equation 3.28 may be written as an integral equation by adding $\frac{1}{2} q^2 x$ (continuity equation) and integrating on y from $0 \to \delta$. Assuming negligible free stream turbulence, the result is

$$\frac{1}{2} \int_0^\delta \frac{\partial}{\partial x} (\rho u q^2) dy = \int_0^\delta (\tau_t \frac{\partial u}{\partial y} - (\tilde{u}^2 - \tilde{v}^2) \frac{\partial u}{\partial x}) dy$$

$$- \int_0^\delta \rho \Phi \, dy - j \int_0^\delta \frac{\rho u q^2}{2R} \frac{dR}{dx} \, dy \qquad (3.29)$$

Following McDonald et al. [25,26], Bradshaw et al. [24], and Collins and Simpson [27] it is assumed that

$$a_1 q^2 = F \left| \frac{\tau}{\rho} \right|$$

$$- \frac{(\tilde{u}^2 - \tilde{v}^2) \frac{\partial u}{\partial x}}{\tau_t \frac{\partial u}{\partial y}} = \frac{\text{Normal Stress Production}}{\text{Shear Stress Production}} = F \qquad (3.30)$$

$$\Phi = \left(F \left| \frac{\tau}{\rho} \right| \right)^{3/2} / L$$

where

$a_1 \simeq$ const $\simeq 0.15$

F = function of x only $\simeq \left[1 + 2 \left| \frac{\partial u / \partial x}{\partial u / \partial y} \right|_{\substack{\max \\ \text{shear}}} \right]^{-1}$

L = dissipation length = $L(y/\delta)$

It is pointed out that only Collins and Simpson consider normal stress turbulence production significant; the models of McDonald et al. [25,26] and Bradshaw et al. [24] are obtained by setting $F \equiv 1$. Substituting 3.30 into 3.29 and expressing the resulting equation in

terms of the parameters $M_e, \lambda, \delta, u_\beta$, we get

$$\{(3-M_e^2)\frac{1}{M_e}\frac{T_e}{T_o}\int_0^1\phi|\bar{\tau}|d\xi + \int_0^1(|\bar{\tau}|\frac{\partial\phi}{\partial M_e} + \phi\frac{\partial|\bar{\tau}|}{M_e})d\xi\}\frac{dM_e}{dx}$$

$$+ \{\int_0^1(|\bar{\tau}|\frac{\partial\phi}{\partial\lambda} + \phi\frac{\partial|\bar{\tau}|}{\partial\lambda})d\xi\}\frac{d\lambda}{dx}$$

$$+ \{\int_0^1(|\bar{\tau}|\frac{\partial\phi}{\partial\delta} + \phi\frac{\partial|\bar{\tau}|}{\partial\delta})d\xi\}\frac{d\delta}{dx}$$

$$+ \{\int_0^1(|\bar{\tau}|\frac{\partial\phi}{\partial u_\beta} + \phi\frac{\partial|\bar{\tau}|}{\partial u_\beta})d\xi\}\frac{du_\beta}{dx}$$

$$+ \{\int_0^1\phi\frac{\partial|\bar{\tau}|}{\partial(\ell_\infty/\delta)}d\xi\}\frac{d(\ell_\infty/\delta)}{dx} =$$

$$- (\frac{J}{R}\frac{dR}{dx} + \frac{1}{F}\frac{dF}{dx})\int_0^1\phi|\bar{\tau}|d\xi + \{\int_0^1\bar{\tau}\frac{\partial\phi}{\partial\xi}d\xi$$

$$- F^{1/2}\int_0^1 r^{-1/2}\frac{|(\bar{\tau})|^{3/2}}{(L/\delta)}d\xi\}\frac{2a_1}{\delta} \qquad (3.31)$$

where

$$\bar{\tau} \equiv \frac{\tau_t}{\rho_e u_e^2} = \frac{\varepsilon}{u_e\delta}\frac{\partial\phi}{\partial\xi} \qquad (3.32)$$

If the mixing length model (equations 3.22 and 3.23) is used and if F is formulated in terms of the assumed velocity profile function and its derivatives, then Equation 3.31 becomes a differential equation involving M_e, λ, δ, u_β, ℓ_∞/δ, and their derivatives; in effect a differential equation for ℓ_∞/δ. (It still remains to

specify $L/\delta = f(\xi)$). It must be noted that the formulation is still not complete, since all of the partial derivatives of $|\bar{\tau}|$ have not been presented. They will not be written here but the following two points are listed

(1) The partial derivatives involve many terms, due to the algebraic complexity of the mixing length model itself,

(2) It is necessary to evaluate all of the <u>second</u> derivatives of the velocity profile function.

After all operations have been performed and the indicated integrations performed (numerically) equations 3.8, 3.9, 3.10 or 3.11, 3.12 and 3.31 are five coupled ordinary differential equations for the six parameters Θ, M_e, λ, δ, u_∞, ℓ_∞/δ and can be solved if either of Θ or M_e are specified. Calculations were performed using this set of equations for the Simpson et al. [21] and Alber et al. [13] flows. The results were as follows.

It was first assumed, following McDonald et al. [25,26] Bradshaw [24], and particularly Collins and Simpson [27] that the dissipation length is a function of y/δ only and as approximated by

$$\frac{L}{\delta} = \frac{L_\infty}{\delta} \tanh\left[\frac{k}{L_\infty/\delta}\,\xi\right][1 + 5.5\,\xi^6]^{-1}$$

for attached boundary layers, (3.32)

$$\frac{L}{\delta} = \frac{L_\infty}{\delta}\,[\delta - y_o]$$

for separated boundary layers

where $L_\infty/\delta = 0.09$.

Calculations using this formulation were quite discouraging, being similar to those made with $\ell_\infty/\delta \equiv 0.09$, as indicated by the skin friction plots of Figure 3.5.. It was concluded that the dissipation length formulation of 3.32 was not sufficiently general.

The measurements of Simpson et al. [21] indicate that in a separating boundary layer, the dissipation length (as well as the mixing length) in the outer portion of the boundary layer decreases as separation is approached, accordingly calculations with $L_\infty/\delta = 0.07$ were made; these were inaccurate in regions upstream of separation.

Realizing that L_∞/δ in fact varies with the flow, calculations were then made with

$$L_\infty/\delta = 0.05 + 0.04 \exp(-\beta/4)$$

These calculations were slightly better but by now it should be obvious that specifying L_∞/δ is a function of the mean flow parameters is no different than specifying ℓ_∞/δ as a function of the same mean flow parameter and that the latter is considerably more efficient! As a result, it was concluded that, within the framework of the present method, there is no advantage to using either the extremely complicated (algebraically) turbulence kinetic energy equation or the (artificial) "lag" equation and the simple algebraic mixing length.

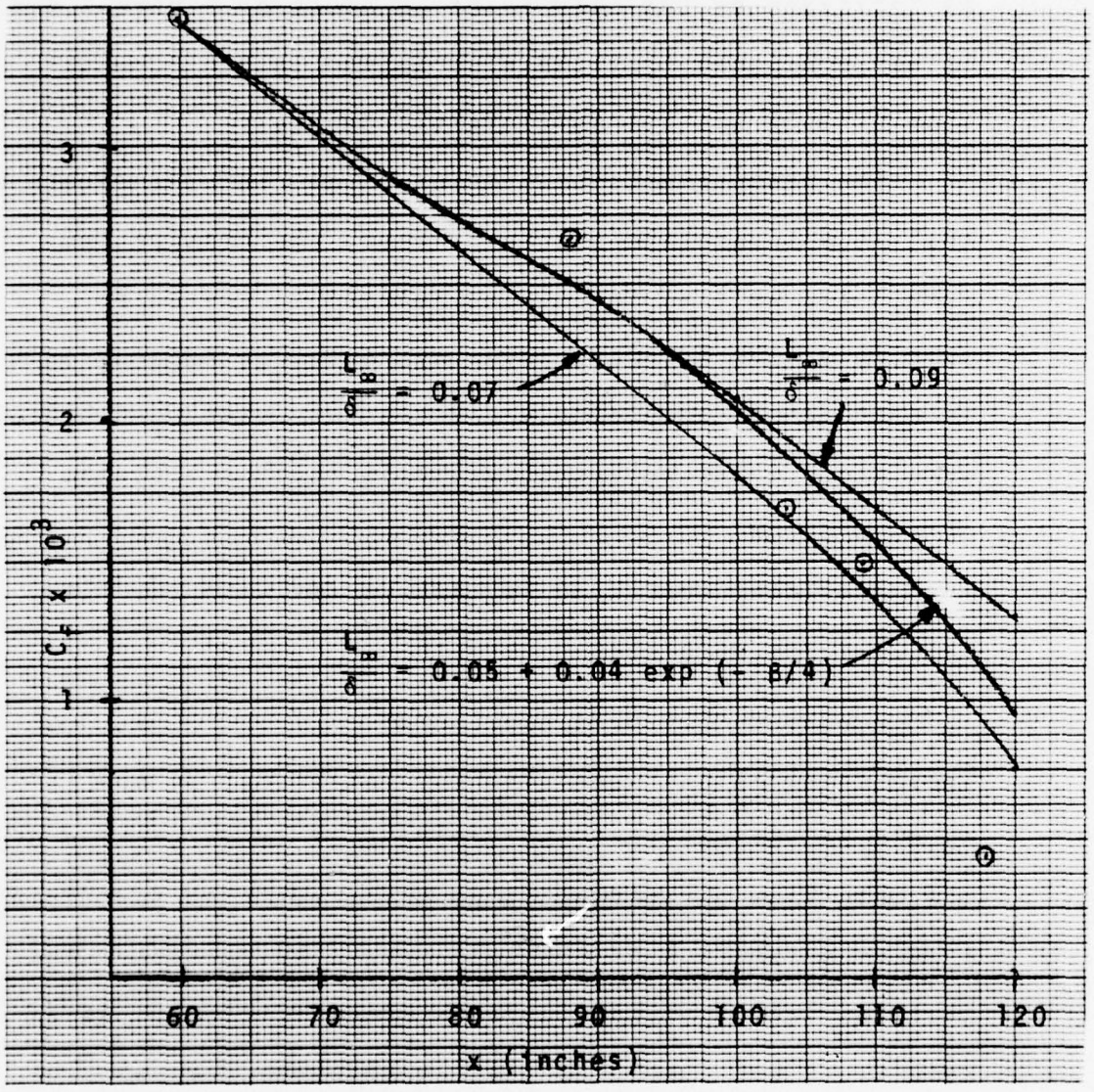

FIGURE 3.5 EFFECT OF USING VARIOUS "DISSIPATION LENGTH" FORMULATIONS IN THE TURBULENCE KINETIC ENERGY EQUATION ON C_f IN THE SIMPSON ET AL. FLOW

correlation embodied in Equations 3.24 - 3.26 was adopted as both simpler and more accurate.

3.4.2 Effects of Turbulent Normal Stresses

Since the work of Newman [28], it has been recognized that as a boundary layer approaches separation, the effects of the turbulent normal stresses ($\rho\underset{\sim}{u}^2$, $\rho\underset{\sim}{v}^2$) are not negligible. These stresses contribute the term

$$+ \frac{\partial}{\partial x} (\rho\underset{\sim}{v}^2 - \rho\underset{\sim}{u}^2)$$

to the right hand side of the partial differential momentum equation of the boundary layer (eqn. 2.2). In addition to their effect on the mean flow equations, Simpson and co-workers [21,27] found that the effects of normal stresses on turbulence production were significant. Collins and Simpson [27] subsequently presented a turbulence kinetic energy equation based turbulence model which accounted for the normal stress production; this is essentially the model of equations 3.30 - 3.32. The work involving the turbulence kinetic energy (integral) equation described herein thus took normal stress turbulence production into account.

Returning to normal stresses in the mean flow equations, it is necessary to model the above term in terms of the other flow parameters. Following Townsend [29], McDonald et al. [25,26] and Collins and Simpson, it is assumed that

$$\underline{\bar{u}}^2 \sim q^2 \quad \text{and} \quad \underline{\bar{v}}^2 \sim q^2$$

thus $\rho(\underline{v}^2-\underline{\bar{u}}^2) \sim \rho q^2 \sim |\tau_t|$

resulting in

$$\rho(\underline{\bar{v}}^2-\underline{\bar{u}}^2) = a_3|\tau_t| = a_3|\rho\varepsilon \frac{\partial u}{\partial y}| \tag{3.33}$$

A value of $a_3 = 2$ was selected in accord with previous workers [25-27].

Upon integrating the normal stress term across the boundary layer, the term

$$-a_3 \int_0^{\delta} \phi^m \xi^n \frac{\partial}{\partial x} |\bar{\tau}| d\xi$$

is added to the right-hand side of the momentum equation 3.2 ($m = n = 0$), moment of momentum equation 3.3 ($m = 0$, $n = 1$), and mechanical energy equation 3.4 ($m = 1$, $n = 0$). Substituting the assumed velocity profile and the mixing length turbulence model and expanding results in the addition of the following terms to the working Equations 3.9 - 3.11:

To the coefficient of $\frac{dM_e}{dx}$ is added:

$$a_3[\int_0^1 \phi^m \xi^n \frac{\partial|\bar{\tau}|}{\partial M_e} d\xi + (2-M_e^2) \frac{T_e}{T_o} \frac{1}{M_e} \int_0^1 \phi^m \xi^n |\bar{\tau}| d\xi]$$

To the coefficient of $\frac{d\lambda}{dx}$ is added:

$$a_3 \int_0^1 \phi^m \xi^n \frac{\partial|\bar{\tau}|}{\partial \lambda} d\xi$$

To the coefficient of $\frac{d\delta}{dx}$ is added:

$$a_3 \int_0^1 \phi^m \xi^n \frac{\partial |\overline{\tau}|}{\partial \delta} d\xi$$

and, to the coefficient of $\frac{du_\beta}{dx}$ is added:

$$a_3 \int_0^1 \phi^m \xi^n \frac{\partial |\overline{\tau}|}{\partial u_\beta} d\xi$$

Attention is directed to the required partial derivatives of the turbulent shear stress function $|\overline{\tau}|$. As in the turbulence kinetic equation, these are algebraic functions of considerable complexity, involving second derivatives of the velocity profile function with respect to the 4 parameters M_e, λ, δ, u_β.

Using the present method calculations were performed in which the effects of normal stresses in both the mean flow and turbulence kinetic equations were included. As regards the turbulence kinetic energy equation, the effects of normal stresses were not found to be significant (the effect of normal stresses are represented by the "F" defined in Equation 3.30, with $F \equiv 1$ when normal stress effects are neglected) and do not influence the conclusion of the previous section that use of the turbulence kinetic energy equation itself is not warranted. As regards the effect of normal stresses on the mean flow equations, calculations of C_f, δ, H for the entire Simpson et al. [21] flow, both with and without the

normal stress terms were carried out. No difference in predicted values of C_f, δ, H, Θ, and M_e were observed; hence, it was concluded that, within the present framework, normal stress terms do not greatly effect the accuracy of the method.

3.5 Mathematical Details of Solution Procedure

In terms of a closed system of equations, the boundary layer calculation problem is now completely formulated. Complete knowledge of the boundary layer flow is given in terms of the parameters Θ, M_e,* λ, δ, u_β as functions of x. Via the velocity profile specification of Section 3. and the turbulence model discussed in 3.4, Equations 3.8 - 3.12 become, ultimately, five first order, non-linear, ordinary differential equations with M_e, λ, δ, u_β, Θ as dependent variables and with x as the independent variable**. Now information from the inviscid outer flow must be input to the boundary layer method, thus either $M_e(x)$ or $\Theta(x)$ is regarded as a known function (the possibility of a mixed specification with M_e known for certain x's and Θ known for other x's is not precluded). To calculate the remaining 4 parameters, only 4 equations are needed,

---

* In incompressible flow, M_e is the ratio of the local edge velocity to a reference velocity.

** Using a differential equation turbulence model introduces an additional parameter, ℓ_∞/δ, and an additional differential equation.

accordingly either the moment of momentum equation (3.10) or the mechanical energy equation (3.11) is dropped. The ultimate selection of one of these over the other will be discussed shortly; the other critical question of whether M_e or Θ is taken as specified will be the subject of a later section.

The algebraic complexity of the velocity derivative integrands and the turbulent shear integrals, as well as the non-linearity of the resulting differential equations make a numerical solution the only possibility. The differential equations to be solved have the form

$$A_i \frac{dM_e}{dx} + B_i \frac{d\lambda}{dx} + C_i \frac{d\delta}{dx} + D_i \frac{du_\beta}{dx} = E_i$$

$$i = 1,4$$

The coefficients A, B, C, D, E are functions of M_e, λ, δ, u_β and involve several integrations, the coefficient E also contains Θ. The integrations in A, B, C, D can be preformed analytically if the flow is incompressible [30]; however, the shear stress integrals in E cannot and for compressible flow, neither can those in A, B, C, D. In the present method, all integrals were evaluated numerically. A large number of integrals had to be calculated (approximately 40 if the turbulence kinetic energy equation is to be solved, 30 if not), requiring a rapid, efficient integration method. Because of its higher accuracy for fewer points (that is fewer calculations of the integrand), Gaussian quadrature formulas

were selected for single integrals. The double integrals required for the moment of momentum equation were evaluated by using a 10 point Simpson's rule for the outer integral with a Gaussian quadrature for the inner integral. All integrals were evaluated in 10 strips from $\xi = 0$ to $\xi = 1$. Because of the more rapid variations near the wall, 6 point quadratures were used for $\xi \leq 0.1$, 4 point for $0.1 \leq \xi \leq 0.3$ and 2 point for $\xi > 0.3$.

Because of the appearance of the same terms in many of the integrands, a great computing time saving was realized by calculating integrals simultaneously rather than one at a time.

The complications involved in calculating double integrals would seem to indicate that the mechanical energy equation (3.11) should be preferred to the moment of momentum equation (3.10). Initial efforts were in fact concentrated on a method using the mechanical energy equation. Numerical experimentation showed that extremely small integration steps were necessary to obtain accuracy in the dissipation integral

$$\int_0^1 \frac{\tau}{\rho_e u_e^2} \frac{\partial \phi}{\partial \xi} \, d\xi$$

The integrand in this term is proportional to $(\partial\phi/\partial\xi)^3$ since

$$\tau \sim \left|\frac{\partial u}{\partial y}\right| \frac{\partial u}{\partial y}$$

and the rapid variation of $\partial\phi/\partial\xi$ near the wall requires extremely small steps of integration. For this reason, the moment of momentum equation was found to be superior to the mechanical energy equation and was adopted for the remainder of the study.

Initially, a fourth order Runge-Kutta method was selected for solving the differential equations; however, this was found to be very slow. A fourth order modified predictor - corrector scheme was then employed which has the ability to change step size to speed up calculations or increase accuracy. As expected, the predictor - corrector method required about half the computing time of the Runge-Kutta method.

In order to start the calculations, initial values of M_e, λ, δ, u_β must be known at some x location. When testing the program using experimental data, values of M_e, $\lambda(C_f)$, δ are usually available at a station upstream of the region of primary interest and calculations are started there. The value of u_β at the initial station is obtained from the "local friction law", equation 3.7 When making a complete calculation starting from a leading edge or front stagnation point, theoretically a laminar boundary layer calculation and transition analysis would be needed; however, in the present work it was assumed that transition occurred very close to the leading edge and the calculations were initialized by setting $\delta = 0$

at a leading edge and using turbulent flat plate boundary layer correlations to estimate δ and $\lambda(C_f)$ at the first point downstream of the leading edge.

3.6 Weak Interaction, Strong Interaction, and the Appearance of Singular Points

The coupling between the viscous and inviscid flow regions requires that either M_e or Θ, as calculated by the inviscid flow model, be specified as known input to the boundary layer model. Of course, in classical boundary layer theory, the edge velocity (M_e) is taken as the known input parameter. This is referred to as the weak interaction model because, to first order accuracy for these boundary layers, the presence of the boundary layer does not affect the pressure distribution. In this approach, the (small) effects of the boundary layer on the pressure distribution are accounted for by adding a "displacement thickness" to the body, effectively modifying the body shape. If the weak interaction approach is adopted, the continuity equation (3.8) can be subtracted from the momentum and moment of momentum equations (3.9, 3.10) thus removing Θ as a variable. After these modified equations, together with 3.12 are solved for λ, δ, and u_β, Θ can be calculated from the continuity equation (and δ^* can be calculated by integrating the velocity profile). That this approach to the calculation of all types of boundary layer flows, both attached

and separating, as desirable is due not only to the simplification resulting from the elimination of ⊖ from the system of equations but also to the fact that methods to calculate inviscid flows with body geometry specified are easier and considerably more plentiful than methods to calculate geometry (i.e. θ) with velocity (M_e) specified. Unfortunately, considerable research has demonstrated that the weak interaction formulation is inadequate for the calculation of separating boundary layers. [1-5,31-34] Typically, application of the weak interaction formulation yields one of two results:

(1) If a pressure distribution predicted from a completely inviscid analysis of the flow over a body is input, the weak interaction method typically breaks down as separation is approached, with numerical divergence occurring. Typically δ, δ^*, H, and ⊖ rapidly increase just before breakdown. The <u>occurrence</u> of separation can be predicted by such a method and its location roughly estimated, but no flow details in the vicinity of separation can be obtained and the effects of the boundary layer on the pressure distribution cannot be obtained.

(2) If an experimentally determined pressure distribution is input, calculations usually do not predict separation; instead the skin friction

levels off at some constant value near the measured separation location. Calculations by Cebeci et al. [32] for several incompressible flows and by Gerhart and Bober [33] for the compressible flow of Alber et al. [13] substantiate this conclusion. Application of the present method (in the weak interaction mode) to the incompressible separating flow of Simpson et al [21] produces similar results as shown in Figure 3.2. Cebeci et al. and Gerhart and Bober have indicated that it is possible to conclude that separation is in fact occurring and to estimate its location from such calculations, but obviously they are of no value for predicting details of the flow.

The first behavior is not a cause for major concern because in a separating flow the inviscid pressure distribution is significantly modified by the viscous-inviscid interaction so some calculation scheme which artificially smooths the pressure distribution for the first few cycles of iteration may possibly be devised. The second behavior is more decisive in its implications since it implies that even if the exact pressure distributions were somehow arrived at, the boundary layer flow could still not be accurately calculated!

The resolution of this dilemma has been presented by a number of researchers [1-5,34] and requires that calculations be made in the so called strong interaction mode in which the pressure is considered as an unknown in the boundary layer calculation with some other parameter being specified as input information. If the interaction formulation of the current method is followed (see equations 2.9, 2.10), the obvious variable to specify as input is the velocity angle at the edge of the boundary layer Θ. The flow angle has been used extensively for coupling in supersonic separated flow calculations [35-37] but has not been employed as extensively in incompressible/subsonic methods. In low speed flows, the displacement thickness has been used [3-5,38], as has the skin friction coefficient [2,3]. The reason for chosing one formulation over another is not so much that one is more appropriate from a physical viewpoint but that some formulations may be more easily coupled to inviscid flow methods than others. In this regard, there is no way that initial guesses of $C_f(x)$ can be iteratively updated by solving for the flow <u>external</u> to the boundary layer; however, guesses of $\delta^*(x)$ or $\Theta(x)$, which lead to a $M_e(x)$ calculated from the boundary layer equations, can be updated by applying the calculated $M_e(x)$ as a boundary condition in an inviscid flow analysis (the "inverse" or "design" problem of inviscid flow theory). As to the choice between δ^* or Θ as the strong interaction variable, it is here pointed

out that, formally, it is the slope of the velocity vector on the surface that is computed by an inverse inviscid flow method, with the corresponding "body surface" i.e. body plus displacement thickness, determined by integrating the surface slopes. In addition, Θ naturally appears as a variable in the integral boundary layer method, δ^* would have to be introduced artificially. * For these reasons, it was decided to employ Θ as the interaction parameter in the strong interaction mode in the present work. Therefore, in the strong interaction mode, $\Theta(x)$ is presumed known and the continuity, momentum, moment of momentum, and skin friction equations 3.8 - 3.10, 3.12 are regarded as 4 equations for calculating the 4 variables M_e, λ, δ, u_β.

Initially, it was proposed to calculate the entire boundary layer flow, attached, separating, fully separated, reattaching, and redeveloping, using the strong interaction formulation. This was ultimately rejected, it being

---

* This is most easily accomplished by putting the boundary layer integral equations in weak interaction form to eliminate Θ and introducing the definition $\delta^* = \delta\int_0^1(1 - \frac{\rho u}{\rho_e u_e}\, dy = \delta^*(M_e,\lambda,\delta,u_\beta) = \delta^*(x)$ as an extra equation, which may be retained in its algebraic form or converted to a differential equation [3].

found that the strong interaction equations are ill conditioned in regions where the boundary layer is non-separated. It is therefore necessary to calculate the boundary layer flow using a combination of weak and strong interaction formulations. With reference to Figure 3.6, calculations are initially begun in the weak interaction mode, near a leading edge or at some point well upstream of separation. Calculations are marched downstream in the weak interaction mode, until at some point it becomes necessary to switch to the strong interaction mode as separation is approached. Calculations are carried through separation to fully separated flow in the strong interaction mode. In flows exhibiting large separated regions, in which the flow essentially develops as a free shear layer, it may be necessary to switch back to the weak interaction mode to make calculations in the free shear layer. If and when the separated boundary layer reattaches, it once again becomes necessary to employ the strong interaction formulation to calculate through the reattachment. At some point downstream of reattachment, the weak interaction formulation may again be used.

The obvious question that arises is when to switch from one mode of calculation to the other. In practice there are two criteria used:

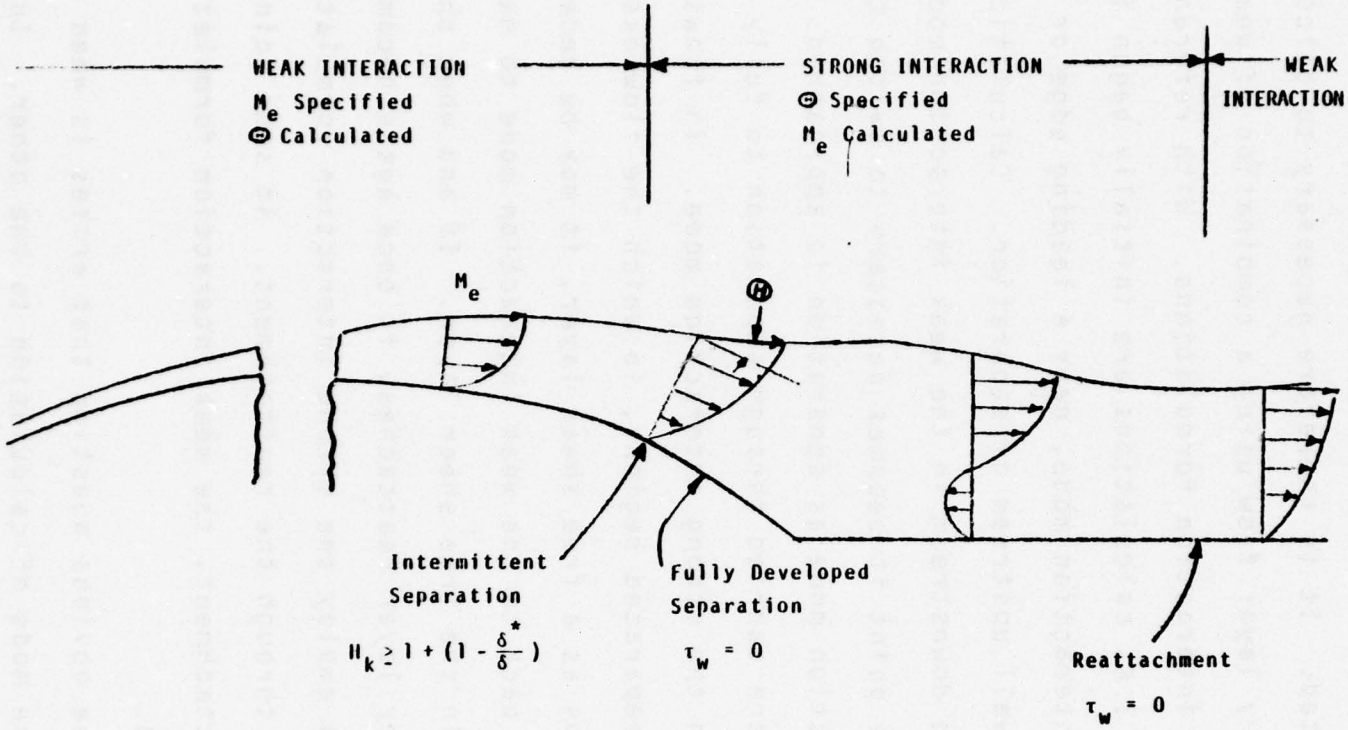

FIGURE 3.6 TYPICAL DEVELOPING AND SEPARATING BOUNDARY LAYER FLOW SHOWING WEAK AND STRONG INTERACTION REGIONS

(1) When separation or reattachment is approached calculations must be switched to the strong interaction mode; when reattachment is "complete" calculations must be switched to the weak interaction mode.

(2) When singular points (the set of equations being used becomes indeterminant) are approached, it is necessary to switch to the opposite formulation to continue calculations.

From previous discussion of the behavior of the weak interaction equations, it is obvious that this formulation must be abandoned before (fully developed) separation. The nearest to separation that these equations might possibly be extended is the point of intermittent separation, discussed by Sandborn and Kline [39]. This criterion indicates that intermittent separation begins at the point where

$$H_k \geq 1 + \left(1 - \frac{\delta_k^*}{\delta}\right)^{-1}$$

This is typically satisfied if H_k is approximately 2.4. It was found that better accuracy could be obtained by switching even before this criteria is satisfied; therefore, the current method used two criteria to indicate the approach to separation and the need to switch from the weak interaction to the strong interaction. These criteria are

$$H_k \geq 2.0$$
$$\text{or} \qquad (3.34)$$
$$\Theta \geq .5$$

The former criteria tends to dominate if experimentally determined inputs ($M_e(x)$) as specified and hence presumably in the later stages of iteration, while the latter tends to dominate if ideal flow pressure distributors are used (i.e. in the early stages of iteration). In flows redeveloping following reattachment, calculations are switched from the strong back to the weak interaction mode if

$$H_k \leq 2.2$$
$$\text{and} \qquad (3.35)$$
$$\frac{dC_f}{dx} > 0$$

The occurance of singularities in the boundary layer equation is a well known fact the stagnation point and separation singularities being two well known examples. Integral boundary layer calculation methods seem to be especially prone to exhibit singularities, especially in the vicinity of separation and reattachment. Singularities may be divided into two types, those which are connected with significant physical occurrences in the flow itself and those which are not necessarily connected with physical occurrences but are rather attributable to mathematical anomalies in the particular calculation method chosen. An example of the former type of singularity is the well known Crocco-Lees [31,35-37]

critical point which appears in supersonic separated and reattaching flow analyses and has been shown to be analogus to the critical point occurring in the throat of a subsonic-supersonic nozzle. Examples of the latter type are the "velocity profile critical points" discussed by Shammroth and McDonald [40-41] and further by Gerhart [34]. The latter type of critical point is identified with the failure of a finite set of integral equations coupled with a particular velocity profile function to produce a completely independent set of equations at all times. Calculation difficulties associated with the latter type of singularity can be overcome by using an over-constrained set of equations [40,41] or by switching from the weak to strong interaction formulation or vice versa [34]. It is important that these latter types of singularities not be assigned physical significance and it is questionable if smooth passage through such singular points should be made a criterion for arbitrary adjustment of flow parameters (see Shammroth and McDonald's [40,41] discussion of the work of Green [42], and also Tai [43,44]).

In the current work, both types on singularity were encountered. As pointed out by Kuhn and Nielsen [3], if the wall-wake velocity profile (equation 3.5) is assumed, the coefficients of $d\lambda/dx$ in all of the differential equations (3.8 - 3.12) vanish when $\lambda = C_f = 0$,

which becomes a singularity in either the weak or strong interaction formulations. This behavior may be identified with the separation point singularity and has some physical implications. Examination of the wall-wake velocity profile function shows that all influence of the (zero) skin friction disappears. Downstream of the point of zero skin friction, the boundary layer may develop as a recirculating flow above a solid surface, in which case the skin friction attains negative values or as a wake type flow in which the skin friction remains zero; therefore, "critical" point behavior is not inconsistent.

Whatever its cause, if a singularity occurs in the calculations, a method must be devised to calculate through it or jump over it. Kuhn and Nielsen [3] indicate that the singularity can be removed from their formulation which uses δ^* rather than Θ as the strong interaction parameter*. They show that the ratios of coefficients of $d\lambda/dx$ in their differential equation set are finite so that, by dividing the momentum and moment of momentum by the differentiated displacement thickness definition, two independent differential equations are recovered. These are solved together with a prescribed $\delta^*(x)$ and the δ^* definition. Of course, using

---

* Since it occurs where $C_f = 0$ (fully developed separation), this singularity must always be dealt with in the strong interaction formulation.

the δ^* definition twice does not introduce any new information, it simply represents an artificial way of removing a computational difficulty. Kuhn himself states that the method is essentially equivalent to prescribing $\lambda(x)$ as the interaction parameter as in his previous work [2]. Had it been deemed necessary, a similar development could have been undertaken in the present work, however extensive calculations revealed that the singularity associated with the vanishing of λ is very weak. A singularity is of course associated with the vanishing of the determinant of the matrix of the coefficients of the derivative dM_e/dx, $d\lambda/dx$, $d\delta/dx$, du_β/dx of equations 3.8 - 3.12. The predictor-corrector method used for the solution of the differential equations is sensitive to the approaching of a singularity, with the marching step size being automatically reduced as the determinant decreases. Calculations have shown that the skin friction parameter λ, can be reduced to a value of $\pm$ .0000005 without any notable effect on the calculations.* The determinant thus behaves as shown in Figure 3.7, with no zero crossing by the determinant. Since this singularity is so hard to detect, it is extremely unlikely that it would ever effect the calculations significantly. In

---

* The existance of the singularity was nominally verified by setting $\lambda = 0.0$, in the computer program

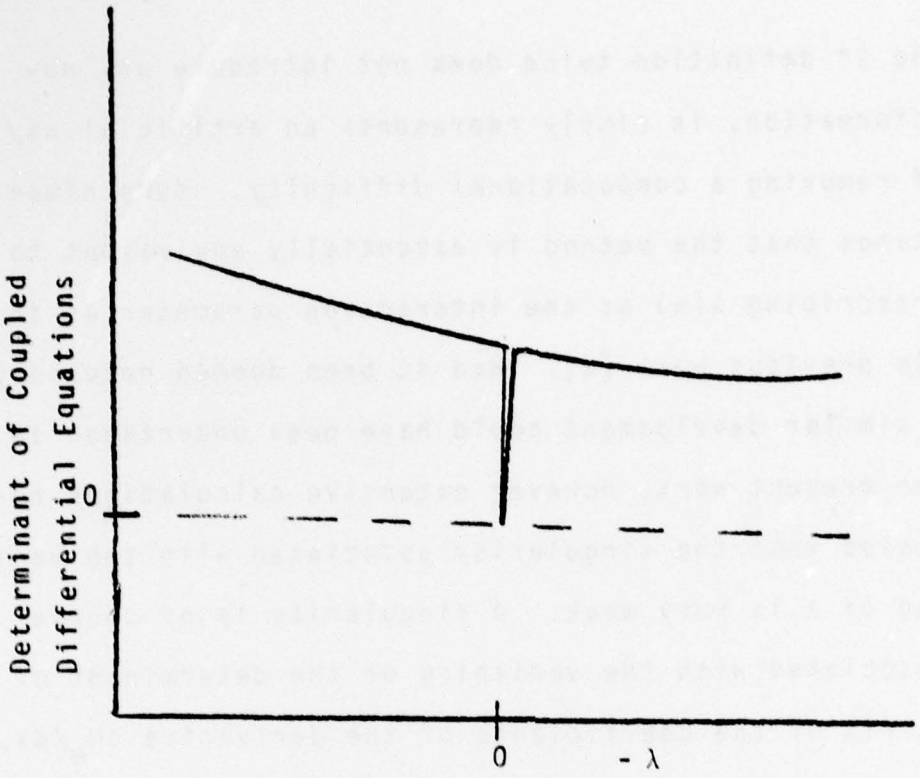

FIGURE 3.7 SINGULARITY ASSOCIATED WITH VANISHING SKIN FRICTION

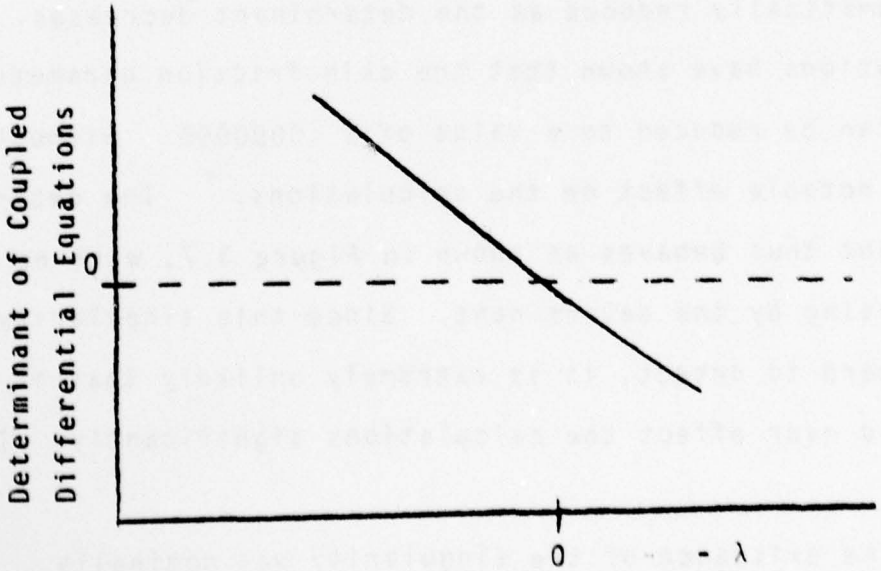

FIGURE 3.8 NON-PHYSICALLY SIGNIFICANT "VELOCITY PROFILE CRITICAL POINT [40]" SINGULARITY

order to account for the possibility of its occurrence, it was decided that if this singularity does occur, the values of the derivatives from the last upstream station are used, thus the variables are linearly extrapolated through the singularity.

Singularities of the "non significant" type also occur in the current method. Typically these singularities are not associated with either a row or column of the differential equation matrix vanishing but simply the appearance of a zero determinant. Singularities of this type involve a "zero crossing" determinant as shown in Figure 3.8. In such a case, the approaching singularity is detected by the differential equation solver, with the result that calculations usually breakdown before the singular point is reached. Numerical experimentation has revealed the following about these types of singularities:

(1) They are more prone to occur in compressible flow calculations, becoming stronger and more plentiful as the Mach number is increased,

(2) The singularities only occur for λ negative or very small positive (i.e. near fully developed separation),

(3) Although these singularities occur in both the weak and strong interaction formulations,

they do not occur simultaneously (e.g. at the same values of M_e, Θ, λ, δ, u_β) in both formulations.

The latter fact provides the key to avoiding these singularities; all that is necessary is to switch from weak to strong interaction calculations (or vice versa) as a singularity is approached. This behavior and remedy were discussed by Gerhart [34] although he apparently had not uncovered the entire picture.

During the course of the calculations, the determinant of the matrix of the differential equations is monitored. If the ratio of the current value to a reference value is less than 0.2, it is assumed that a "zero crossing" or singularity is eminent and the calculation is switched from weak to strong interaction or vice versa. For positive values of λ, the reference determinant is the value at the last point where $C_f \geq .0015$, for negative values of λ, it is the initial value of the determinant at the last mode switch. In practice, the choice of the weak or strong interaction mode is usually dictated by the criterion of equations 3.34 and 3.35, with singularity appearance dictating the switch from strong to weak interaction only in the regions of reverse flow (after separation, during free shear layer development).

At this point, a further discussion of the method of solving the differential equations of the viscous layer is in order.

These equations have the form

$$A_{1i} \frac{dM_e}{dx} + A_{2i} \frac{d\lambda}{dx} + A_{3i} \frac{d\delta}{dx} + A_{4i} \frac{du_\beta}{dx} = B_i$$

$$i = 1,4$$

In the strong interaction formulation, M_e is an unknown and there are 4 differential equations to solve; in the weak interaction formulation, M_e is known and since Θ does not appear in a derivative, it can be eliminated with the result that only 3 differential equations remain. The predictor-corrector method employed for the solution of the differential equations requires knowledge of the derivatives of 4 previous points to march the solution forward; therefore, it must be started by a Runge-Kutta method, which turns out to be a rather time consuming and sensitive process. Now if in switching from weak to strong interaction, we add an extra differential equation to the set, it is obvious that the calculations must be restarted. In order to avoid this, both weak and strong interaction calculations are arranged to solve 4 differential equations; when making weak interaction calculations, the continuity equation ($i = 1$ above) is subtracted from the momentum and momentum equations ($i = 2,3$) and discarded. It is replaced by the equation

$$\frac{dM_e}{dx} = \frac{d}{dx}\,(M_e(x)) \quad \text{[a given function]}$$

Thus $A_{1,1} = 1$, $A_{1,2} = A_{1,3} = A_{1,4} = 0$, B_1 = known function of x. At each station, after a solution has been obtained, the criteria for switching modes are all checked, a decision as to whether to advance the calculations via the weak interaction or strong interaction formulation is made, and the differential equations are set up accordingly.

3.7 Verification of the Boundary Layer Method

Since exact solutions are lacking, the ultimate test of any (separating) turbulent flow calculation procedure is confrontation with experimental data. Since, for attached flows, in the weak interaction mode, the current method is quite similar to several of those presented at the Stanford Conference [19,23,25], it might be expected to perform in roughly the same manner; preliminary calculations verified this.

In order to verify the ability of the method to make calculations of separating boundary layers, it was necessary to calculate such flows. The flows to be calculated should meet the following criteria

(A) Both incompressible and subsonic (or transonic) flows should be considered,

(B) Extensive details of the measured flow are needed, especially including both pressure (M_e) and edge angle (Θ) distributors, as well as C_f and δ information,

(C) Both two-dimensional and axisymmetric geometries are desirable,

(D) Both separation and reattachment of the experimental flow are desirable,

(E) Separation must be caused by adverse pressure gradients, not by sudden geometry changes such as back steps.

Few experimental flows following satisfying all of these criteria were found; however, two excellent test cases were found.

Simpson et al. [21] have made exhaustive measurements in an incompressible, two dimensional separating boundary layer. Then experimental results include both velocity and edge angle distributions, boundary layer thicknesses, form factors, skin friction coefficients, and details of the turbulence structure. In fact the only thing which keeps this flow from being a complete incompressible test case is the fact that the flow does not reattach.

Alber et al. [13] have presented measurements made in a two-dimensional transonic separating boundary layer

flow.* They present information on pressure distribution, boundary layer thicknesses, form factors and skin friction coefficient. Although edge angles were not presented in the paper, they could be estimated from given δ, δ^*, M_e data via:

$$\tan \Theta = \frac{d\delta^*}{dx} + (M_e^2-1)(\delta-\delta^*) \frac{T_e}{T_o} \frac{1}{M_e} \frac{dM_e}{dx} \qquad (3.36)$$

This flow also included reattachment.

The two flows mentioned satisfy all of the desirable criteria except for axisymmetric geometries. Putnam and Abeyounis [45] surveyed the flow field in the vicinity of a boattailed axisymmetric afterbody and presented Mach numbers and flow angles; however, no boundary layer details were obtained and the published figures giving M and "Θ" were too small to be useful. Attempts to obtain larger scale figures were unsuccessful.

Using the method developed in Sections 3.1 - 3.5, the Simpson and Alber flows were calculated. The results are shown in Figures 3.9 - 3.16. The calculations were started by matching M_e, δ, λ at the furthermost upstream point shown. In both cases, the entire experimentally determined $M_e(x)$ and $\Theta(x)$ distributions were made available so that the parameter required by the choice of interaction mode was always available. The normal stress terms as formulated

---

* I. E. Alber has been kind enough to send the authors extensive details of the experimental data.

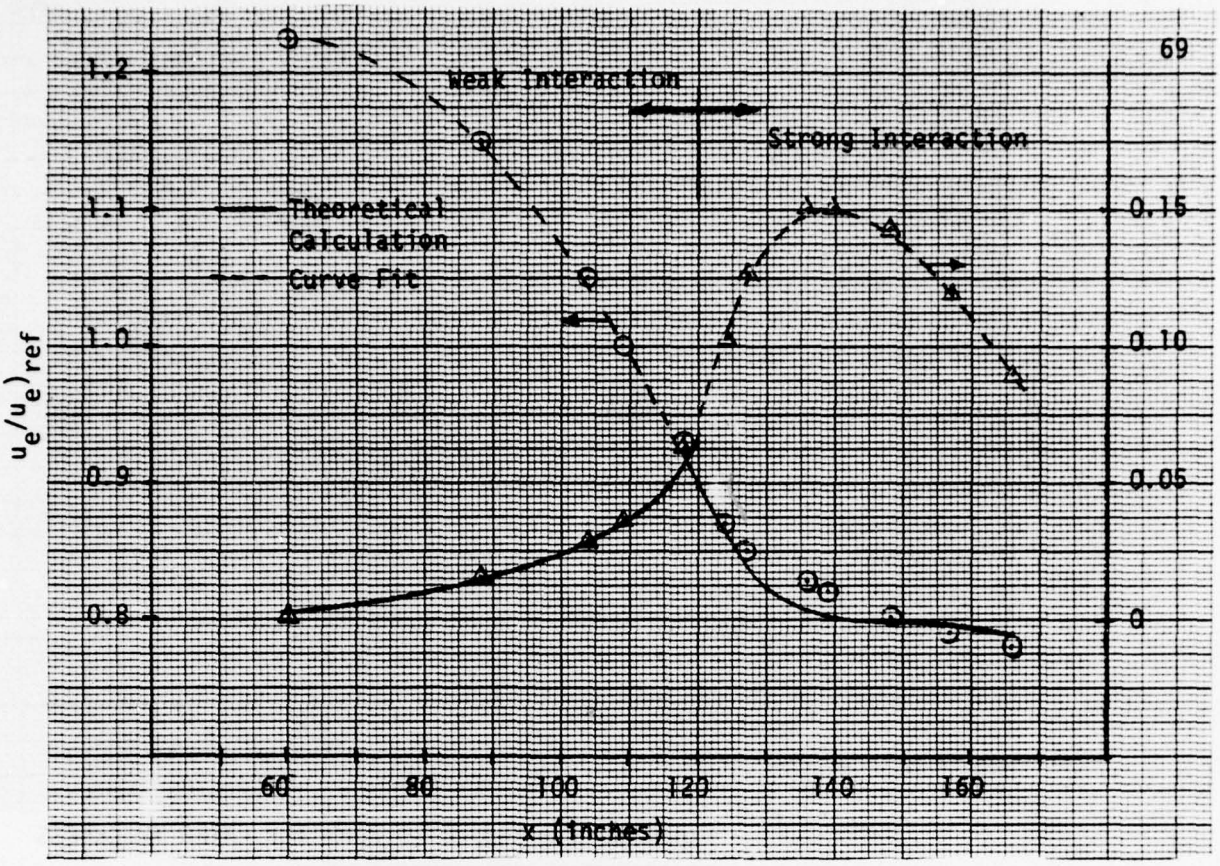

FIGURE 3.9 MEASURED AND PREDICTED VELOCITY AND EDGE ANGLE DISTRIBUTIONS FOR SIMPSON ET AL. FLOW

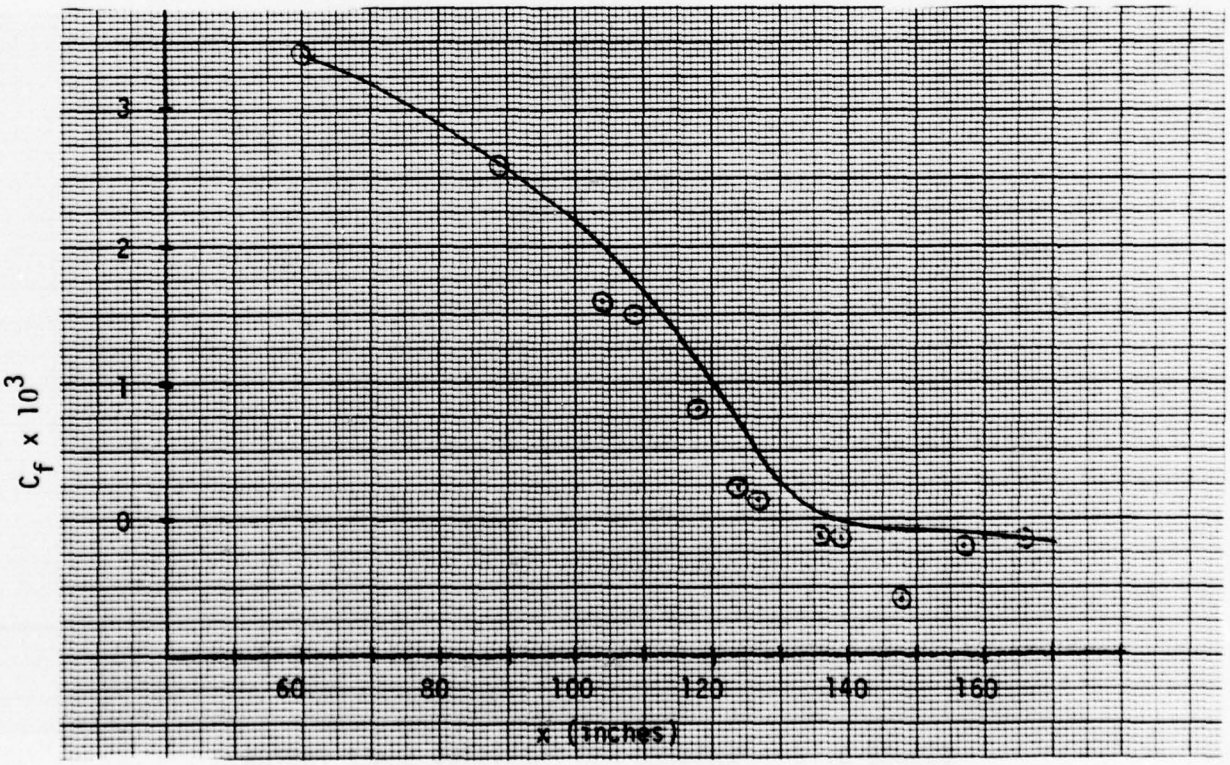

FIGURE 3.10 MEASURED AND PREDICTED SKIN FRICTION COEFFICIENT DISTRIBUTION FOR SIMPSON ET AL. FLOW

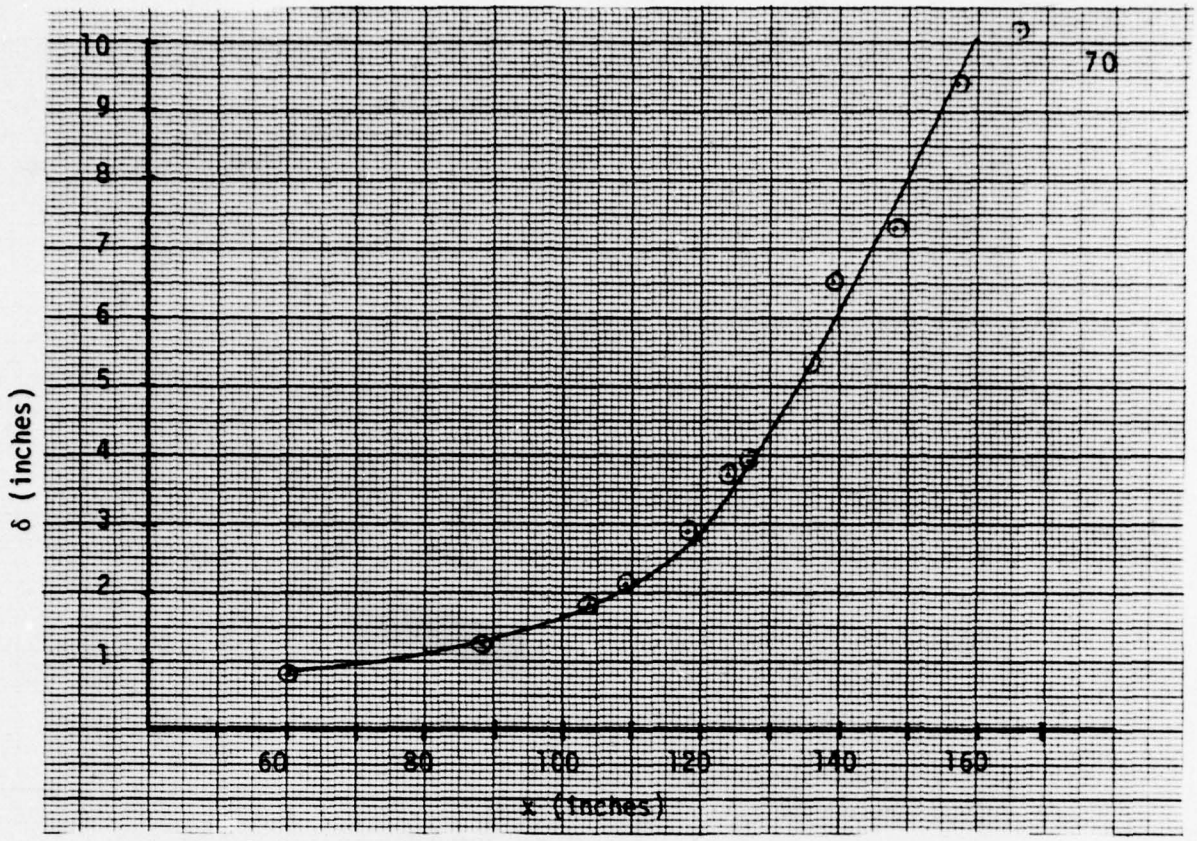

FIGURE 3.11 MEASURED AND PREDICTED BOUNDARY LAYER THICKNESS DISTRIBUTION FOR SIMPSON ET AL. FLOW

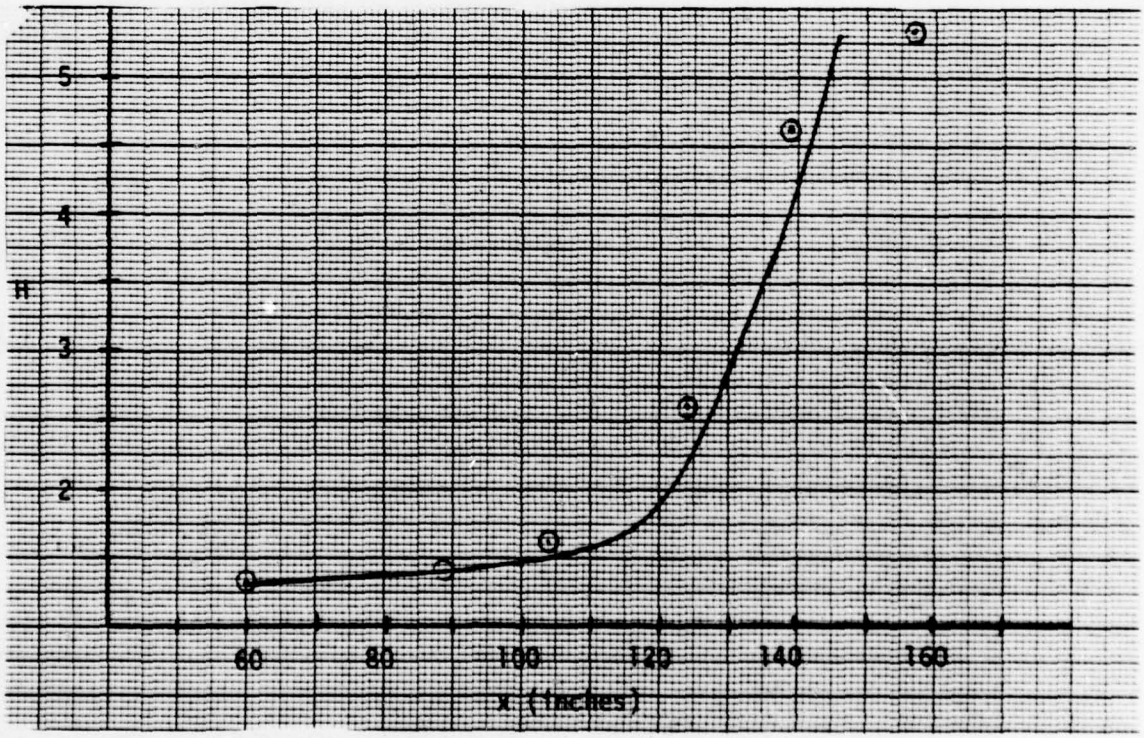

FIGURE 3.12 MEASURED AND PREDICTED SHAPE FACTOR DISTRIBUTION FOR SIMPSON ET AL. FLOW

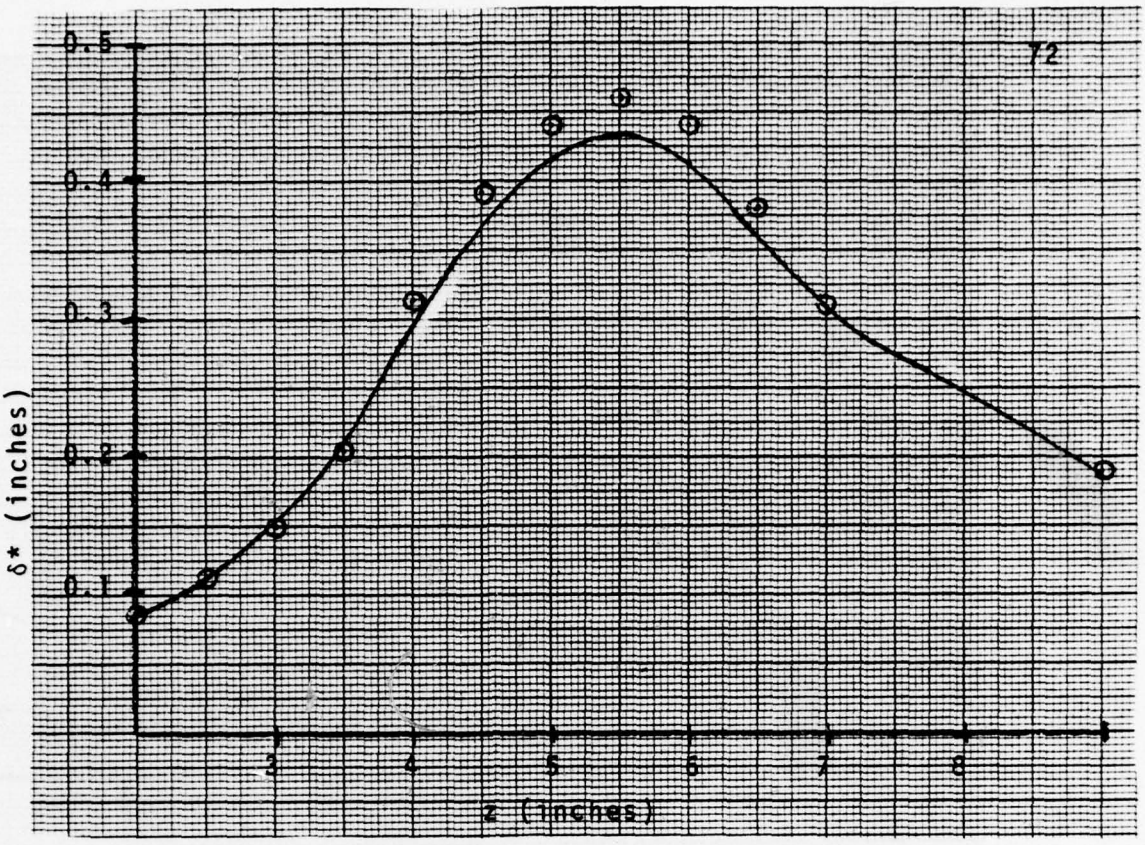

FIGURE 3.15 MEASURED AND PREDICTED BOUNDARY LAYER DISPLACEMENT THICKNESS DISTRIBUTION FOR THE ALBER ET AL. FLOW

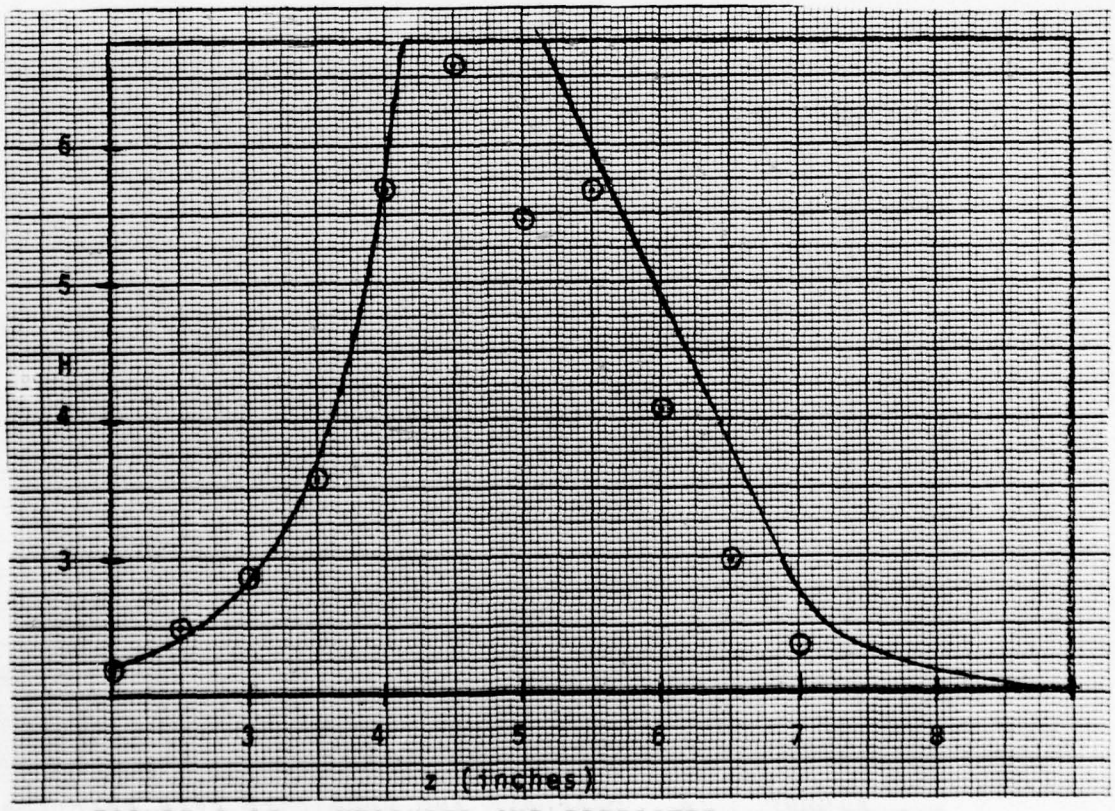

FIGURE 3.16 MEASURED AND PREDICTED SHAPE FACTOR DISTRIBUTION FOR THE ALBER ET AL. FLOW

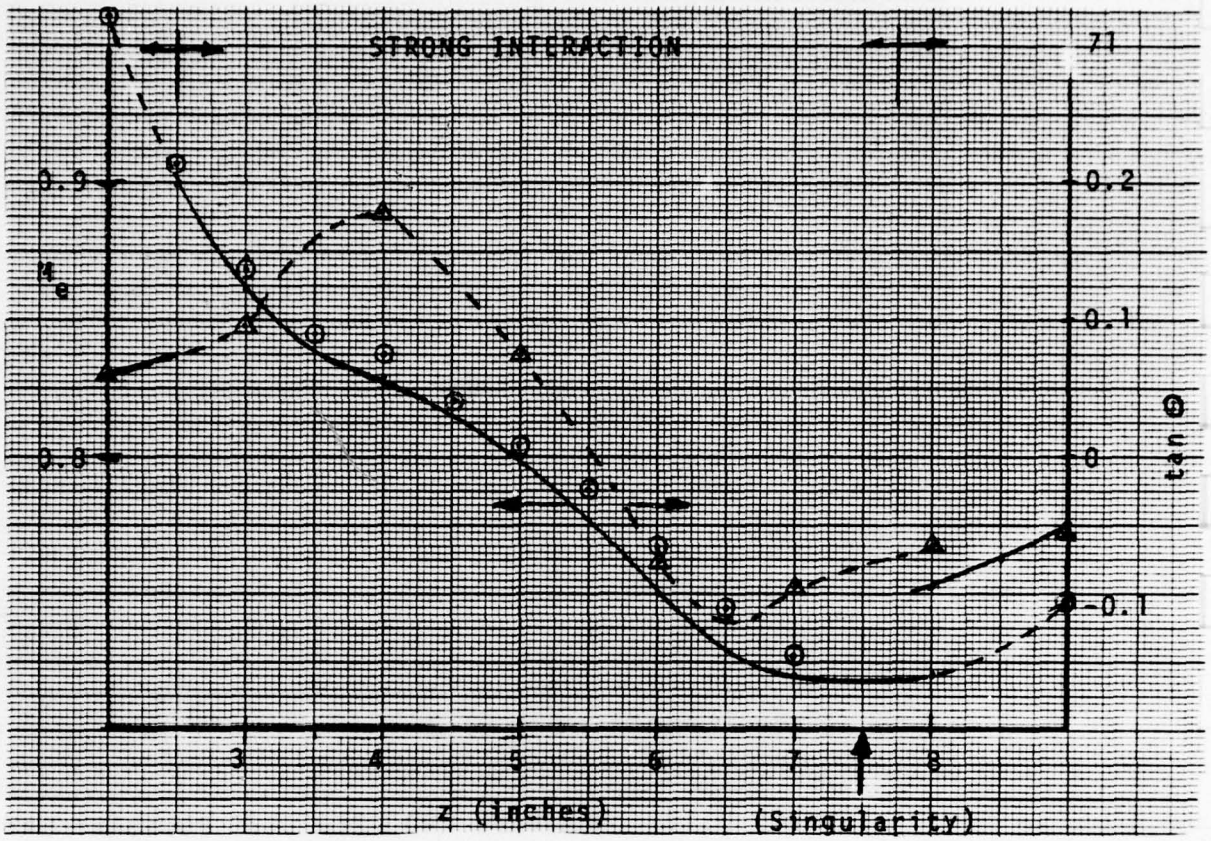

FIGURE 3.13 MEASURED AND PREDICTED MACH NUMBER AND EDGE ANGLE DISTRIBUTIONS FOR THE ALBER ET AL. FLOW

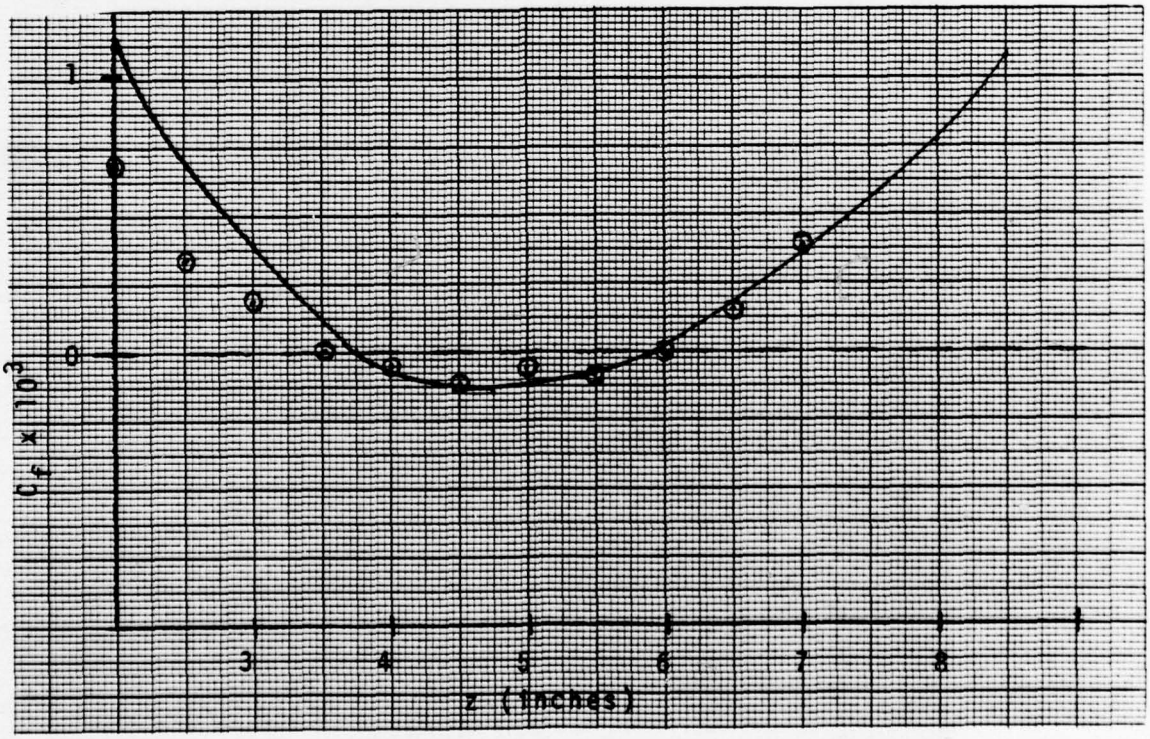

FIGURE 3.14 MEASURED AND PREDICTED SKIN FRICTION COEFFICIENT DISTRIBUTION FOR THE ALBER ET AL. FLOW

in equation 3.33 ff were included in both cases and the algebraic turbulence model of equations 3.24 - 3.26 was employed. * Although the calculations do not show perfect agreement the following are believed to be significant accomplishments.

(1) The agreement is reasonable,

(2) Both compressible and incompressible flows are predicted by a single method,

(3) Separation, reverse flow, negative shear, and reattachment are all evident and, given the difficulty of even measuring negative shear, are considered rather accurate,

(4) The pressure (M_e) distribution is calculated reasonably well by the strong interaction method.

Based on the results of these trial calculations and in comparison with the experience of other investigators in calculating these flows [27,33], it was concluded that the integral method developed herein is sufficiently accurate to be used as part of an a priori separated flow prediction procedure.

---

* It should be pointed out that slightly better calculations could be obtained by adjusting the constants in equation 3.24 for each flow. These "constants" might be a function of Mach number but information is insufficient to pursue this point further.

4. Inviscid Flow Calculation Procedure

The boundary layer method described in the previous chapter represents only half (or less!) of the entire calculation procedure for a priori prediction of separating boundary layer flows. In this section, results of efforts aimed at finding solutions to the inviscid "half" of the flow will be described.

Methods for calculating the inviscid (compressible or incompressible) flow over arbitrary prescribed plane two-dimensional and/or axisymmetric bodies are quite plentiful and need not be described here. These methods basically solve the partial differential equations 2.4 and 2.5, subject to the boundary conditions of 2.7, 2.8 and 2.10. The boundary conditions of 2.10 is applied at the surface of the body in question, it being assumed that the boundary layer is nonexistent, in which case Θ is zero; that is the slope of the velocity vector is required to be equal to the body slope. This constitutes the so called "direct" or "analysis" problem of inviscid flow theory.

A few authors have presented methods for calculating the body which will yield an arbitrarily prescribed pressure distribution over its surface [46-48]. Such methods formally solve equations 2.4 and 2.5 subject to the boundary conditions of 2.7, 2.8 and 2.9 (again, typically $\delta = 0$ so the boundary condition is applied at the body surface). In this method,

it is actually the slope of the body surface which is computed, with the geometry being determined by an integration of the surface slope. This constitutes the "inverse" or "design" problem of inviscid flow theory.

An inviscid flow method satisfactory for coupling with the separating boundary layer method of Chapter 3 must combine elements of both the direct and inverse problems. We have seen that, at most stations along the flow surface, only one formulation, weak or strong, of the boundary layer equations will apply. Now the weak interaction formulation requires that M_e be specified from outside information (e.g. the inviscid flow procedure) and computes an updated velocity slope Θ, for handing to the inviscid flow procedure; on the other hand the strong interaction formulation requires that Θ be specified and calculates an M_e which is handed to the inviscid flow procedure. It is therefore obvious that the inviscid flow procedure must be capable of accepting mixed boundary conditions, with direct type (θ specified) conditions at some points and inverse type (M_e specified) conditions at other points and that which points are of which type are predetermined by the boundary layer calculations. Two other complications arise. First, because the boundary layer may change from iteration to iteration, the type of boundary condition to be applied at a particular point may change from iteration to iteration. Second, the boundary conditions are not applied on a "solid surface" which is both impermeable and fixed from iteration to iteration but instead on a surface *

---

* Hereafter called the "δ surface"

representing the edge of the boundary layer (the surface $y = \delta(x)$, $r = R + \delta(x) \cos \alpha(x)$) which is neither impermeable (not a significant problem) nor fixed from iteration to iteration (a significant problem).

It should not be surprising that no currently available inviscid flow procedure incorporating all of these requirements was found; therefore, it was necessary to attempt to develop a satisfactory procedure. In the research efforts described herein, 3 different methods were investigated. These were

(1) The method of integral relations

(2) The surface singularity method

(3) The finite element method

The formulations for the methods of integral relations and finite elements were done for either plane two-dimensional or axisymmetric bodies. The formulation of the surface source method was for axisymmetric geometries only.

Each of these methods will be the subject of a separate section.

4.1 The Method of Integral Relations

The method of integral relations was the method initially investigated for the solution of the external compressible flow problem. As the method is conceptually and numerically similar to integral boundary layer methods, it appeared to have certain advantages over more conventional inviscid flow methods for the interaction problem.

Briefly, the method involves integration of the system of flow equations in the transverse direction. To perform this integration, the transverse variation of the integrands must be known. A general approach is to approximate this variation with polynomials. The result is that the original elliptic partial differential equations of the flow are reduced to a parabolic two-point boundary value problem that may be solved numerically using a standard Runge-Kutta or predictor-corrector subroutine, also needed for the viscous flow problem.

It was hoped that reduction of the problem to ordinary differential equations would result in solution scheme that was consistent with the integral boundary layer method, able to handle arbitrary flow geometries, and still be simpler and faster than finite difference methods.

Experience with the method of integral relations eventually demonstrated that any advantages gained by reduction of the problem to ordinary differential equations were outweighed by the algebraic complexity of the resulting system. The equations were difficult to derive and program, and ran slowly. Furthermore, the iteration schemes required to handle the two-point boundary valve problems were physically unrealistic. For this and other reasons detailed in the following,

research on the method of integral relations was discontinued in favor of the finite element method.

4.1.1 Literature Review

A. A. Dorodnicyn first introduced the method of integral relations in 1959 for mixed elliptic-hyperbolic aerodynamic problems [49]. He and his colleagues solved subsonic flow over ellipses and ellipsoids, transonic flow over an ellipse, and supersonic flow over a cylinder, although his paper presents few details. Holt of the University of California at Berkeley used the method to solve the transonic flow over a cylinder [50]. Melnik and Ives of Grumman Aerospace solved compressible flows over a cylinder, an ellipse, and simple non-lifting airfoil sections using the method of integral relations [51].

T. C. Tai of the Naval Ship Research and Development Center has used the method for more practical problems. He reports considerable success using the method to solve the supercritical flow over symmetric airfoils [5]] and lifting airfoils [53], and matched to laminar and turbulent boundary layer computations [43-44]. Tai's work is impressive, but a typical airfoil problem takes considerable computer time and requires interactive graphics capabilities [54].

4.1.2 Formulation

The basic equations for an inviscid compressible fluid in Cartesian or cylindrical coordinates can all be written in divergence form as follows:

Continuity

$$\frac{\partial}{\partial z}(\rho v_z) + \frac{\partial}{\partial r}(\rho v_r) + j\frac{\rho v_r}{r} = 0$$

z-momentum

$$\frac{\partial}{\partial z}(KP + \rho v_z^2) + \frac{\partial}{\partial r}(\rho v_z v_r) + j\rho\frac{v_z v_r}{r} = 0$$

r-momentum

$$\frac{\partial}{\partial z}(\rho v_z v_r) + \frac{\partial}{\partial r}(KP + \rho v_r^2) + j\frac{\rho v_r^2}{r} = 0$$

$$K = 1/\gamma M_\infty^2 = \text{constant}$$

All velocities are non-dimensionalized by V_∞, lengths by some typical length (usually the body length), and pressure and density by their free-stream values.

Further, density may be related to the velocity field by the energy equation, and pressure may be related to density by the isentropic relation. For incompressible flow, $\rho = 1$, and pressure is related to velocity by the Bernoulli equation.

Finally, the boundary conditions are as follows: At a solid surface, the normal velocity is zero. At

"infinity", the flow is undisturbed, i.e. $v_z = \rho = P = 1$, $v_r = 0$.

4.1.3 Development of the Method of Integral Relations Equations

To apply the method of integral relations, the flow equations must be written in divergence form:

$$\frac{\partial}{\partial z} A(z,r,v_z\ldots) + \frac{\partial}{\partial r} B(z,r,v_z\ldots) = R(z,r,v_z\ldots)$$

Like an integral boundary layer method, the method of integral relations relies on integration of the flow equations in the r direction, reducing the partial differential equations to ordinary ones with independent variable z. To do so, the r-variation of the integrands must be known. If the flow field is divided into strips bounded by typical streamlines, the integrands may be approximated by polynomials of the form:

$$A \simeq \sum_{i=0}^{N} a_i (r-r_o)^i \quad , \quad R \simeq \sum_{i=0}^{N} b_i (r-r_o)^i$$

where N is the number of strips and a_i and b_i are constants evaluated on strip boundaries.

After tedious integration and rearrangement, the equations can be reduced to the forms:

$$\frac{dv_{zo}}{dz} = f_o(v_{zn}, v_{rn}) \frac{dA_n}{dz}, \frac{dr_n}{dz} \ldots)$$

$$v_{ro} = v_{zo} \frac{dr_o}{dz}$$

$$\frac{dv_{zn}}{dz} = f_n \left(v_{zn}, v_{rn}, \frac{dAn-1}{dz}, \frac{dr_n}{dz} \ldots\right)$$

$$\frac{dv_{rn}}{dz} = g_n \left(v_{zn}, v_{rn}, \frac{dAn-1}{dz}, \frac{dr_n}{dz} \ldots\right)$$

where the subscript $()_o$ refers to the stagnation streamline, and the subscript $()_n$ is the number of a strip boundary as shown in Figure 4.1. The full equations for two-dimensional flow may be found in [53]].

It is unreasonable to expect to approximate all flow quantities from r_o to r_∞ with a simple polynomial. Instead, the flow domain is treated as a series of effective strips, using a second-order polynomial approximation across each pair of strips, as shown in Figure 4.1. Given a pair of strips bounded by r_o, r_{n-1}, and r_n, the flow equations can be integrated along r_{n-1} if the flow properties are known at r_n. Thus, the solution can be found along r_1 given properties on r_2. Similarly, the solution can be found along r_2 given properties on r_3, and so on until the free stream boundary is reached where the flow properties are known. The integration of all sets of equations is carried out simultaneously at successive z-stations. Strips may be added at any point in the flow to increase accuracy.

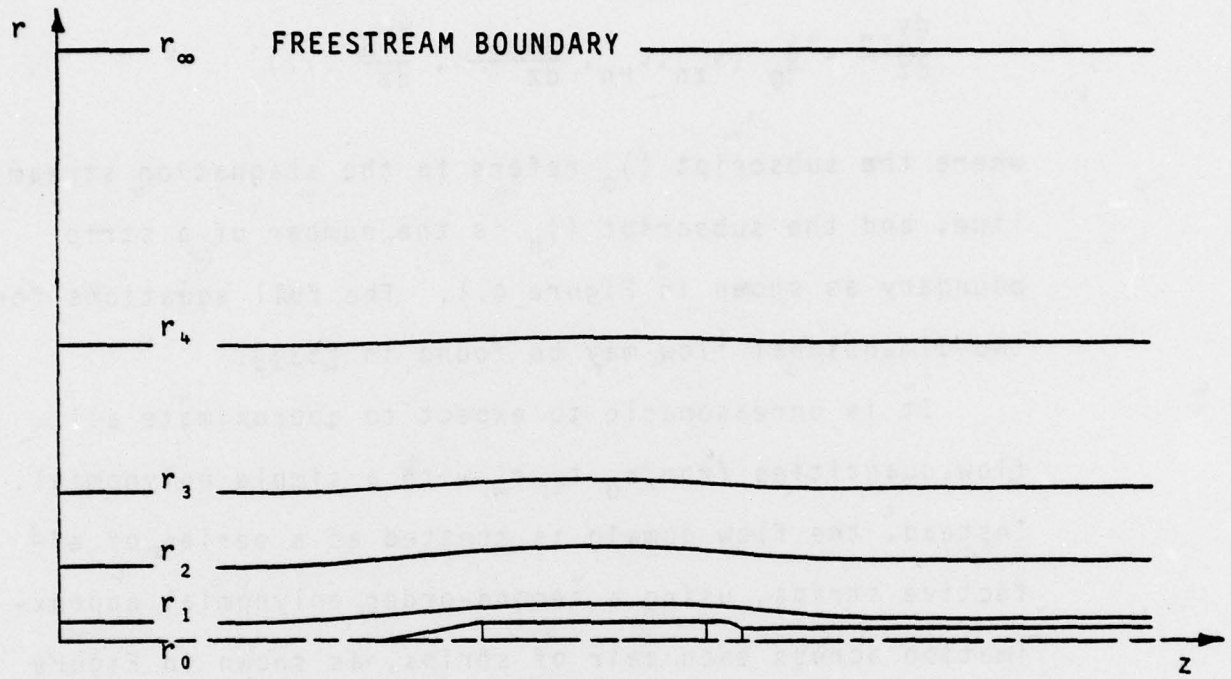

FIGURE 4.1 A MULTI-STRIP SCHEME IS USED TO APPLY THE FREESTREAM BOUNDARY CONDITIONS AND TO IMPROVE ACCURACY. THE METHOD OF INTEGRAL RELATIONS REDUCES THE PARTIAL DIFFERENTIAL EQUATIONS OF THE FLOW TO ORDINARY ONES ALONG STREAMLINES. FREESTREAM CONDITIONS ACT AS BOUNDARY CONDITIONS FOR THE EQUATIONS ALONG r_4. THE SOLUTION ALONG r_4 THEN BECOMES BOUNDARY CONDITIONS FOR THE EQUATIONS ALONG r_3, ETC.

4.1.4 Iteration Procedures for Subsonic Flow Over Symmetric Bodies

Integration reduces the elliptic partial differential equations of the flow to ordinary differential equations. Two iteration schemes used to solve these boundary value problems preserve the elliptic nature of the flow.

Flow integration starts well upstream where free-stream conditions are imposed. A mathematical disturbance, based on predicted stagnation conditions, must be applied along the stagnation streamline for the flow to vary at all. Details may be found in [53]. When the flow begins to vary stably, the disturbance is removed, and integration proceeds to the body. There, the predicted conditions may be evaluated, and the new values are used to start another iteration. This procedure repeats until convergence is achieved.

Integration proceeds from stagnation, along the body, and well downstream, where the pressure is expected to return to its free-stream value. It turns out that this condition is extremely dependent on the location of the free-stream boundary r_∞, apparently since the polynomial approximations involve r_∞. Hence, iterating on r_∞ to force the downstream pressure to converge provides feedback from downstream to upstream.

4.1.5 Results and Conclusion

The upstream iteration for a symmetric Joukowsky airfoil at $M_\infty = 0.5$ was completed on a simple two strip grid. In general, the flow behavior was correct, but cannot be compared to other solutions since the downstream iteration never converged to an "exact" value of r_∞. Similar test runs were made using multiple strip grids. From these tests, the computer time required for the solution of the flow over a typical body was predicted to be seven minutes on an IBM 370/158.

Several objections to the method of integral relations led to termination of the research before any complete solutions were obtained.

An initial objection was that the integrated equations are algebraically cumbersome. Second order approximations are very difficult to derive and program, third order would be prohibitive.

A second objection is that although the equations are in primitive variable form, that is, the unknown quantities are the velocities, density, and pressure rather than a potential function, the quantities solved for are combinations of these variables and must be decoupled algebraically at each step.

The major objection is that the iterative schemes required to preserve the elliptic nature of the flow are artificial. Upstream it is annoying that a disturbance

is required to cause the flow to vary at all. Near the body, the method of integral relations equations become unstable, and the solution must be extrapolated to the stagnation point. It is comforting to note that the upstream disturbance is based on physically realistic stagnation properties, and that the upstream iteration converges quickly. Regarding the downstream iteration, it is unrealistic that the location of the free stream boundary should have a pronounced effect on convergence of the downstream pressure, yet this is a most sensitive iteration.

Finally, the large computing times predicted for a simple airfoil demonstrated that the method of integral relations is not competitive with finite difference or finite element methods.

4.2 Surface Singularity Method

When the research described herein was begun, it was decided that of all inviscid flow methods available, the surface singularity method held the most promise of being easily adopted to the special needs of separated flow computation. This method has undergone extensive development by researchers at the McDonnell-Douglas Corporation [55-58]. The work by Hess and Smith [55] may be considered classic. Computer programs for solving the direct problem are widely available and modifications to solve the inverse problem have been documented [48,52,58].

Basically, the surface singularity method constructs a solution to the velocity potential differential equation, which replaces 2.4 and 2.5 by the single equation (the adiabatic-isentropic energy equation is also included)

$$(1-M_\infty^2)\frac{\partial^2\phi}{\partial z^2} + \frac{\partial^2\phi}{\partial r^2} + \frac{j}{r}\frac{\partial\phi}{\partial r} = 0 \qquad (4.1)$$

The velocity is $v_z = V_\infty + \frac{\partial\phi}{\partial z} = V\cos\theta$, $v_r = \frac{\partial\phi}{\partial r} = V\sin\theta$

This equation is equivalent to 2.4 and 2.5 for incompressible flow ($M_\infty = 0$) and a small perturbation approximation for $M_\infty > 0$. The equation is apparently accurate up to $M_\infty \simeq 0.8$.

It can be shown that 4.1 can be satisfied by various singularities such as sources, sinks, doublets, and for plane flow, vorticies. Since the equation is linear, combinations or distributions of singularities also satisfy the equation. In the surface singularity method, singularities are distributed over surfaces (usually corresponding to body surfaces) in the flow field. The singularities generate a flow field which satisfies (4.1) identically; the strengths of the singularities (the intensity of the distribution) are determined by requiring that the flow field generated satisfy the boundary conditions (usually tangency at a solid surface). The result is a Fredholm integral equation of the second kind for the unknown singularity density function. As

developed by Hess and Smith [55], the corresponding numerical procedure involves distributing source (sink) singularities in a stepwise fashion over a piecewise linear approximation (inscribed) to the actual surface. This results in a set of linear algebraic equations with the (piecewise) source densities ad unknowns as an approximation to the integral equation. Subsequent improvements have introduced curved surface elements, doublet or combination singularities, and polynomial singularity distributions over each element [56-58].

To apply the method to the current problem, we recognize that our goal is to calculate the flow on and external to a predetermined surface in the flow field, the surface describing the edge of the boundary layer. This surface is given by

$$r(z) = R(z) + \delta(z) \cos \alpha(z)$$

External to this surface, it is assumed that the flow is irrotational and inviscid, thus the flow satisfies 4.1.

Introducing the transformations

$$Z = \sqrt{1-M_\infty^2}\, z_o = \beta z_o$$

$$r = r_o$$

$$\phi = 1/\beta\ \phi_o$$

$$V_\infty = V_o$$

results in

$$\frac{\partial^2 \phi_o}{\partial z_o^2} + \frac{\partial^2 \phi_o}{\partial r_o^2} + \frac{j}{r_o} \frac{\partial \phi_o}{\partial r_o} = 0 \ ,$$

the "incompressible" form of the equation. The "incompressible" velocities are related to the compressible velocities by

$$\frac{v_{zo}+V_o}{V_o} = 1 + \frac{v_{zo}}{V_o} = 1 - \beta^2 + \beta^2 \frac{V}{V_\infty} \cos\theta$$

$$\frac{v_{ro}}{V_o} = \beta \frac{V}{V_\infty} \sin\theta$$

The "δ surface" is first modified by replacing x by x_o, transforming to an "incompressible" geometry. Next the "δ surface" is divided into n segments and (source) singularities are distributed in stepwise fashion on the "δ surface". Once these singularities have been distributed, we can form the influence coefficient matrix following identically the steps and calculations of Hess and Smith [55]. In the current method, computer subroutines adapted directly from a computer program written at the Douglass Aircraft Company ("EODA") were used. The influence coefficient matrices are written X_{ij} and Y_{ij} and are the z and r components of velocity induced at the midpoint of the "i"th surface element by a unit source density on the "j"th element. If σ_j is the actual source density on the "j"th element, then the total induced velocities on the "i"th element are

$$\left.\frac{v_{zo}}{V_o}\right)_i = \sum_{j=1}^{n} X_{ij}\sigma_j \qquad \text{and}$$

$$\left.\frac{v_{ro}}{V_o}\right)_i = \sum_{j=1}^{n} Y_{ij}\sigma_j$$

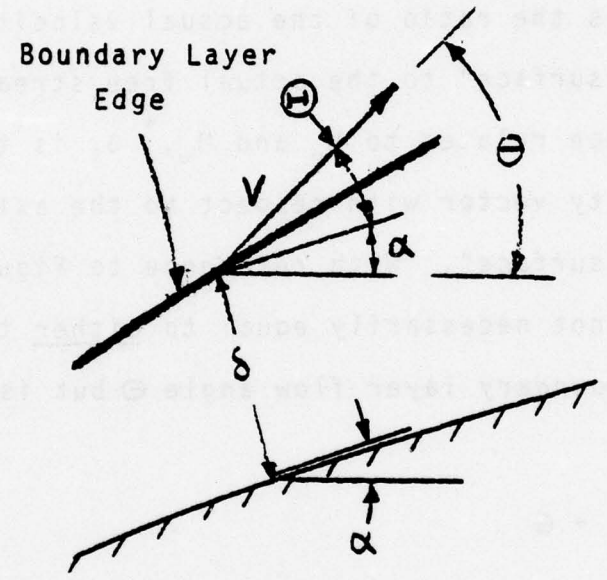

FIGURE 4.2 RELATION AMONG ANGLES AT BOUNDARY LAYER EDGE

AD-A051 535 AKRON UNIV OH DEPT OF MECHANICAL ENGINEERING F/G 20/4
DEVELOPMENT OF A METHOD FOR PREDICTING SUBSONIC TURBULENT SEPAR--ETC(U)
FEB 78 P M GERHART, R V CHIMA DAHC04-75-G-0026
UNCLASSIFIED ARO-12437.1-E NL

2 OF 2
AD A051535

END
DATE FILMED
4-78
DDC

Introducing the relationship between the "incompressible" and actual (compressible) velocities:

$$\sum_{i=1}^{n} X_{ij}\sigma_j = \beta^2\left[\frac{V}{V_\infty}\cos\theta\right)_i - 1] \qquad (4.2)$$

$$\sum_{i=1}^{n} Y_{ij}\sigma_j = \beta\,\frac{V}{V_\infty}\sin\theta\Big)_i \qquad (4.3)$$

Now $\frac{V}{V_\infty})_i$ is the ratio of the actual velocity at point i on the "δ surface" to the actual free stream velocity and is hence related to M_e and M_∞,* θ_i is the angle of the velocity vector with respect to the axis at point i on the "δ surface". With reference to Figure 4.2, note that θ is not necessarily equal to <u>either</u> the body angle α <u>or</u> the boundary layer flow angle Θ but is related to them by:

$$\theta = \alpha + \Theta \qquad (4.4)$$

Note that is there were *no boundary layer*, the "δ surface" would correspond to the body surface, Θ would be zero, and θ would equal the body angle α.

Now consider equations 4.2 and 4.3. From a previous boundary layer calculation, $\delta(x)(\rightarrow \delta(z))$ is known, thus the geometry of the "δ surface" can be determined and the influence coefficient matrices X and Y can be calculated. At each point on the "δ surface", either M_e (which can be used together with M_∞ to find V/V_∞) <u>or</u> Θ

---

* $V/V_\infty = \frac{M_e}{M_\infty}\left(\frac{1+\frac{\gamma-1}{2}M_\infty^2}{1+\frac{\gamma-1}{2}M_\infty^2}\right)^{1/2}$

(which determines θ via 4.4) has been calculated by the boundary layer method. Equations 4.2 and 4.3 thus provide 2n equations for nσ's (irrelevant to the overall method) and n of <u>either</u> V/V_∞ <u>or</u> θ, which provide new estimates of M_e or Θ for use in a further cycle of boundary layer calculations. At any point, it is (theoretically) possible to calculate <u>either</u> M_e or Θ, given the other. Note that the variable which must be calculated at a particular point might change with each (overall) iteration.

All that remains is to construct a method for solving 4.2 and 4.3 which allows for <u>either</u> V/V_∞ or θ to be determined. Now if all of the θ's are known, with all of the V/V_∞'s to be determined, the equations are <u>linear</u>; in addition, if (β cos θ) x (equation 4.3) is subtracted from (sin θ) x (equation 4.2), the resulting equation is easily solved for the (n)σ's; the velocity is then easily calculated. This is in effect identical to the applications of the method to the calculation of the flow over specified arbitrary geometries as developed by Hess and Smith.

If any of the θ's are unknown (a case which arises at any point at which we were obliged to use the strong interaction boundary layer formulation), 2 non-linear equations are introduced at that point and standard matrix methods can no longer be used. In a typical

separated flow calculation, θ will have to be calculated from the inviscid flow equation at several points so a method of solving the mixed set of 2n linear and non-linear algebraic equations arising from 4.2 and 4.3 with V/V_∞ known and θ unknown was developed.

Now 4.2 and 4.3 can be written:

$$\left.\begin{aligned} \frac{1}{\beta^2}\,\Sigma X_{ij}\sigma_j - V_i\sqrt{1-S_i^2} + 1 \equiv F_i^{(1)}(x_i) = 0 \\ \frac{1}{\beta}\,\Sigma Y_{ij}\sigma_j - V_i S_i \;\; = F_i^{(2)}(X_j) = 0 \end{aligned}\right\} \qquad (4.5)$$

where $V_i = V/V_\infty)_i$

$S_i = \sin\theta_i$

$x_j = \sigma_j \quad j=1\rightarrow n$

$x_j = V_i \;\underline{\text{or}}\; S_i \quad j=n+1\rightarrow 2n$.

It was found necessary to use $\sin\theta$ as the unknown rather than $\cos\theta$ The two are related via the square root identity e.g. $\sin\theta = \pm\sqrt{1-\cos^2\theta}$ or $\cos\theta = \pm\sqrt{1-\sin^2\theta}$ Cos θ can be assumed to always have the positive sign since the external flow is not expected to flow "upstream"; however, the sign of sin θ cannot be determined since the flow could have an "up" or "down" component. Viewed another way, although we can always preassign the proper sign to cos θ, we cannot to sin θ and must rely on the calculations to set the sign of sin θ.

The equations (4.5) are solved via Newton iteration:

$$x_j^{m+1} = x_j^m + \delta x_j^m \tag{4.6}$$

where

$$\frac{\partial F_i}{\partial x_j}\Big|_{x=x^m} \delta x_j^m = - F_i(x_j^m) \tag{4.7}$$

and

$$\frac{\partial F_i}{\partial x_j} = \left[\begin{array}{c|c} \frac{1}{\beta^2} X_{ij} & \begin{array}{ccc} 0 & 0 \ldots & 0 \\ -\sqrt{1-S_i^2} & 0 \ldots & 0 \\ 0 & \underline{\text{or}} & 0..0 \\ 0\ 0 & V_i S_i / \sqrt{1-S_i^2} & \\ 0 \ldots & 0 & \end{array} \\ \hline \frac{1}{\beta} Y_{ij} & \begin{array}{ccc} 0\ 0 & \ldots & 0 \\ -S_i & 0\ 0 & \ldots 0 \\ 0 & \underline{\text{or}} & \\ 0\ 0 & -V_i & \ldots 0 \\ 0\ 0\ 0\ 0\ 0 & & \end{array} \end{array}\right] \tag{4.8}$$

If V_i is to be determined, the upper term appears on the right half of the matrix, if S_i is to be determined, the lower term appears. Solution of these equations proceeds as follows: First $\delta\sigma_j$, is solved from:

$$\frac{1}{\beta^2}[A_{ki}^{(2)} X_{ij} - \frac{1}{\beta} A_{ki}^{(1)} Y_{ij}]\delta\sigma_j = - A_{ki}^{(2)} F_i^{(1)}(x_j^m) + A_{ki}^{(1)} F_i^{(2)}(x_j^m)$$

(a set of nxn linear algebraic equations)

where $A^{(1)}_{m,n}$ is the (nxn) diagonal matrix in the upper right hand corner of 4.8 and $A^{(2)}_{m,n}$ is the (nxn) diagonal matrix in the lower right hand corner of 4.8. Then δV_i or δS_i (whichever is required) is calculated from

$$\delta V_i = (-F_i^{(1)}(x^m_j) - \frac{1}{\beta^2} \Sigma X_{ij}\delta\sigma_j)/A^{(1)}_{ii}$$

or

$$\delta S_i = (-F_i^{(2)}(x^m_j) - \frac{1}{\beta} Y_{ij}\delta\sigma_j)/A^{(2)}_{ii}$$

It was found necessary to calculate δV_i and δS_i using the separate formulations above. This is felt to be due to the "dominance" of the "z" direction over the "r" direction in the velocity.

The development outlined here is equally applicable to either plane 2-dimensional (non-lifting) or axisymmetric geometries. The only difference would appear in the formulation of the influence coefficient matrices X_{ij} and Y_{ij}. In this work, since the senior author was considerably more familiar with the axisymmetric method, only axisymmetric formulations were programmed.

The "direct-inverse" inviscid flow method outlined above was tested in the following manner. An axisymmetric body geometry, typical of those used in the experimental investigation of nozzle afterbody drag [45], was specified (see Figure 4.3). The inviscid flow over the body surface was calculated by specifying

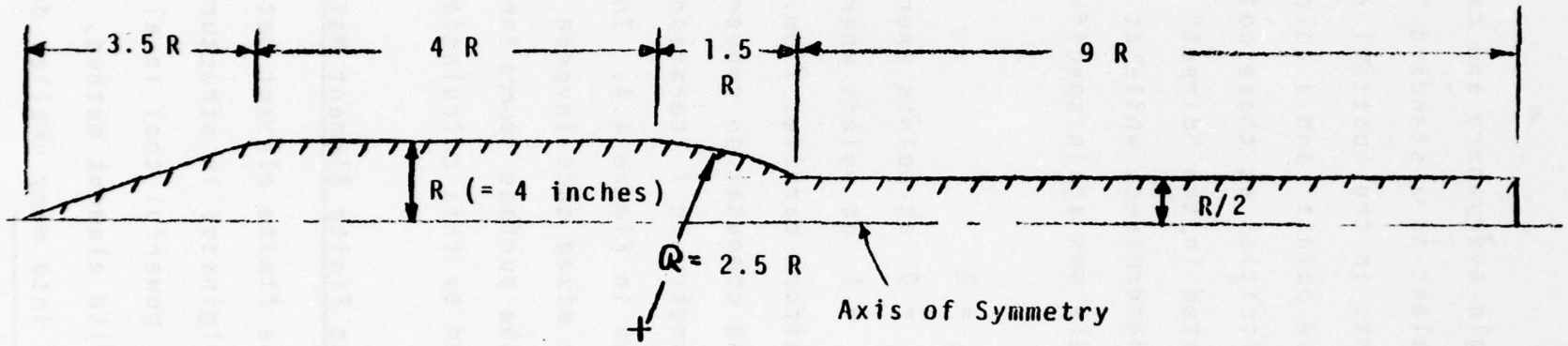

FIGURE 4.3 TEST GEOMETRY FOR INVISCID FLOW AND FULLY SEPARATED FLOW CALCULATIONS

the angle everywhere and calculating the velocities. (Equivalent to a standard "direct" problem.) A number of points in the boattail region were then selected as "inverse points" and a calculation was done in which the velocities at these points were assigned the values calculated in the "direct" calculation with the angles to be determined, while at the remaining body points the angle was again specified. The initial guesses were

$$\sigma_i = 0$$

$$\theta_i = 0 \quad \text{at points where } \theta \text{ is to be determined}$$

$$V/V_\infty)_i = 1 \quad \text{at points where } V \text{ is to be determined}$$

i.e. uniform parallel flow.

The computation converged to the correct velocity and geometry in 7 iterations.* The iteration history is shown in Figure 4.4. The (possibly limited) ability to make mixed duct-inverse inviscid flow calculations using the surface source formulation was believed to be verified by this calculation.

4.3 The Finite Element Method

The finite element method is a numerical technique that originated in structural analysis, but is proving to be a powerful tool in all continuum problems. In the finite element method, the domain of interest is divided into many smaller domains or finite elements.

* The values of V/V_∞ and σ were obtained in 3 iterations, the values of θ converged most slowly.

Corners of the elements are known as nodes. The dependent variables of the problem are approximated by interpolation functions across each element. The Galerkin method, a subclass of the method of weighted residuals, is used to minimize the error resulting from use of the interpolation functions in the governing equations. Assembly of the Galerkin equations from each element results in a global system of algebraic equations for the nodal values of the dependent variables, which may be solved by standard matrix methods.

A finite element program was developed to solve inviscid compressible flows over arbitrary two-dimensional or axisymmetric bodies. Finite difference methods are by far more popular for this type of problem, but the finite element method has certain advantages. The most obvious is the ability of the method to fit arbitrary geometries by judicious placement of the elements, a necessity in the boundary layer interaction problem. Secondly, work by Popinsky and Baker [59] indicates that on coarse grids finite element methods are more accurate than finite difference methods. Third, the inviscid compressible flow problem is best formulated in terms of the potential function for finite difference solution. As will be discussed later, the finite element solution is more conveniently formulated in terms of primitive variables. Two unknowns, the velocity components, are solved for directly at each node,

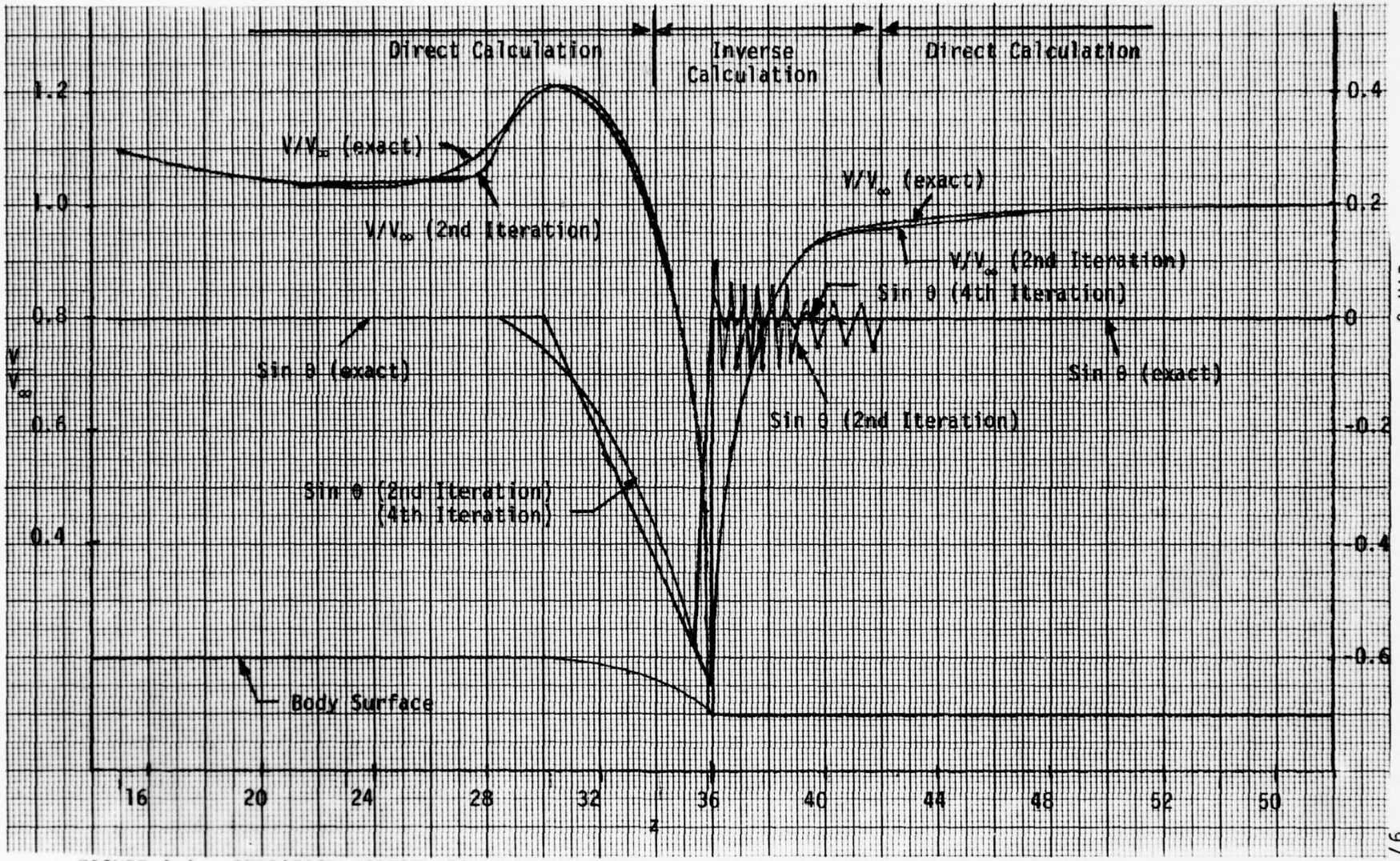

FIGURE 4.4 ITERATION HISTORY FOR INVERSE INVISCID FLOW CALCULATION OF BOATTAILED BODY

Corners of the elements are known as nodes. The dependent variables of the problem are approximated by interpolation functions across each element. The Galerkin method, a subclass of the method of weighted residuals, is used to minimize the error resulting from use of the interpolation functions in the governing equations. Assembly of the Galerkin equations from each element results in a global system of algebraic equations for the nodal values of the dependent variables, which may be solved by standard matrix methods.

A finite element program was developed to solve inviscid compressible flows over arbitrary two-dimensional or axisymmetric bodies. Finite difference methods are by far more popular for this type of problem, but the finite element method has certain advantages. The most obvious is the ability of the method to fit arbitrary geometries by judicious placement of the elements, a necessity in the boundary layer interaction problem. Secondly, work by Popinsky and Baker [59] indicates that on coarse grids finite element methods are more accurate than finite difference methods. Third, the inviscid compressible flow problem is best formulated in terms of the potential function for finite difference solution. As will be discussed later, the finite element solution is more conveniently formulated in terms of primitive variables. Two unknowns, the velocity components, are solved for directly at each node,

and do not have to be computed from derivitives of a velocity potential. Finally, the finite element method tends to produce "neat" algorithms that are easy to program.

The computer program was tested extensively against analytic incompressible solutions. Excellent results were obtained for the pressure coefficients on Rankine ovals and ovoids, on a sphere and a cylinder, and on a 14% thick Joukowsky airfoil. Compressible results agreed well with those predicted by compressibility transformations. The pressure coefficient over a NASA boattail model was computed, and the results agreed well with a published finite difference solution [60] over a range of subsonic Mach numbers.

The inviscid flow program was also coupled iteratively with a Sasman-Cresci integral boundary layer program [61], using the classical method of augmenting the body by the displacement thickness. Results for the NASA boattail model agreed reasonably well with published data [60]. This work clearly demonstrated the ease with which the finite element method can be made to follow a variable geometry.

Finally, inverse or design calculations have been attempted in which the inviscid flow program was to be used iteratively to compute the axisymmetric geometry corresponding to a prescribed pressure distribution. Two formu-

lations of the problem were tested, the sole difference being the boundary condition applied on the non-converged body. Only one method gave promising results, but a converged solution was not obtained. Development of this approach is continuing.

4.3.1 Literature Review

Incompressible ideal flow has been the topic of many finite element papers. Habashi [10] solved lifting airfoil problems by mapping the airfoils to near circles, then discreetizing the resulting finite field with triangular elements spanned by linear interpolation functions. As a free-stream boundary condition, Habashi applied the asymptotic form of the analytic solution for flow over a cylinder. The circulation, and hence the lift, was solved for directly as a problem unknown. Habashi's program is efficient and accurate, and demonstrates the utility of the finite element method.

T. J. Chung's notes from the short course "Finite Element Methods in Fluid Dynamics", University of Alabama, Huntsville, 1976 [62], include complete formulations and computer programs for two-dimensional ideal flow using triangular elements, and for axisymmetric flow using quadrilateral elements. Other papers on simple ideal flows include those by Norie and de Vries [63], Schmidt [64], Shen [65] and Street [66].

An excellent paper using the finite element method for inviscid compressible flow is Hirsch's computation of turbomachine through flow [67].

Chung [62] and Heubner [68] have both presented finite element formulations of the full potential equation. Chung and Hooks [69] have used this type of formulation to obtain some initial shockless results for flow over a small bump, but their primary objective is to use an element with discontinuous interpolation functions to solve flows with shock waves. Chung and Chiou have formulated unsteady compressible flow in terms of the equations of continuity, momentum, energy, and state, using primitive variables [20]. Using this formulation, they have solved for two points in the unsteady boundary layer behind a moving shock wave, with reasonable results.

The most common use of the finite element method in compressible flow so far has been in the solution of small perturbation forms of the potential equation. Carey solved the incompressible flow over a cylinder then used this result to obtain a first order correction [71,72]. Leonard used a similar method to solve the supersonic flow over a Prandtl-Meyer expansion corner [73]. Habashi used the Prandtl-Glauert similarity form of the potention equation to solve the flow over a cylinder [74].

The preceeding references indicate that the finite element has been applied at least initially to many compressible flow problems. However, by no means can it be said that the method has been fully investigated.

4.3.2 Formulation of Method for Inviscid Compressible Flow

The common forms of the inviscid compressible continuity equation, z and r momentum equation, and energy equation are listed below.

Continuity

$$\frac{\partial}{\partial z}(\rho v_z) + \frac{\partial}{\partial r}(\rho v_r) + j\frac{\rho v_r}{r} = 0 \qquad (2.4)$$

z-momentum

$$v_z \frac{\partial v_z}{\partial z} + v_r \frac{\partial v_z}{\partial r} = -\frac{1}{\rho}\frac{\partial p}{\partial z} \qquad (4.10)$$

r-momentum

$$v_z \frac{\partial v_r}{\partial z} + v_r \frac{\partial v_r}{\partial r} = -\frac{1}{\rho}\frac{\partial p}{\partial r} \qquad (4.11)$$

Energy

$$c^2 = c_\infty^2 + \frac{(\gamma-1)}{2}(V_\infty^2 - v_z^2 - v_r^2) \qquad (4.12)$$

One consequence of the inviscid flow assumption is that the flow must remain irrotational, as given by:

$$\frac{\partial v_z}{\partial r} - \frac{\partial v_r}{\partial z} = 0 \qquad (2.5)$$

After multiplying the z and r momentum equations by v_z and v_r, it is possible to use the identity

$$\frac{\partial P}{\partial x_i} = \frac{dP}{d\rho}\frac{\partial \rho}{\partial x_i} = c^2 \frac{\partial \rho}{\partial x_i}$$

along with the equations above, to reduce the z momentum equation to the form

$$\frac{\partial v_z}{\partial z} + \frac{\partial v_r}{\partial r} + j\frac{v_r}{r} = M_\infty^2\{[\frac{(1-\gamma)}{2} + \frac{(\gamma+1)}{2} v_z^2 + \frac{(\gamma-1)}{2} v_r^2] \frac{\partial v_z}{\partial z}$$

$$+ [\frac{(1-\gamma)}{2} + \frac{(\gamma-1)}{2} v_z^2 + \frac{(\gamma+1)}{2} v_r^2] \frac{\partial v_r}{\partial r}$$

$$+ \frac{(\gamma-1)}{2}(v_z^2 + v_r^2 - 1)j\frac{v_r}{r} + 2v_z v_r \frac{\partial v_z}{\partial z}\} = 0 \qquad (4.13)$$

All velocities have been normalized by V_∞ and all lengths by some arbitrary length ℓ.

This equation is to be solved along with the normalized irrotationality condition:

$$\frac{\partial v_z}{\partial r} - \frac{\partial v_r}{\partial z} = 0 \qquad (4.14)$$

Equations (4.13) and (4.14) are a coupled set of first order non-linear partial differential equations for the normalized velocity components v_z and v_r. Note that (4.14) is linear, and that (4.13) is of the form:

linear terms = M_∞^2 * non-linear terms

so that as $M_\infty \to 0$, (4.13) reduces to the linear (incompressible) continuity equation.

The boundary conditions are (2.8 - 2.10).

If the direct or analysis problem is solved, 2.10 becomes

$$V_{nb} = v_{rb} \cos \theta_b - v_{zb} \sin \theta_b = 0 \qquad (4.15)$$

where u_b and v_b are the components of velocity on the body, with the body at an angle θ_b measured counter-clockwise from the z-axis.

These equations are said to be in primitive variable form, that is, they are still in terms of the quantities of interest, the velocity components. Note, however, that the set of equations (4.13) and (4.14) are fully equivalent to the potential equation commonly used for inviscid flows.

The pressure coefficient is found in terms of the dimensionless velocity components from:

$$C_p = \frac{P-1}{\frac{1}{2}\gamma M_\infty^2} \quad \text{where} \quad P = \left[1 + \frac{(\gamma-1)}{2} M_\infty^2 (1-v_z^2-v_r^2)\right]^{\gamma/(\gamma-1)} \qquad (4.16)$$

In the limit of $M_\infty \to 0$ (incompressible flow), this becomes:

$$C_p = 1 - (u^2 + v^2) \qquad (4.17)$$

The finite element formulation of (4.13) and (4.14) requires that the dependent variables v_z and v_r, and for axisymmetric flow the independent variable r, be approximated across each element by interpolation functions of the form

$$\begin{aligned} v_z &\simeq \Omega_N v_{zN} = \Omega_1 v_{z1} + \Omega_2 v_{z2} + \ldots + \Omega_n v_{zn} \\ v_r &\simeq \Omega_N v_{rN} = \Omega_1 v_{r1} + \Omega_2 v_{r2} + \ldots + \Omega_n v_{rn} \\ r &\simeq \Omega_N r_N = \Omega_1 r_1 + \Omega_2 r_2 + \ldots + \Omega_n r_n \end{aligned} \qquad (4.18)$$

where Ω_N are the interpolation functions, v_{zN}, v_{rN} and r_N are values of v_z, v_r and r at the Nth node, and n is the number of nodes per element.

The simplest possible element is triangular, and has three nodes and linear interpolation functions. Other elements may have other shapes and higher order interpolation functions. Each element in the flow field gives rise to a n * n coefficient matrix. Thus, linear triangular elements require computation of a 3 * 3 matrix. Higher order interpolation functions may increase accuracy, but also require lengthy computation of large coefficient matrices. Linear triangular elements assure that the final solution will have continuous values of the dependent variables throughout the flow field (called C° continuity). Other elements have been devised that also assure continuity of the first m derivitives of the variable (called C^m continuity). With these elements, values of the variable and its first m derivitives must be solved for at the nodes, increasing solution time.

The potential equation commonly solved by finite difference methods is second order, demanding second order elements with large coefficient matrices. The solution must be differentiated to obtain the velocity components, making C^1 continuity desirable. Both requirements add up to large computer times.

The primitive variable formulation given by equations (4.13) and (4.14) contains only first derivitives, and so requires only first order elements with C° continuity. To minimize requirements on the interpolation functions and thereby reduce computer time, the primitive variable formulation of subsonic inviscid flow was chosen over the potential formulation.

Isoparametric quadrilateral elements, as shown in Fig. 4.5 employ the same interpolation functions for all variables of interest in arbitrarily shaped quadrilateral elements. They were chosen over triangular elements since their shape is more suited to a roughly rectangular flow field, and since their interpolation functions, while almost linear, include a cross product term that increases accuracy.

Figure 4.5 shows an arbitrary quadrilateral element. A non-dimensional or "natural" coordinate system (ε,η) is established at the centroid of the element, such that the coordinates of the four nodes are $\pm$ 1. This simplifies the resulting expressions for the interpolation functions. Note that the node numbering must proceed counterclockwise around each element. Otherwise, interpolation functions may take on negative values.

It is impractical to derive the expressions for the interpolation functions and their derivitives here. Details are available in [62] or [68], and all results are presented here for convenience.

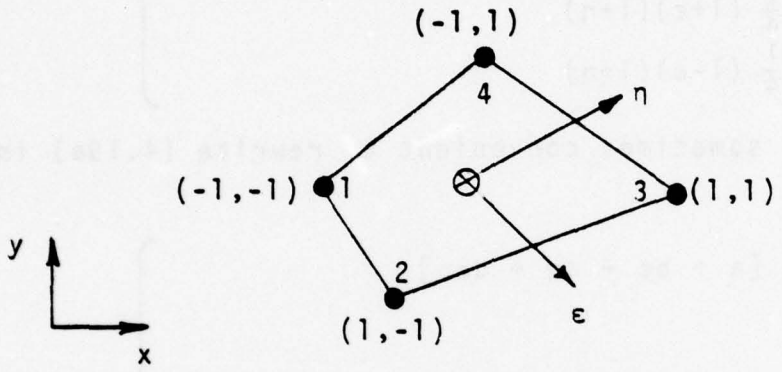

FIGURE 4.5 ISOPARAMETRIC QUADRILATERAL ELEMENTS. NON-DIMENSIONAL (OR "NATURAL") COORDINATES (ϵ , η) ARE ESTABLISHED AT THE CENTROID OF THE ELEMENT SUCH THAT THE COORDINATES OF THE NODES ARE $\pm$ 1. THIS SIMPLIFIES THE EXPRESSIONS FOR THE INTERPOLATION FUNCTIONS. NODES MUST BE NUMBERED COUNTER CLOCKWISE AROUNG THE ELEMENT.

Interpolation for any Variable ϕ:

$$\left.\begin{aligned} \phi &= \Omega_N \phi_N = \Omega_1 \phi_1 + \Omega_2 \phi_2 + \Omega_3 \phi_3 + \Omega_4 \phi_4 \\ &\text{where} \\ \Omega_1 &= \frac{1}{4}(1-\varepsilon)(1-\eta) \\ \Omega_2 &= \frac{1}{4}(1+\varepsilon)(1-\eta) \\ \Omega_3 &= \frac{1}{4}(1+\varepsilon)(1+\eta) \\ \Omega_4 &= \frac{1}{4}(1-\varepsilon)(1+\eta) \end{aligned}\right\} \quad (4.19a)$$

It is sometimes convenient to rewrite (4.19a) in the form:

$$\left.\begin{aligned} \phi &= \frac{1}{4}[a + b\varepsilon + c\eta + d\varepsilon\eta] \\ &\text{where} \\ a &= \phi_1 + \phi_2 + \phi_3 + \phi_4 \\ b &= -\phi_1 + \phi_2 + \phi_3 - \phi_4 \\ c &= -\phi_1 - \phi_2 + \phi_3 + \phi_4 \\ d &= \phi_1 - \phi_2 + \phi_3 - \phi_4 \end{aligned}\right\} \quad (4.19b)$$

Derivitives of Interpolation Functions:

The finite element formulation of (6) and (7) requires first derivitives of the interpolation functions given in (4.19a). These are as follows:

$$\left.\begin{aligned} \frac{\partial \Omega_N}{\partial z} &= \frac{1}{8|J|}(A_{N_1} + B_{N_1}\varepsilon_1 + C_{N_1}\eta) \\ \frac{\partial \Omega_N}{\partial r} &= \frac{1}{8|J|}(A_{N_2} + B_{N_2}\varepsilon + C_{N_2}\eta) \end{aligned}\right\} \quad (4.20a)$$

where A_{Ni}, B_{Ni}, and C_{Ni} are functions of nodal coordinates in the (x,y) system.

$$
\left.\begin{array}{lll}
A_{11} = r_2 - r_1 & B_{11} = r_4 - r_3 & C_{11} = r_3 - r_2 \\
A_{12} = z_4 - z_2 & B_{12} = z_3 - z_4 & C_{12} = z_2 - z_3 \\
A_{21} = r_3 - r_1 & B_{21} = r_3 - r_4 & C_{21} = r_1 - r_4 \\
A_{22} = z_1 - z_3 & B_{22} = z_4 - z_3 & C_{22} = z_4 - z_1 \\
A_{31} = r_4 - r_2 & B_{31} = r_1 - r_2 & C_{31} = r_4 - r_1 \\
A_{32} = z_2 - z_4 & B_{32} = z_2 - z_1 & C_{32} = z_1 - z_4 \\
A_{41} = r_1 - r_3 & B_{41} = r_2 - r_1 & C_{41} = r_2 - r_3 \\
A_{42} = z_3 - z_1 & B_{42} = z_1 - z_2 & C_{42} = z_3 - z_2
\end{array}\right\} \quad (4.20b)
$$

The Jacobian matrix [J] relates derivitives in the local (ξ,η) and global (z,r) coordinate systems.

$$
[J] = \left| \begin{array}{cc} \frac{\partial z}{\partial \epsilon} & \frac{\partial z}{\partial \eta} \\ \frac{\partial r}{\partial \epsilon} & \frac{\partial r}{\partial \eta} \end{array} \right| \quad \left.\right\} \quad (4.21a)
$$

and its determinant $|J|$ is given by

$$
|J| = \frac{1}{8} [\alpha_0 + \alpha_1 \epsilon + \alpha_2 \eta]
$$

where α_i are functions of the global nodal coordinates

$$
\left.\begin{array}{l}
\alpha_0 = (z_1 - z_2)(r_1 - r_3) - (z_1 - z_3)(r_4 - r_2) \\
\alpha_1 = (z_3 - z_1)(r_1 - r_2) - (z_1 - z_2)(r_3 - r_4) \\
\alpha_2 = (z_4 - z_1)(r_2 - r_3) - (z_2 - z_3)(r_4 - r_1)
\end{array}\right\} \quad (4.21b)
$$

Integration

The Galerkin formulation of (4.13) and (4.14) requires integration of various functions over the area

of an element. The relation between integrations in global and local coordinates is:

$$\int_{Area} f(z,r)dzdr = \int_{-1}^{1}\int_{-1}^{1} |J| f(\varepsilon,\eta)d\varepsilon d\eta \qquad (4.22a)$$

Since analytic integration is often impossible due to the term J, Gaussian numerical integration is used.

$$\int_{Area} f(z,r)dzdr = \sum_{j=1}^{L}\sum_{k=1}^{L} \omega_j\omega_k |J| f(\varepsilon,\eta) \qquad (4.22b)$$

where $\omega_j\omega_k$ are the Gaussian weight functions available elsewhere, and L is the order of the Gaussian integration, (L=3 has proven to be sufficient).

Galerkin Formulation

Now the approximations for v_z, v_r and r given by equation (4.18) are substituted into the equations of motion (4.13) and (4.14). In general, the right hand sides will no longer equal zero; indeed, they will each equal some residual. The Galerkin method, a subclass of the method of weighted residuals, is used to minimize these residuals.

The Galerkin method uses the interpolation functions Ω_N as weight functions, and requires that these functions be orthogonal to the residuals over the volume of any element. Gartling [75] and Oden [76] have shown that this method is equivalent to an integral mechanical energy

balance; so the method has physical significance.

Details of this formulation are unnecessary. The Galerkin formulation of (4.13) and (4.14) may be written in the following matrix form:

$$\begin{bmatrix} C-M_\infty^2[F(v_z,v_r)+G(v_z,v_r)], & (D+jE)-M_\infty^2[H(v_z,v_r)+jI(v_z,v_r)] \\ A \quad , & B \end{bmatrix} \begin{bmatrix} v_z \\ v_r \end{bmatrix} = 0 \tag{4.23}$$

Here, the upper row is the Galerkin formulation for the compressible continuity equation (4.13) and the bottom row is the formulation of the irrotationality condition (4.14).

The terms A through I are each (4*4) coefficient matrices given by the following integrals.

$$A_{NM} = \int_A \Omega_N \frac{\partial \Omega_M}{\partial r} r^j \, dzdr$$

$$B_{NM} = -\int_A \Omega_N \frac{\partial \Omega_M}{\partial z} r^u \, dzdr$$

$$C_{NM} = \int_A \Omega_N \frac{\partial \Omega_M}{\partial z} r^j dzdr = -B_{NM}$$

$$D_{NM} = \int_A \Omega_N \frac{\partial \Omega_M}{\partial r} r^j dzdr = A_{NM}$$

$$E_{NM} = \int_A \Omega_N \Omega_M \, dzdr$$

$$F_{NM} = \int_A \left[\frac{(1-\gamma)}{2} + \frac{(\gamma+1)}{2}(\Omega_L u_L)^2 + \left(\frac{(\gamma-1)}{2}(\Omega_L v_L)^2\right]\Omega_N \frac{\partial \Omega_M}{\partial z} r^j dzdr\right.$$

$$G_{NM} = 2\int_A (\Omega_K u_K)(\Omega_L v_L)\Omega_N \frac{\partial \Omega_M}{\partial r} r^j dzdr$$

(4.24 continued)

$$H_{NM} = \int_A \left[\frac{(1-\gamma)}{2} + \frac{(\gamma-1)}{2}(\Omega_L u_L)^2 + \frac{(\gamma+1)}{2}(\Omega_L v_L)^2\right]\Omega_N \frac{\partial \Omega_M}{\partial r} r^j dz dr$$

$$I_{NM} = \frac{(\gamma-1)}{2} \int_A \left[(\Omega_L u_L)^2 + (\Omega_L v_L)^2 - 1\right]\Omega_N \Omega_M \, dz dr \qquad (4.24)$$

$N = 1,2,3,4$

$M = 1,2,3,4$

This set of algebraic equations is non-linear due to the terms F, G, H, and I. In the incompressible limit of $M_\infty = 0$, these terms vanish and the system becomes linear.

A similar set of equations may be written for each element in the flow field. Equations from each element are assembled into a global matrix equation using standard techniques available in [62] or [68].

Dirichlet boundary conditions (specified values of u or v as given by equations 2.7 and 2.8 can now be substituted directly into the global matrix. Movement of known terms to the right-hand side makes the right-hand side non-zero and the equation set non-singular.

Neumann boundary conditions (e.g. the tangency condition given by equation (4.15)) are applied via LaGrange multipliers. Details may be found in [62] or [68]. The tangency constraint is applied at each node on a body, giving rise to extra equation for the LaGrange multiplier at each body node. Physically, the LaGrange multiplier represents the "energy" required to hold the Neumann boundary constraint. Practically, the value of the multiplier is useless.

Iterative Solution of the Non-linear Algebraic Equations

Gartling's work with a primitive variable form of the Navier-Stokes equations [75,77] lead to the following iterative scheme for solving the non-linear algebraic set (4.23)

$$\begin{bmatrix} C-M_\infty^2[F(v_z^{n-1},v_r^{n-1}) + G(v_z^{n-1},v_r^{n-1})] & , & (D+JE)-M_\infty^2[H(v_z^{n-1},v_r^{n-1}) + jI(v_z^{n-1},v_r^{n-1})] \\ A & , & B \end{bmatrix} \begin{bmatrix} v_z^n \\ v_r^n \end{bmatrix} = 0 \tag{4.25}$$

where the superscript $()^n$ refers to the iteration number. For the first iteration (n=1), the non-linear terms F, G, H and I are set to zero, and the resulting linear set is solved using a Gauss-Jordan scheme for banded matrices. Thus, the n=1 solution is the incompressible solution, which is always useful for comparison. In subsequent iterations, the non-linear terms are calculated from the previous (n-1) values of u and v.

The solution is considered to be converged when all $v_z^n - v_z^{n-1}$ and all $v_r^n - v_r^{n-1}$ are less than 0.0001. This invariably occurs in 3 or 4 iterations, unless the flow goes locally supersonic, in which case the solution almost never converges.

4.3.3 Results

In each of the following examples, an automatic mesh generation subroutine was used to simplify input to the program and to minimize the band with of the resulting equations. As shown in Figure 4.6 this subroutine installs nodes along vertical columns and along roughly parallel rows. If the number of nodes per column is designated Nr, the number of nodes per row is Nz, and the number of nodes on the body is NB, then the total number of nodes is NzxNr, the number of elements is (Nz-1)*(Nr-1), and the number of equations solved is 2*Nz*Nr+NB.

All computer times given below are for an IBM 370/158.

Sphere

Flow over a sphere was computed on a 9*27 node grid. The resulting incompressible pressure coefficient is shown in Figure 4.7 (circles), compared to the exact solution (solid line). The compressible solution at M_∞ = 0.5 (plus signs) is compared to the Gothert's rule compressibility correction (dashed line) on the same plot. The solutions are good near the stagnation region, but worsen near the peak of the sphere where the finite free stream boundary has the most effect. Computer times were 22 seconds for the incompressible solution, and 149 seconds for the compressible solution. The compressible solution required 7 iterations since the flow approached the critical Mach number of M_∞ = 0.57.

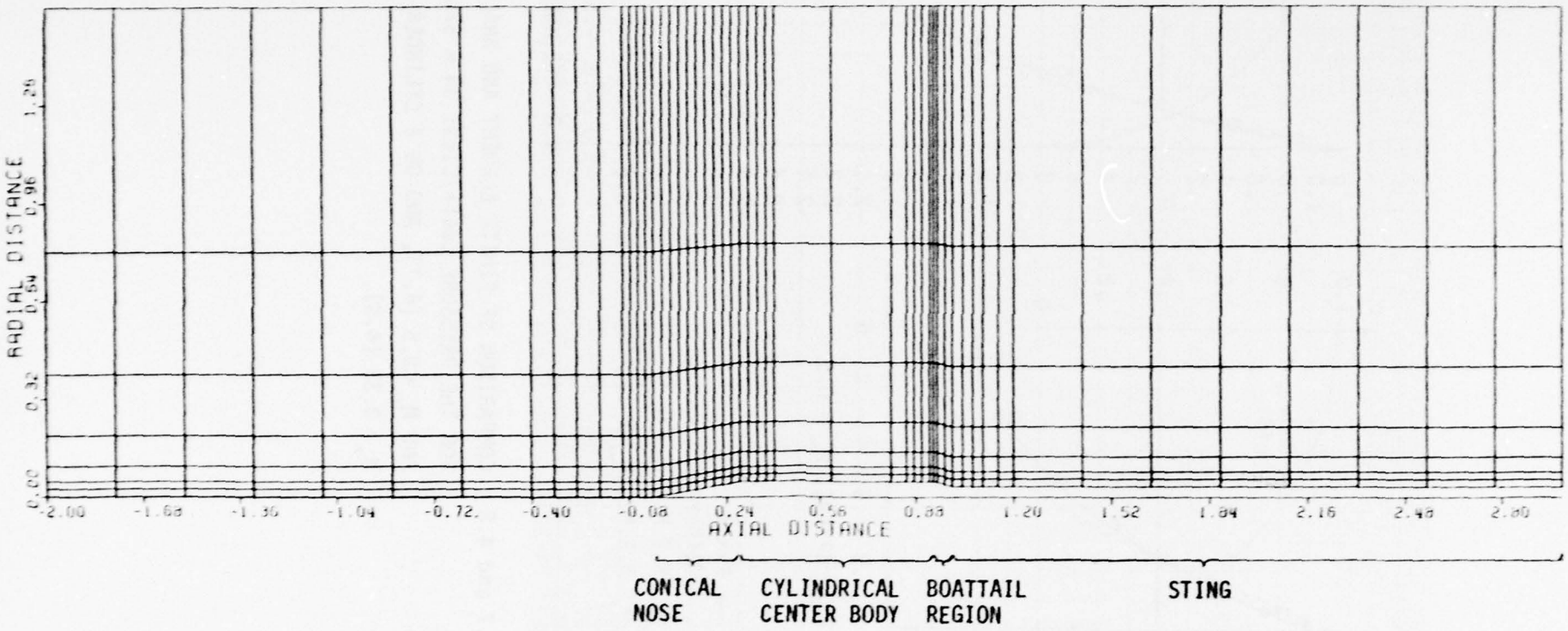

FIGURE 4.6 THE 7*52 ELEMENT GRID OF AN AXISYMMETRIC NASA BOATTAIL MODEL USED FOR BOUNDARY LAYER COUPLING STUDY. THERE ARE 7*52 = 364 ELEMENTS, (7+1)*(52+1) = 424 NODES, 38 BODY NODES, AND 2*424 + 38 = 886 EQUATIONS. THE GRID WAS GENERATED AUTOMATICALLY BY THE COMPUTER PROGRAM.

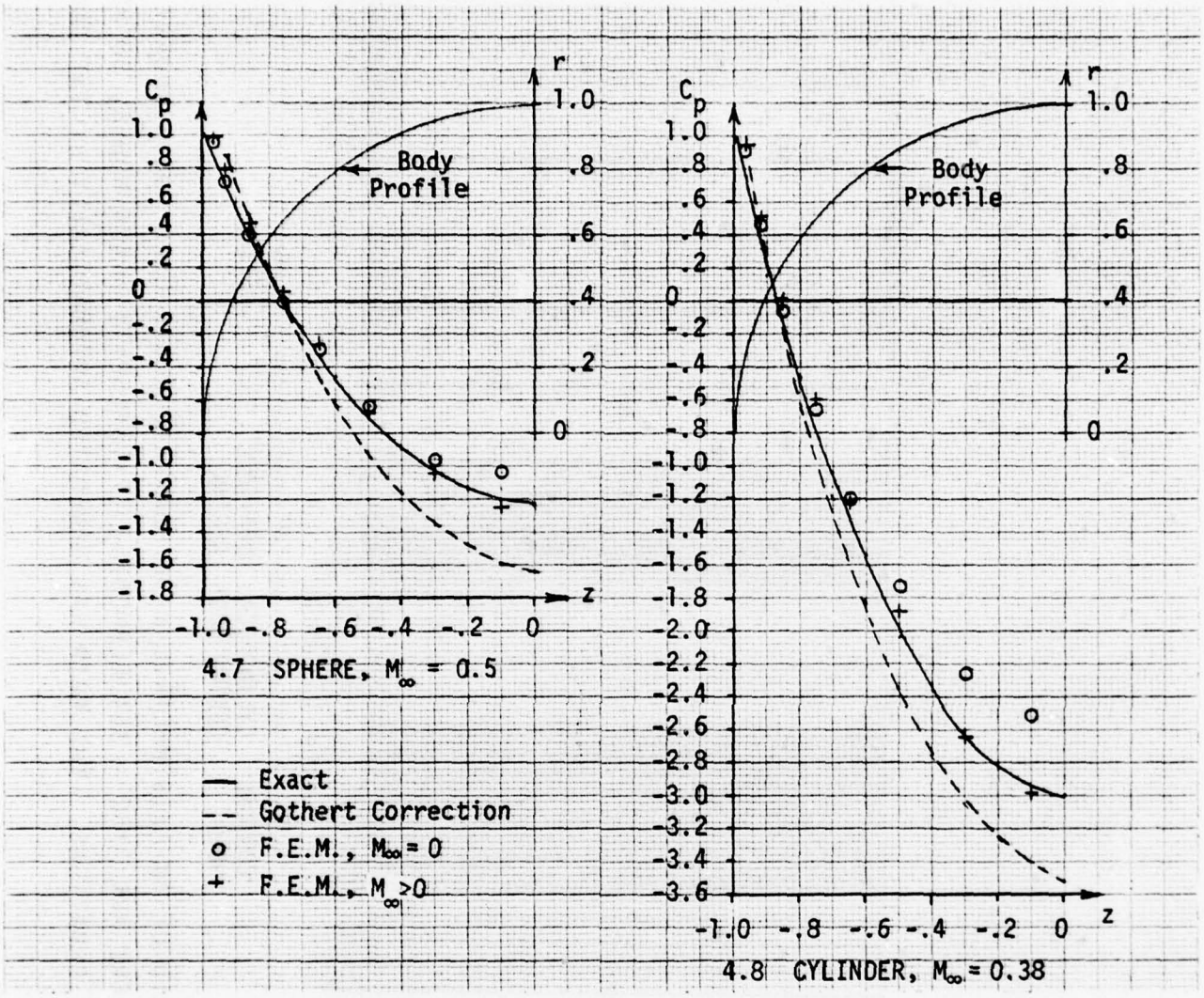

FIGURE 4.7 and 4.8 COMPARISON OF FINITE ELEMENT AND ANALYTIC SOLUTIONS FOR THE PRESSURE COEFFICIENT ON A SPHERE AT $M_\infty = 0$ AND $M_\infty = 0.5$ (4.7), AND ON A CYLINDER AT $M_\infty = 0$ AND $M_\infty = 0.38$ (4.8).

Cylinder

The grid used for the sphere was also used to compute the pressure coefficient over a cylinder, as shown in Figure 4.8. Agreement with the analytic solution is similar to that of the sphere, but slightly worse. This was expected, since the two-dimensional cylinder represents a larger flow disturbance than the axisymmetric sphere. Computer times were 22 seconds for the incompressible solution and 110 seconds for the M_∞ = 0.38 solution (5 iterations).

Rankine Ovoid

Figure 4.9 compares the calculated and exact pressure coefficients on a 3.16:1 aspect ratio axisymmetric Rankine ovoid. At M_∞ = 0, the finite element solution (circles) and the exact solution (solid line) agree almost exactly. At M_∞ = 0.6, the finite element solution (plus signs) compares well with the Gothert's rule compressibility correction. A 10*29 node mesh was used over the quarter body. Incompressible and compressible solution times were 29 seconds and 120 seconds respectively.

Rankine Oval

Figure 4.10 compares the calculated and exact pressure coefficients on a 3.16:1 aspect ratio two-dimensional Rankine oval. It should be noted that the body profile is not the same as that of the ovoid mentioned above.

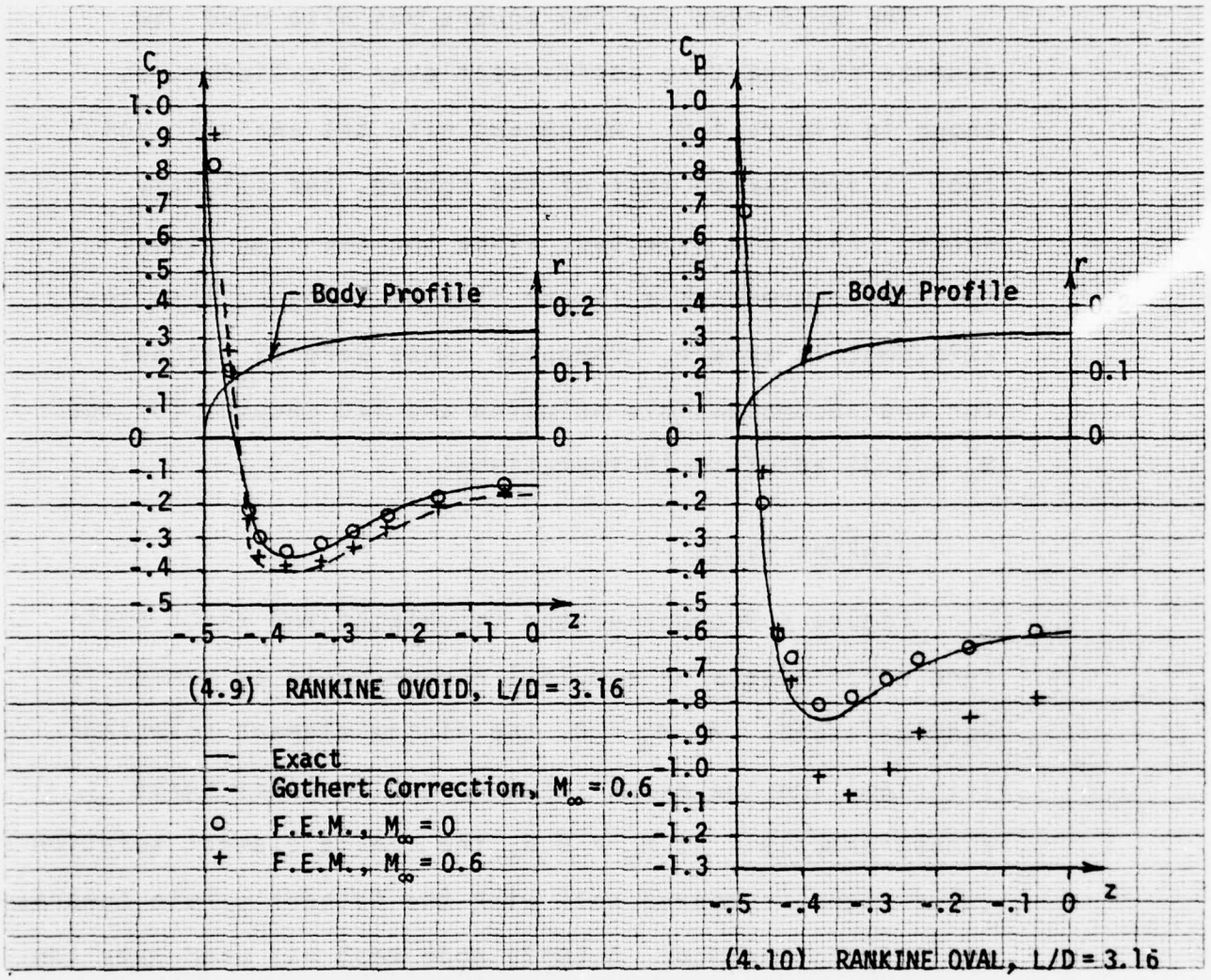

FIGURE 4.9 and 4.10 COMPARISON OF FINITE ELEMENT AND ANALYTIC SOLUTIONS FOR THE PRESSURE COEFFICIENT ON A 2-D RANKINE OVOID (4.9) AND ON AN AXISYMMETRIC RANKINE OVAL (4.10), BOTH AT $M_\infty = 0$ AND $M_\infty = 0.6$

The finite element incompressible solution (circles) and the exact solution (solid line) compare well, except in the region of peak negative pressure, where grid spacing may have been too coarse. A 9*29 node grid was used over the quarter body. The $M_\infty = 0.6$ solution is also shown (plus signs). Computer times were 25 seconds at $M_\infty = 0$ and 123 seconds at $M = 0.6$.

14% Joukowsky Airfoil

The finite element program has been used to solve for the flow over a 14% thick symmetric Joukowsky airfoil at $M_\infty = 0$ and $M_\infty = 0.6$. Figure 4.11 shows the exact pressure coefficient (solid line), the incompressible finite element solution (circles), the $M_\infty = 0.6$ finite element solution (plus signs), and the $M = 0.6$ Gothert's rule compressibility correction to the exact solution. Both the incompressible and compressible solutions show excellent agreement with the analytic solutions. The only error is again in the peak negative pressure region, probably indicating inadequate mesh spacing. The mesh consisted of 7 node rows by 37 node columns, for a total of 259 nodes (13 on the body). This amounts to 216 elements and 531 simultaneous equations. The incompressible solution took 21 seconds, and the $M_\infty = 0.6$ solution took 83 seconds (4 iterations). These times are not out of line with finite difference methods.

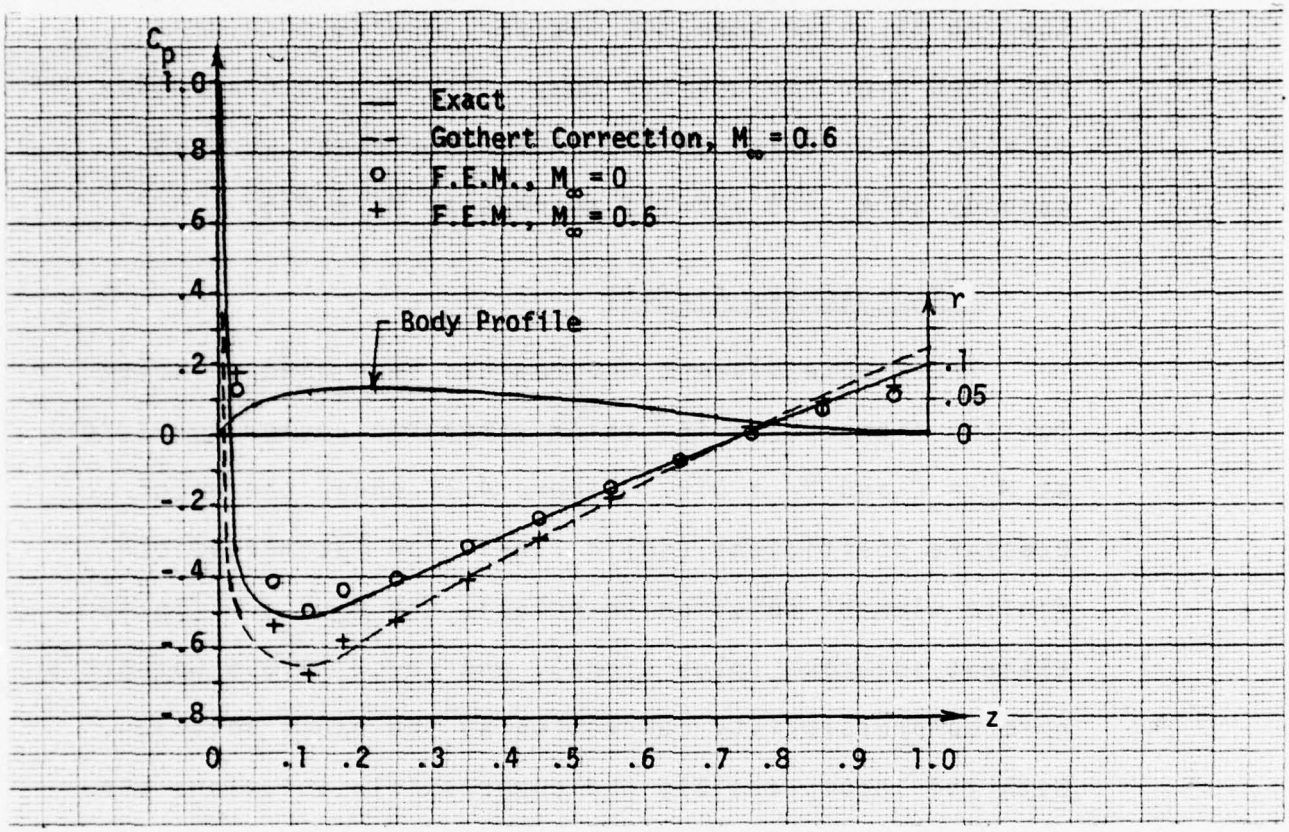

FIGURE 4.11 COMPARISON OF FINITE ELEMENT AND ANALYTIC SOLUTIONS FOR THE PRESSURE COEFFICIENT ON A 14% THICK SYMMETRIC JOUKOWSKY AIRFOIL AT $M_\infty = 0$ AND $M_\infty = 0.6$.

Axisymmetric Boattail Model

Chow, Bober and Anderson [60] published experimental data and finite difference calculations for the pressure coefficient on a NASA axisymmetric boattail model. Figure 4.5 shows the 8*53 node finite element grid used to re-compute this flow in the present study.

Figure 4.12 shows the incompressible finite element solution (solid line) compared to a surface source method (dashed line). Qualitative agreement is good, but quantatively there is some disagreement in the results. It is thought that this is due to the finite location of the free-stream boundary. This boundary is 30 body radii away, but only 1.6 body lengths (excluding the sting) away. A compressible $M_\infty = 0.8$ solution is also presented (circles).

Boundary Layer Coupling

Sasman and Cresci's compressible turbulent boundary layer program [61] was coupled iteratively to the finite element inviscid flow prgoram using the classical method of augmenting the body by the displacement thickness.

Briefly, Sasman and Cresci reduce the integral momentum and moment of momentum equations to an "incompressible" form via a Mager type transformation. They use power law velocity profiles and the Ludweig-Tillman skin friction correllation. Their dependent variables

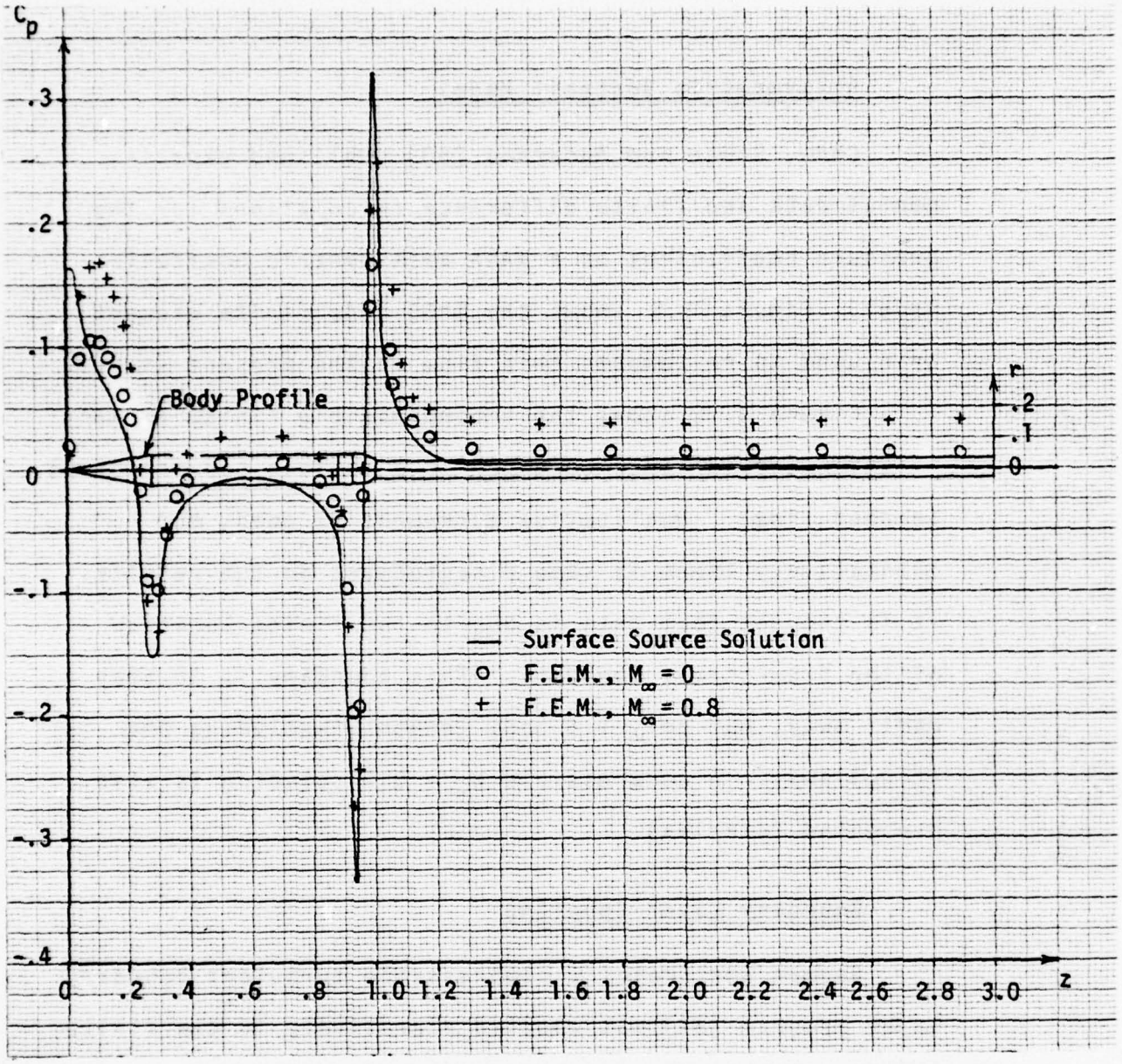

FIGURE 4.12 COMPARISON OF FINITE ELEMENT AND SURFACE SOURCE SOLUTIONS FOR THE PRESSURE COEFFICIENT ON A NASA BOATTAIL MODEL, AND THE COMPRESSIBLE FINITE ELEMENT SOLUTION FOR $M_\infty = 0.8$.

are the momentum thickness θ and the shape factor $H = \delta^*/\theta$, where δ^* is the displacement thickness. Chow, Bober and Anderson [60] used this method for their boattail work at Mach numbers from .56 to .9, with good results at all but the highest Mach number.

Figure 4.13 compares the pressure coefficients over the boattail model at $M_\infty = 0.8$ calculated by the inviscid method alone (circles), and by the inviscid/viscous interaction (solid line).

Figure 4.14 is an enlargement of the boattail region from Figure 4.13 compared with the results of Chow, Bober and Anderson [60]. The finite element/Sasman-Cresci method underestimates the pressure coefficient in this region. It should be noted, however, that the finite element grid for this problem was 8 nodes high by 53 nodes long, while the grid used by Chow, et al. was 26 nodes high and 101 nodes long. Furthermore, Chow, Bober and Anderson used an infinite-to-finite transformation on the flow field in the r direction, while the present study used a finite free-stream boundary. Chow, Bober and Anderson's finite-difference interaction problem took 7 minutes on a CDC 6600, while the finite element method took 13 minutes on an IBM 370/158.

Finally, Figure 4.15 compares the displacement thicknesses in the boattail region calculated by Chow, et al. and by the present study. The disagreement is undoubtedly due to discrepancies in the inviscid solutions.

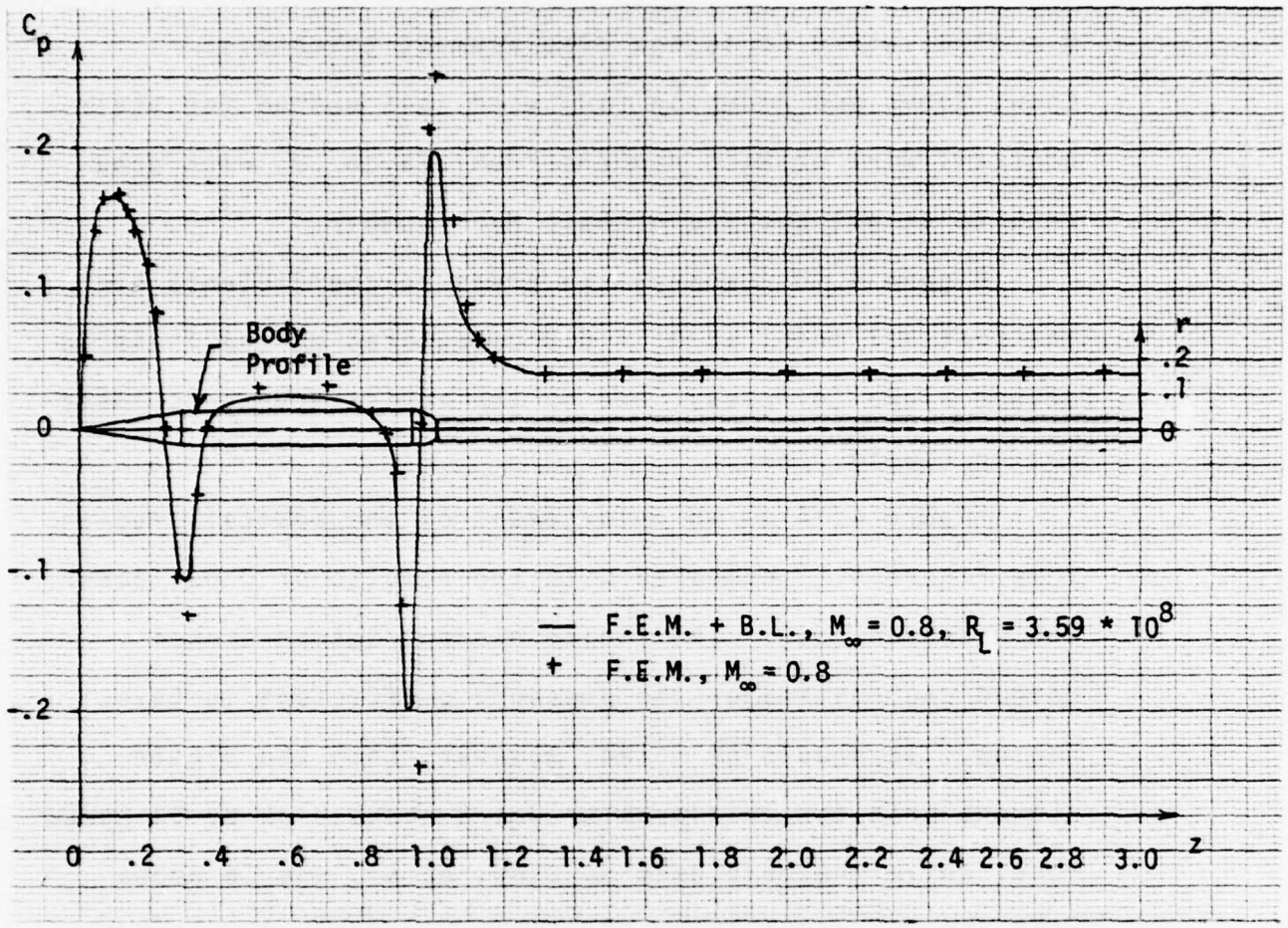

FIGURE 4.13 COMPARISON OF PRESSURE COEFFICIENTS ON A NASA BOATTAIL MODEL AT $M_\infty = 0.8$. THE "+" SIGNS ARE THE INVISCID SOLUTION ON THE ACTUAL BODY. THE SOLID LINE IS THE INVISCID SOLUTION ON THE BODY AUGMENTED BY THE DISPLACEMENT THICKNESS δ^* CALCULATED ITERATIVELY FROM A SASMAN-CRESCI TURBULENT BOUNDARY LAYER DECK AT $M_\infty = 0.8$, $R_L = 3.59 * 10^8$

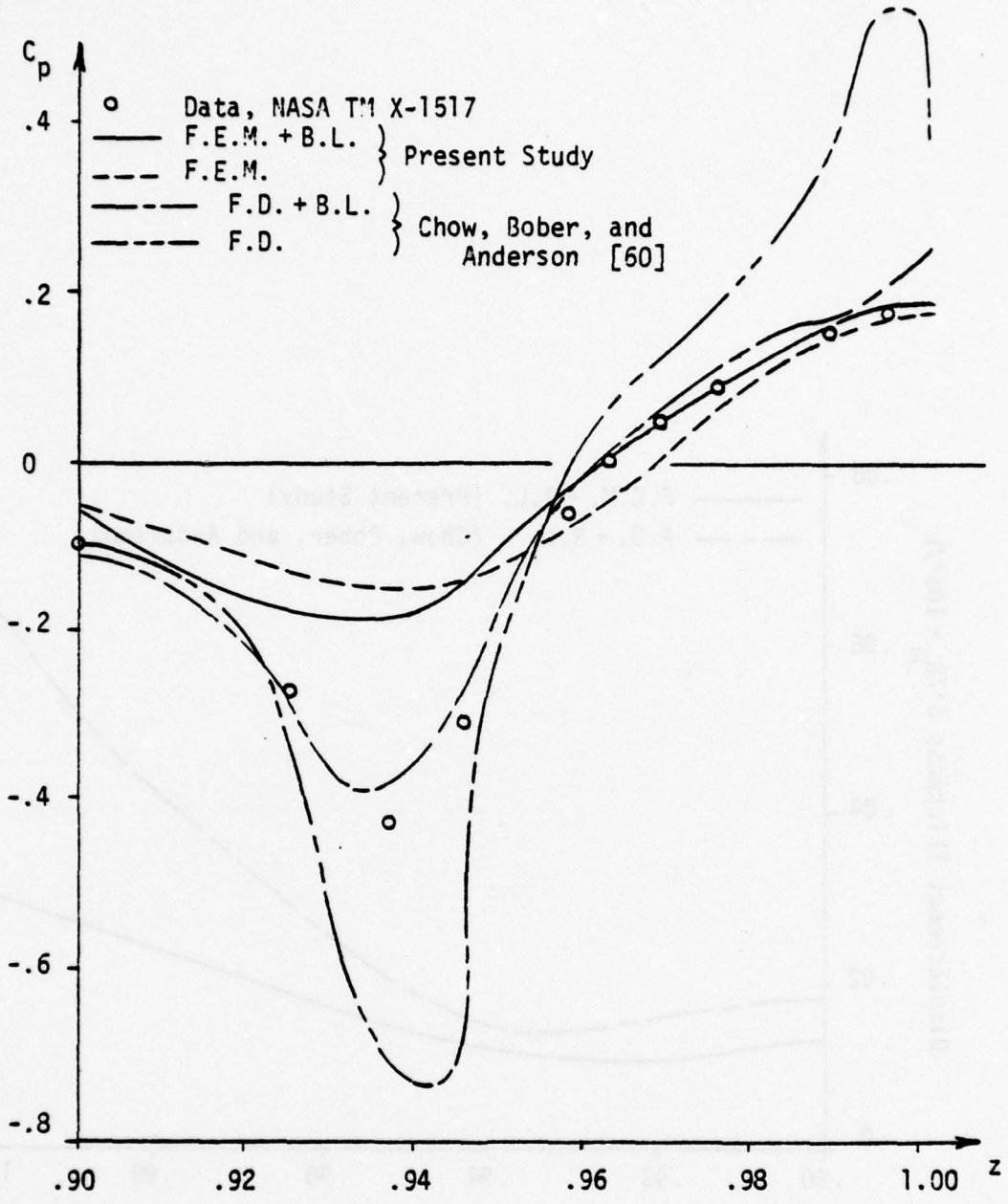

FIGURE 4.14 COMPARISON OF FINITE ELEMENT AND FINITE DIFFERENCE SOLUTIONS FOR THE PRESSURE COEFFICIENT ON A NASA BOATTAIL MODEL AT $M_\infty = 0.8$. BOTH ARE SHOWN WITH AND WITHOUT BOUNDARY LAYER INFLUENCE, CALCULATED USING A SASMAN-CRESCI TURBULENT BOUNDARY LAYER DECK.

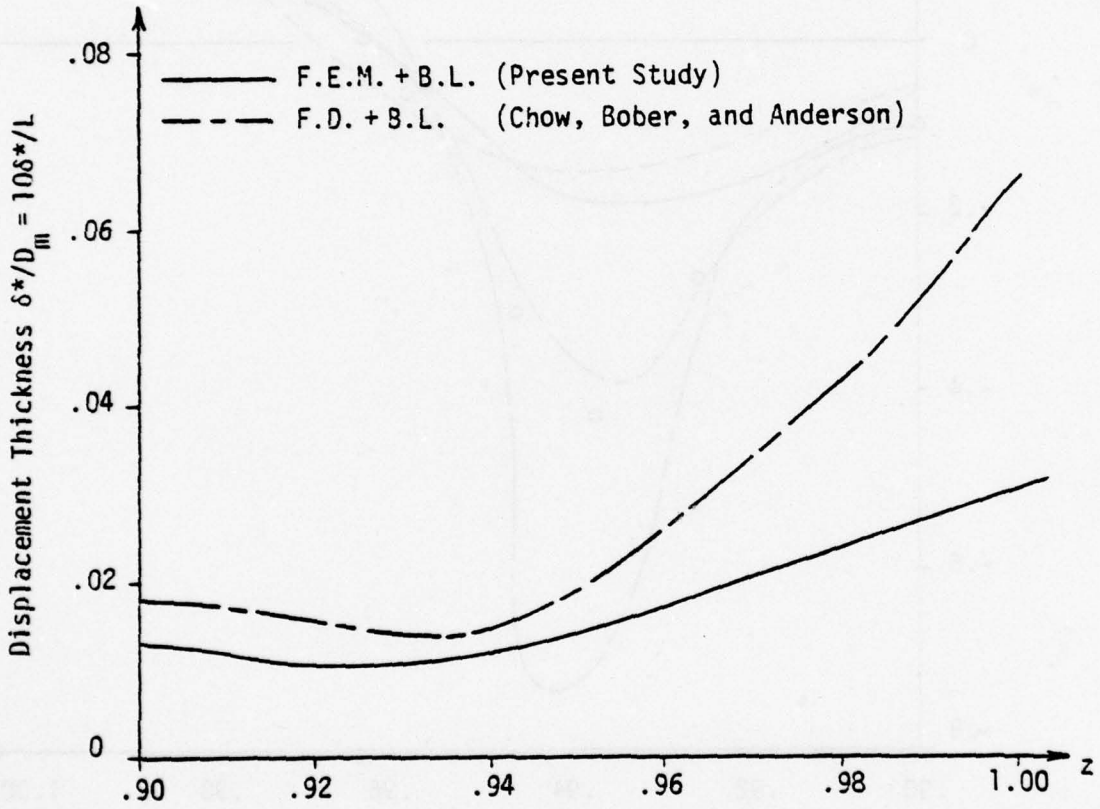

FIGURE 4.15 DISPLACEMENT THICKNESSES ON THE BOATTAIL CALCULATED USING SASMAN-CRESCI TURBULENT BOUNDARY LAYER METHOD

4.3.4 Design or Inverse Problem

Inverse boundary layer coupling requires that the inviscid flow method be capable of determining the edge angle θ given the edge Mach number M_e or the total edge velocity V_e. This problem is roughly equivalent to the classic design problem in which a body geometry is to be determined from a specified pressure coefficient C_p.

Design calculations were attempted with the finite element program using the following iterative scheme.

An initial guess is made at the body geometry, and hence the edge angle θ. Assuming that the flow follows the initial geometry, the pressure coefficient, edge Mach number, or total edge velocity may be algebraically resolved into v_r and v_z velocity components on that body.

In an analysis problem, the Neumann boundary condition of flow tangency is applied on the body. In the inverse or design problem, that condition is replaced by a Dirichlet boundary condition in which one of the two velocity components, either v_r or v_z, is specified on the initial geometry. The finite element method solves for the other component.

Since the geometry guessed initially probably does not correspond to the desired distribution of C_p, M_e, or V_e, the velocity component specified and the velocity component solved for will not satisfy the requirement of flow tangency. Physically, the solution represents a body with blowing or suction, which displaces the stagnation

streamline from the guessed body.

The displacement of the stagnation streamline may be used as a basis for updating the guessed geometry. L. A. Carlson [47] developed a finite-difference design method. In his work, he found the location of the stagnation streamline by integrating the expression

$$\frac{dr}{dz} = \frac{v_r}{v_z}\Big|_{\text{Guessed Body}}$$

then used the location of this streamline as an updated body geometry for the next iteration.

T. L. Tranen [46] developed a design method that used a more complex update technique. This technique was based on adding to the guessed body a kind of displacement thickness of sufficient height to exactly carry the normal mass flow resulting from the blowing or section. During the course of the present study, it was discovered that certain terms in Tranen's scheme were insignificant, so that his update scheme reduced numerically to Carlson's.

One advantage of the finite element method over finite difference methods in this problem is that interpolation functions are available for the terms v_r and v_z. Hence, the differential equation for the updated geometry can be evaluated analytically from node to node.

Initially, a small region of the boattail model was to be "designed" from a specified pressure distribution determined from a previous finite element analysis. To test the method, the exact corresponding geometry was input as the first guess.

When the v_z velocity components were applied as the Dirichlet boundary conditions on the region to be "designed", the finite element method behaved unstably and returned a physically unrealistic flow solution. No explanation is currently available for this phenomena, except that the method is numerically unable to handle this particular boundary condition.

When the v_r velocity components were specified, the method returned the correct solution for the v_z components. Thus, this approach appears promising. When the initial body guess was not the body corresponding exactly to the specified pressure, the method still returned reasonable values of v_z in the region to be designed. However, the update scheme tended to diverge from the true body.

Conclusions

Experience with the finite element formulation of inviscid compressible flow in primitive variables indicates that the analysis method is both fast and accurate. The ability of the method to conform to arbitrary bound-

aries is a major advantage over finite difference methods in the analysis problem and particularly in the iterative problem of boundary layer coupling. For the inverse or design problem, the method appears promising, but further investigation is needed.

Recommendations for Further Research

Further research should be conducted on use of the finite element method as an inviscid flow solution technique. The method should be tested on finer grids and faster machines.

The problem of a finite free-stream boundary could be overcome using an infinite-to-finite transformation of the r-coordinate. This approach was used by Chow, et al., in their finite difference boattail study [60]. Habashi developed a semi-infinite boundary element [74] that appears to be more consistent with the present work.

Convergence problems of the design or inverse method need to be explored and eliminated, so that inverse boundary layer coupling may be tested in fully compressible flow.

Finally, extensions of the analysis method to lifting surfaces and three-dimensional bodies would be highly desirable.

5. Combination of the Boundary Layer and Inviscid Flow Methods Into a Complete Separated Flow Prediction Method

Of the inviscid flow methods discussed in Chapter 4, only the surface source method has thus far been developed to the point of being ready to combine with the (successful) boundary layer method of Chapter 3. In this chapter, experiences with the attempt to combine the two methods will be reported.

5.1 Flow Geometry Selected

The flow geometry which was selected for the attempts at a complete calculation of a flow exhibiting separation is shown in Figure 4.3. Separation is expected to take place on the boattail, with subsequent reattachment on the sting. This geometry is typical of that employed to study nozzle afterbody drag and considerable effort has been expended on research into the development of an adequate method for calculating the flow over such a body [6,45,60] with a view to analytical predictions of afterbody drag. The separation bubble occuring in such a flow is relatively thin and short and may be expected to be steady. It was assumed that the surface was smooth. Air at a free stream reference Reynolds number (c_o/ν_o) of $1.7 \times 10^6 \left\{\frac{1}{\text{inch}}\right\}$ was assumed to approach the body at Mach numbers of

0.5 to 0.8. It was expected that separation would occur earlier at higher Mach numbers; this was verified by the calculations.

5.2 Geometric Problems Involved in Combining the Boundary Layer and Inviscid Flow Methods

Several details must be worked out in order to successfully combine the methods and make iterative calculations. The source of most of the trouble is due to three items:

(1) The boundary layer method is formulated in a coordinate system parallel to and perpendicular to the body surface, while the inviscid flow procedure is formulated in a coordinate system with axes along an axis of symmetry and perpendicular to it.

(2) The boundary layer thickness is added on <u>perpendicular</u> to the body to define the "δ surface". The "edge Mach number" M_e and angle Θ at a surface point x are actually the values <u>above</u> $z(x) + \Delta z$ a distance of $\delta \cos \alpha$ (see Figure 5.1).*

---

* The assumption that dominant cross stream coordinate "y" is perpendicular to the surface is of less validity in the neighborhood of separation, however, it is nevertheless retained.

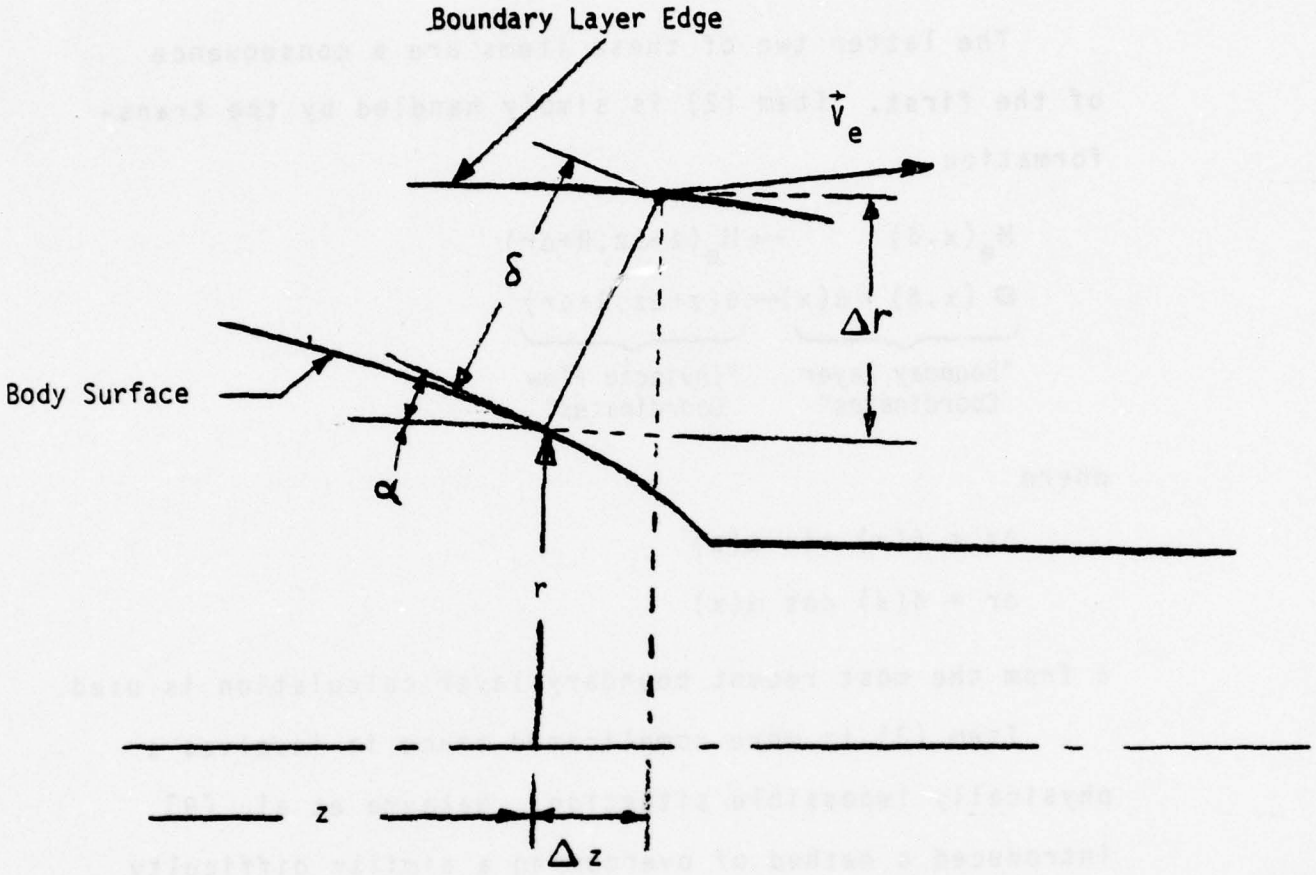

FIGURE 5.1 LOCATION OF POINT AT EDGE OF BOUNDARY LAYER IN z, r COORDINATE SYSTEM

(3) The adding of a finite δ perpendicular to the surface results in an "overlapping" of the δ surface in the immediate vicinity of a concave corner such as the boattail-sting juncture.

The latter two of these items are a consequence of the first. Item (2) is simply handled by the transformation

$$M_e(x,\delta) \quad \leftrightarrow \quad M_e(z+\Delta z, R+\Delta r)$$

$$\underbrace{\Theta(x,\delta) + \alpha(x)}_{\text{"Bounday Layer Coordinates"}} \leftrightarrow \underbrace{\theta(z+\Delta z, R+\Delta r)}_{\text{"Inviscid Flow Coordinates"}}$$

where

$$\Delta z = \delta(x) \sin \alpha(x)$$

$$\Delta r = \delta(x) \cos \alpha(x)$$

δ from the most recent boundary layer calculation is used.

Item (3) is more complicated since it involves a physically impossible situation. Nakayma et al. [9] introduced a method of overcoming a similar difficulty by defining a triangular control volume with the concave corner at one vertex and with sides perpendicular to the upstream and downstream surfaces. The boundary layer equations are solved up to the inlet face of the control volume and terminated. The calculations are restarted at the downstream face with parameters determined by mass

and momentum balances for the control volume. A similar method was investigated for the present purposes, employing a control value composed of two congruent triangles as shown in Figure 5.2. This approach was finally considered too complicated and time consuming for the accuracy gained. The treatment finally employed simply marches the boundary layer calculations through this region (the "corner" is not recognized in the surface oriented boundary layer coordinate system). Points in the region of interference (that is points between the tail location, z_T, and $z_T + \delta_T \sin \alpha_T$) are simply discarded when transforming to the inviscid flow geometry. In this way, a smooth, continuous "δ surface" was defined.

5.3 The Iterative Procedure and Initial Guesses

Because the boundary layer equations are parabolic and the inviscid flow equations are elliptic *, simultaneous solution of the boundary layer and inviscid flow equations is not possible (as it is in supersonic separated flow calculations [35-37]) and iteration between a complete boundary layer calculation and a complete inviscid flow calculation must be employed. The critical variables of the iteration are the fluid

---

* Thus preserving the well known elliptic nature of the separated flow problem.

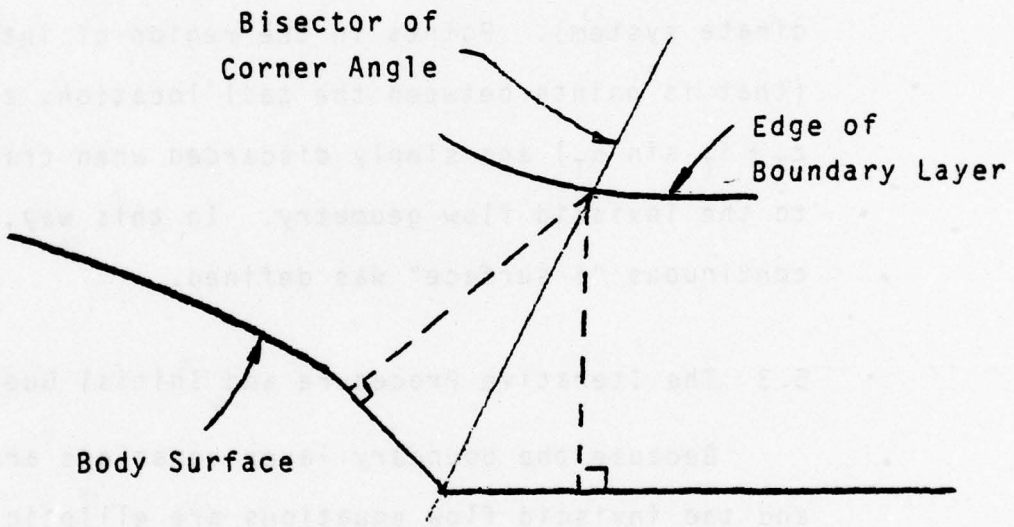

FIGURE 5.2 CONTROL VOLUME FOR CORNER FLOW

velocity (or Mach number) and angle along the boundary between the viscous ("boundary layer") region and the external inviscid flow region. The calculation procedure in each region calculates "new" values for one of these variables at each point, which is handed to the procedure for the other region where the opposite variable is updated and so on until convergence is achieved.

There are several possibilities for starting the calculations. The most obvious is to first calculate the inviscid flow over the body assuming there is no boundary layer (a "direct" or analysis calculation) and then use the pressure (velocity) distribution thus calculated as input to the boundary layer method to update the geometry, etc. Another obvious alternative is to first calculate the boundary layer on the body assuming no "effect" of the inviscid flow, that is calculate the boundary layer under the assumption of constant pressure and then use the calculated edge angle and "δ-surface" as input to the inviscid flow method and so on. In actual practice these approaches are essentially identical; the "constant pressure" boundary layer does not significantly modify the body shape so that the "bare body" pressure distribution results from the inviscid calculation in the second case. Thus in either case, the calculations "start"

with a pressure distribution essentially identical to the value for the completely inviscid flow, and the first significant problems develop in the boundary layer routine.

The boundary layer calculations are started in the weak interaction mode and continue in this mode up to a position about midway down the boattail, where a (typical) sharp rise in δ, δ^*, H, and Θ occur. These are of course an indication of impending boundary layer separation. As soon as one of the criteria of equations 3.34 are satisfied (typically both are satisfied at the same calculation step), the calculations switch to the strong interaction mode. A major problem is immediately encountered in that the strong interaction mode, Θ is required as input, with M_e to be calculated; thus a Θ distribution must be assumed to continue the calculations. In order to obtain a realistic boundary layer calculation, the Θ distribution must be realistic. The distribution must have the general shape shown in Figure 5.3. The rapid increase of Θ associated with separation must be maintained for a distance but the value of Θ must not be too large or numerical problems will occur. In order to "turn" the flow back toward the sting and "force" a reattachment Θ must decrease and attain negative values. As the boundary layer is expected to redevelop in typical fashion

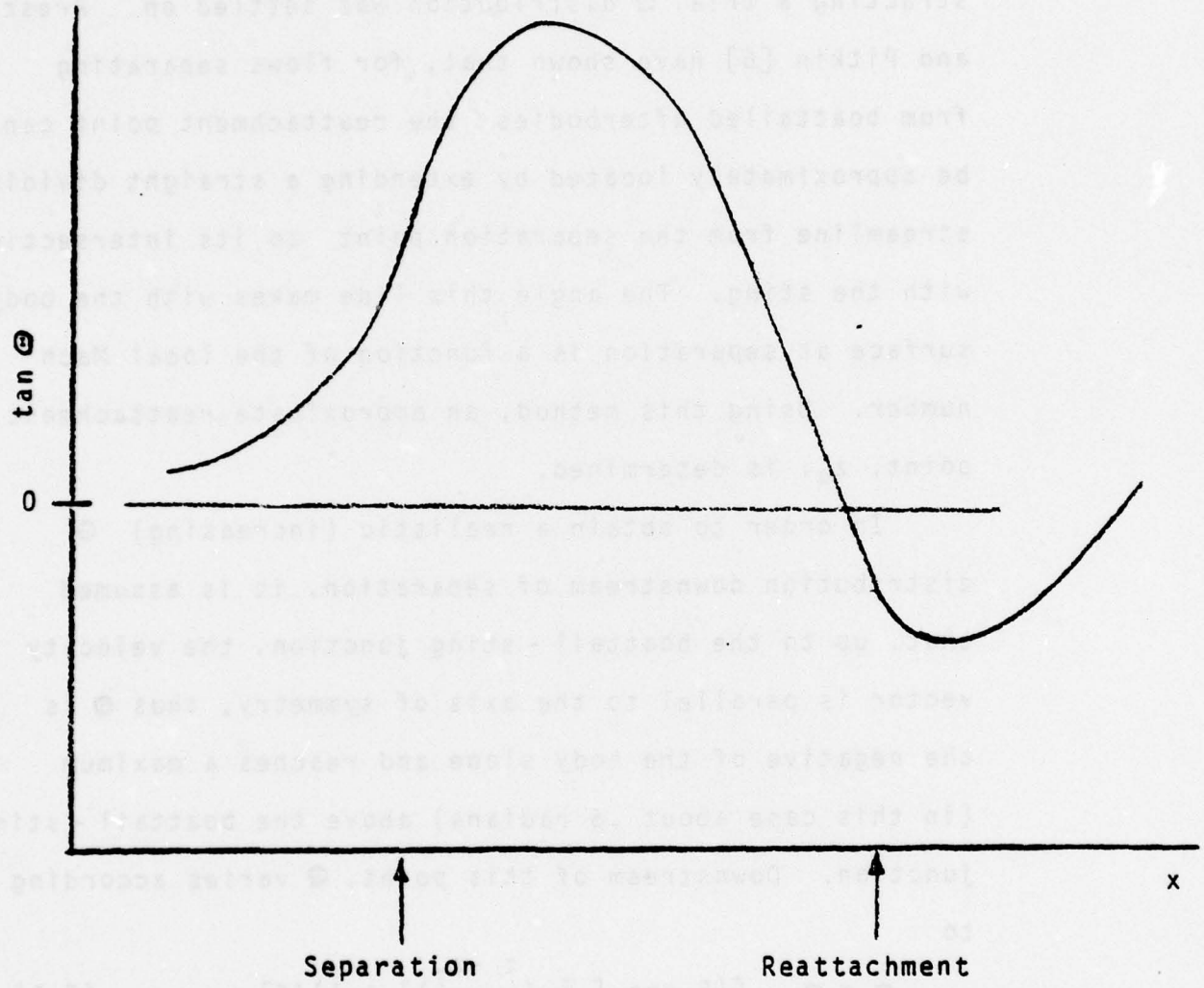

FIGURE 5.3 EXPECTED TAN Θ DISTRIBUTION FOR SEPARATING AND REATTACHING BOUNDARY LAYER

after reattachment, an eventual return to positive (small) Θ values is anticipated. After a considerable amount of "cut and try", the following procedure for constructing a trial Θ distribution was settled on. Presz and Pitkin [6] have shown that, for flows separating from boattailed afterbodies the reattachment point can be approximately located by extending a straight dividing streamline from the separation point to its intersection with the sting. The angle this line makes with the body surface at separation is a function of the local Mach number. Using this method, an approximate reattachment point, z_R, is determined.

In order to obtain a realistic (increasing) Θ distribution downstream of separation, it is assumed that, up to the boattail - sting junction, the velocity vector is parallel to the axis of symmetry, thus Θ is the negative of the body slope and reaches a maximum (in this case about .6 radians) above the boattail - sting junction. Downstream of this point, Θ varies according to

$$\Theta = \Theta_{max}\left[\left(5 \cos\left[\frac{\pi}{2}\left(\frac{z - z_T}{z_R - z_T}\right)\right] + 1\right)/6\right] \qquad (5.1)$$

Thus Θ is a minimum at the estimated reattachment point. When Θ reaches a value of zero downstream of z_R, Θ is continued at zero.

This distribution of Θ is sufficient to continue calculations downstream of the point where the switch from weak to strong interaction occurs; however, the values of Θ calculated by the weak interaction formulation at the last few stations before the switch are usually too large; often larger than Θ max. Those values of Θ which are greater than 0.3 radians are replaced by values computed from a second order curve fit between Θ = 0.3 and the initial value of $\Theta(=-\alpha)$ at the switch point.

Having completely specified Θ, calculations are continued in the strong interaction mode; typical results are shown in Figure 5.4. At some point following reattachment, the conditions of equations 3.35 are satisfied and the calculations are switched back to the weak interaction mode (M_e specified). The values of M_e needed to continue the calculation are available from the previous (initial) inviscid calculation; however, it usually occurs that the last M_e computed from the strong interaction mode is not equal to the inviscid value at that point so a discontinuity results. This is removed by an exponential fairing between the last strong interaction value and the value of M_e five boundary layer thicknesses downstream. Calculations are then continued to the tail of the sting far downstream.

The results of the boundary layer calculation are a set of values of $\delta(x)$, "new" values of $\Theta(x)$ at points

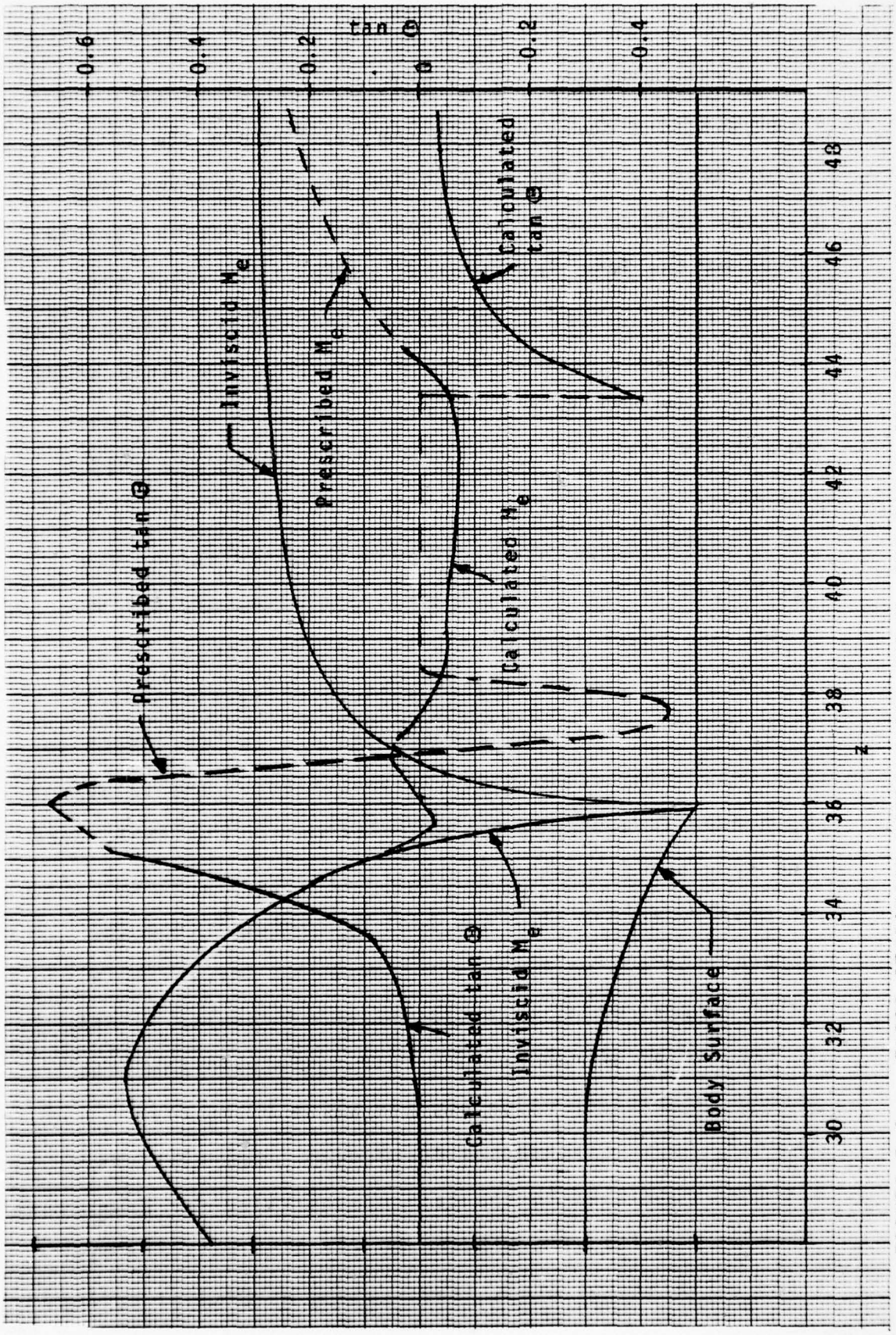

FIGURE 5.4a FIRST ITERATION PREDICTIONS FOR M_e AND TAN Θ FOR BOATTAILED BODY, $M_\infty = 0.7$

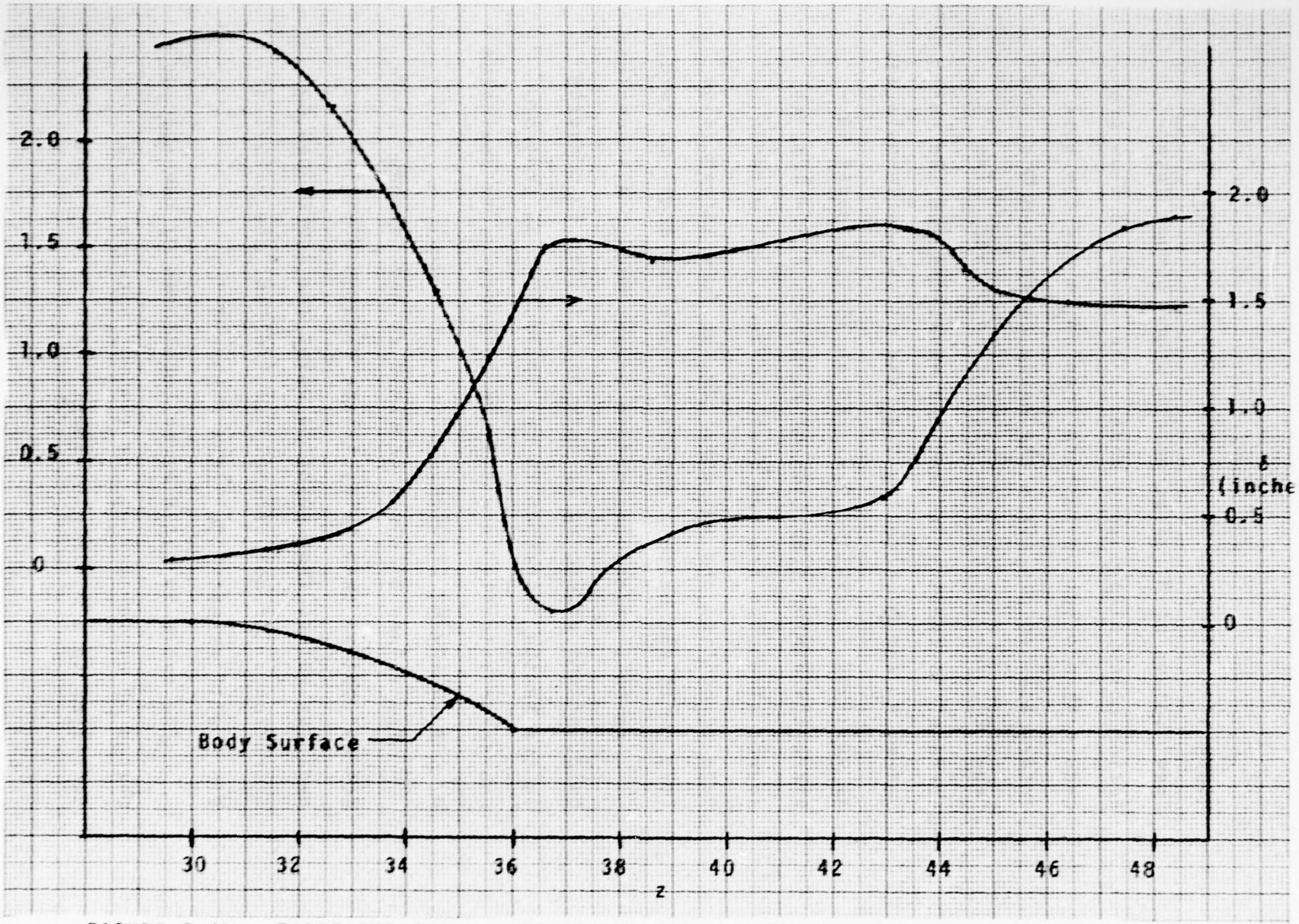

FIGURE 5.4b FIRST ITERATION PREDICTIONS FOR C_f AND δ FOR BOATTAILED BODY, $M_\infty = 0.7$

where weak interaction calculations were made, and "new" values of $M_e(x)$ at points where strong interaction calculations were made. The inviscid flow procedure is now set up to find "new" M_e's for the weak interaction points (from the newly calculated Θ's) and "new" Θ's for the strong interaction points. The "δ surface" is constructed and the equations for the required M_e and Θ (actually V/V_∞ and θ) values formulated, as outlined in Section 4.2. As an initial guess to start the Newton iteration of equations 4.6 - 4.8, all source strengths are set equal to zero, all unknown edge velocities are set equal to the free stream value ($V/V_\infty = 1$) and unknown angles (θ) are set equal to zero.

At this point, the method breaks down. All complete calculations attempted to date have failed to converge in the Newton iteration in the inviscid flow program. Characteristically, the failure to converge is dominated by the following problems:

The values of sin θ computed at the "strong interaction" points tend to oscillate between positive and negative values from point to point and iterations to iterations. If not strongly controlled, the values of sin θ will exceed 1.0. (See Figure 4.4.)

The cycle to cycle error (monitored by the <u>average</u> change of either $V/V_\infty)_i$ or $\sin\theta)_i$ between iterations decreases to a minimum of about 4 iterations then in-

creases. The relative minimum error is rather large. The "solutions" in the neighborhood of switch points are discontinuous.

Several "obvious" remedies to alleviate this behavior were tried; these include:

(1) Undercorrection using only a portion of the newly calculated (from the boundary layer method) δ, M_e, Θ combined with the previous values e.g.

$$\delta_{new} = \frac{1}{2}\,\delta_{old} + \frac{1}{2}\,\delta_{new}$$

(2) "Smoothing" of the δ surface and the M_e, Θ distributions.

(3) Using the flow over the "bare body" or the (assumed solid) "δ surface" as the initial guess for the Newton iteration.

None of these "fixes" was observed to improve the situation.

A possible explanation and resolution of the problem is as follows. By considering the boundary layer calculation method, one may conclude that although calculations are possible, one must tread a very tortuous path to make them. In developing the boundary layer method, it was assumed that whatever was needed to continue could be obtained i.e. mode switch was possible where necessary, singularities were carefully avoided, etc.

Using measured data with the boundary layer method verified its ability to make calculations if "good" information is available as input. In a complete calculation, since all liberties have been taken with the boundary layer method, the inviscid flow method must take up the slack, making exactly the calculations required by the boundary layer method. We cannot "play" with the inviscid routine to find out what types of boundary conditions are most efficient or acceptable at various points.

It is still felt that the method is capable of making complete separated flow calculations but that the inviscid flow method will converge only if called upon to "improve" M_e or Θ values which are close to actual values; in other words, an initial guess close to the final result must be provided. Two methods are suggested for providing this initial guess. Firstly, a semi-empirical approximate method of estimating the flow parameters (especially pressure distribution) such as those proposed by Presz and Pitkin [6] or Kuhn [78] could be used to generate an initial guess for the present method.

Secondly, an interactive computer terminal, hopefully with graphics capability, could be employed. The "man in the loop" could postrate various reasonable initial guesses until one which allowed calculations to proceed is found.

At the time this research was carried out, the latter possibility was not available to the authors. Toward the end of the project, attempts were made to persue a method of the first type, similar to the method of Kuhn, in which a polynominal distribution of θ is assumed in the strong interaction region, with coefficients selected in order to minimize the deviation of the calculated edge velocities from the prescribed values. No formal procedure for constructing the polynominal approximation to minimize the deviation was programmed; efforts to select a set of coefficients by "cut and try" were finally abandoned as too time consuming.

At the present time, it is hoped that the finite element procedure, still under development, will be capable of combination with the boundary layer method for a complete calculations routine.

6. Conclusions and Recommendations for Further Research

The following are considered to be the major accomplishments of this work and conclusions that may be drawn from it.

(1) The strong interaction formulation is a viable framework for separating boundary layer analysis.

(2) The "boundary layer equations" are adequate representations of the flow in the viscous region.

(3) It is possible to develop a general integral method for solving the boundary layer equations in cases involving flow separation.

(4) Simple algebraic (non-equilibrium) turbulence models are adequate for use with such a method and the effects of "normal stresses", both in the mean flow equations and in the turbulence model are not significant.

(5) The integral boundary layer method is especially prone to the appearance of "singularities". These singularities are usually mathematical rather than physical and smooth passage through them should not be a forced condition on the analysis. The singularity can usually be avoided by switching between the "strong" and "weak" interaction modes of calculation.

(6) The integral method probably does not offer any advantage over a finite difference or finite element formulation in terms of ease of formulation, ease of programming, and computation time. The advantages of the method thus lie in the fact that the desired interaction parameters (M_e, Θ, δ) are explicit in the formulation, and it seems rather forgiving in terms of the turbulence model employed.

(7) Experience with the method of integral relations for the inviscid flow indicates that the method is too complex and several of the required steps too artificial for the method to be given serious consideration.

(8) It is possible to develop an a priori "inverse" or "design" calculation procedure for inviscid flow over axisymmetric bodies using the surface singularity method.

(9) The ability to make complete a priori separated flow calculations is apparently restricted by the need for initial guesses close to the final answer.

(10) The finite element method is a viable alternative to the finite difference method for computing compressible (non-linear) flows in the "direct" or "analysis" mode and can be successfully combined with boundary layer calculations via "displacement thickness" interaction.

(11) Problems still remain in the development of the finite element approach to the "inverse" or "design" problem of inviscid flow.

The following are recommendations for further work suggested by the results of this study.

(1) The development of an "inverse" finite element procedure should continue.

(2) A procedure such as that of Presz and Pitkin [6] Kuhn [78] should be incorporated to obtain an initial estimate of the flow parameters, which can be improved by the present method.

(3) Apparently, the use of curved rather than straight body elements, polynominal rather than uniform singularity distributions, and combined singularities rather than simple sources offers considerable improvement in the speed, stability, and accuracy of the surface source method, especially for the design problem [56-58]. Accordingly, such improvements should be introduced into the current method.

(4) "Displacement thickness" interaction, especially in the strong interaction calculation (δ^* rather than Θ specified in the boundary layer equations) should be investigated for the present program.

(5) A finite element formulation of the boundary layer flow should be investigated. In this (differential) framework, the algebraic turbulence model should be compared with one and two equation models.

(6) Finite difference models of both the boundary layer and inviscid flow, retaining the strong interaction formulation of Chapter 2, should be investigated.

APPENDIX A

Below, the various derivatives of the velocity profile equations 3.5 and 3.7 are tabulated.

$$\frac{\partial a}{\partial M_e} = \frac{4a^2}{(\gamma-1)RF\ M_e}$$

$$\frac{\partial r}{\partial M_e} = (\gamma-1)RF\ M_e(\phi^2-1)r^2$$

$$\frac{\partial y^+}{\partial M_e} = y^+/M_e\left[1-9/4\ \frac{(\gamma-1)M_e^2}{1+\frac{\gamma-1}{2}M_e^2} - 7/4\ \frac{RF(\gamma-1)M_e^2}{1+RF(\frac{\gamma-1}{2})M_e^2}\right]$$

$$\frac{\partial \delta^+}{\partial M_e} = \delta^+/M_e\left[1-9/4\ \frac{(\gamma-1)M_e^2}{1+\frac{\gamma-1}{2}M_e^2} - 7/4\ \frac{RF(\gamma-1)M_e^2}{1+RF(\frac{\gamma-1}{2})M_e^2}\right]$$

$$\frac{\partial \phi}{\partial \lambda} = \sqrt{1-a^2\phi^2}\ \left[\frac{1}{k}\ln\ (1+y^+) + B - (1.5y^+ + B)e^{-.18y^+}\right]$$

$$\frac{\partial F}{\partial \lambda} = \sqrt{1-a^2\phi^2}\ \left[\frac{1}{k}\ln\ (1+\delta^+) + B - (1.5\delta^+ + B)e^{-.18\delta^+}\right]$$

$$\frac{\partial y^+}{\partial \lambda} = y^+/\lambda$$

$$\frac{\partial \delta^+}{\partial \lambda} = \delta^+/\lambda$$

$$\frac{\partial \phi}{\partial \delta} = -\sqrt{1-a^2\phi^2}\ \left[\frac{\pi}{\delta}\ \xi\ u_\beta\ \sin\ (\frac{\pi}{2}\xi)\ \cos\ (\frac{\pi}{2}\xi)\right]$$

$$\frac{\partial \delta^+}{\partial \delta} = \delta^+/\delta$$

$$\frac{\partial F}{\partial \delta^+} = \sqrt{1-a^2\phi^2}\ \left[\frac{\lambda}{k(1+\delta^+)} + .18\lambda e^{-.18\delta^+}(1.5\delta^+ + B - 8.333)\right]$$

$$\frac{\partial \phi}{\partial y^+} = \sqrt{1-a^2\phi^2}\ \left[\lambda\left[\frac{1}{k(1+y^+)} + .18e^{-.18y^+}(1.5y^+ + B - 8.333)\right]\right.$$

$$\frac{\partial \phi}{\partial \xi} = \sqrt{1-a^2\phi^2}\ \left[\lambda\delta^+\left(\frac{1}{k(1+y^+)} + .18e^{-.18y^+}(1.5y^+ + B - 8.333)\right)\right.$$

$$\left. + \pi u_\beta \sin\left(\frac{\pi}{2}\xi\right)\cos\left(\frac{\pi}{2}\xi\right)\right]$$

$$\frac{\partial \phi}{\partial u_\beta} = \sqrt{1-a^2\phi^2}\ \sin^2\left(\frac{\pi}{2}\xi\right)$$

$$\frac{\partial F}{\partial u_\beta} = \sqrt{1-a^2\phi^2}$$

$$\frac{\partial r}{\partial \phi} = (\gamma-1)RF\ M_e^2\ \phi\ r^2$$

$$\frac{\partial \phi}{\partial a} = -\phi/a + \sqrt{\frac{1}{a^2} - \phi^2}\ \left(\frac{\sin^{-1} a\phi}{a}\right)$$

$$\frac{\partial F}{\partial a} = -F/a + \sqrt{\frac{1}{a^2} - \phi^2}\ \left[\frac{1}{k}\ln(1+\delta^+) + B - (1.5\delta^+ + B)e^{-.18\delta^+} + u_\beta\right]$$

Where

$$\delta^+ = R_\delta M_e|\lambda|\ (1 + \tfrac{\gamma-1}{2}\ M_e^2)^{-9/4}(1 + RF(\tfrac{\gamma-1}{2})M_e^2)^{-7/4}$$

$$y^+ = \xi\delta^+$$

$$R_\delta = \frac{c_0 \delta}{\nu_0} \qquad \text{(compressible flow)}$$

For incompressible flow, a = 0, all derivatives with respect to a are 0 and

$$R_\delta = \frac{V_\infty \delta}{\nu_\infty}$$

List of Symbols

a	Mach number function defined in Appendix A
B	"Law of the wall" constant
c	Speed of sound
C_f	Skin friction coefficient $C_f \equiv \tau_w / \frac{1}{2} \rho_e u_e^2$
F	Ratio of shear to normal stress turbulence production
H	Boundary layer form factor $H = \delta^*/\theta$
H_k	Boundary layer form factor $H_k = \delta_k^*/\theta_k$
j	= 0 for plane 2-D flow, = 1 for axisymmetric flow
$\|J\|$	Jacobian determinant
ℓ	Mixing length
M	Mach number
P	Pressure
q	Turbulence kinetic energy $q^2 = \underline{u}^2 + \underline{v}^2 + \underline{w}^2$
R	Body radius
r	Radial coordinate; density ratio ρ/ρ_e
$\mathcal{R}$	Longitudinal radius of curvature
RF	Recovery factor
R_δ	Reynolds number $R_\delta = \frac{c_0 \delta}{\nu_0}$
T	Temperature (absolute)
u	Velocity parallel to body surface
u_τ	Friction velocity $u_\tau = \sqrt{\tau_w/\rho_w}$
u_β	"Wake velocity"
v	Velocity perpendicular to body surface
v_r	Velocity component in radial direction

v_z Velocity component parallel to axis of symmetry

V Total velocity $V = u^2 + v^2 = v_r^2 + v_z^2$

x Coordinate parallel to body surface

X_{ij} Influence coefficient matrix for v_z

y Coordinate perpendicular to body surface

y^+ $y\ u_\tau/\nu_w$

Y_i Influence coefficient matrix for v_r

z Coordinate parallel to axis of symmetry

α Body slope (angle)

β Boundary layer equilibrium parameter

γ Specific heat ratio

δ Boundary layer thickness

δ^* Displacement thickness $\delta^* \equiv \int_0^\delta \left(1 - \frac{\rho u}{\rho_e u_e}\right) dy$

δ_k^* "Kinematic displacement thickness"

$\delta_k^* \equiv \int_0^\delta (1 - u/u_e)dy$

ε Kinematic eddy viscosity

ζ Dummy variable of integration

η Isoparametric element coordinate

θ Angle of velocity vector with respect to z axis;
momentum thickness $\theta \equiv \int_0^1 \rho u/\rho_e u_e\ (1-u/u_e)dy$

Θ Angle of velocity vector with respect to body surface

k von Karman constant

λ Skin friction parameter $\lambda = C_f/|C_f|^{1/2}$

μ Dynamic viscosity

ν Kinematic viscosity

ξ y/δ; isoparametric element coordinate

ρ Density

σ Surface source density

τ Shear stress

τ_L Laminar shear stress

τ_t Reynolds shear stress $\tau_t = -\overline{\rho u v}$

$\bar{\tau}$ $= \tau/\rho_e u_e^2$

ϕ Velocity ratio u/u_e

Φ Turbulence dissipation

Ω Finite element interpolation function

Subscripts

e Edge of boundary layer

∞ Reference upstream value

w evaluated at wall

— Fluctuating turbulent quantity

o Stagnation; incompressible flow

T "Tail" of body

References

1. Klineberg, J., and Steger, J., "Calculation of Separated Flows at Subsonic and Transonic Speeds," 3rd International Conference on Numerical Methods in Fluid Dynamics, Paris, 1972.

2. Kuhn, G., and Nielsen, J., "Prediction of Turbulent Separated Boundary Layers," AIAA Paper 73-663, 1973.

3. Kuhn, G., and Nielsen, J., "Prediction of Turbulent Separated Flow at Subsonic and Transonic Speeds Including Unsteady Effects," AGARD Conference Proceedings 168 - Flow Separation, 1975.

4. Briley, W.R., and McDonald, H., "Numerical Prediction of Incompressible Separation Bubbles," J. Fluid Mech., 69, 4, pp 631-656.

5. Carter, J.E., "Solutions for Laminar Boundary Layers With Separation and Reattachment," AIAA Paper 74-583, 1974.

6. Presz, W., and Pitkin, E., "Analytical Model of Axisymmetric Afterbody Flow Separation," J. Aircraft, 13, 7, 1972.

7. Deiwert, G., "Computation of Separated Transonic Turbulent Flows," AIAA J., 14, 6, 1976.

8. Chow, W., "Recompression of a Two-Dimensional Supersonic Turbulent Free Shear Layer," 12th Midwestern Mechanics Conference, Notre Dame, Indiana, 1971.

9. Nakayama, A., Patel, V.C., and Landweber, L., "Flow Interaction Near the Tail of a Body of Revolution: Part II - Iterative Solution for Flow Within and Exterior to Boundary Layer and Wake," J. Fluids Engrg., Sept. 1976.

10. Coles, D., "The Law of the Wake in the Turbulent Boundary Layer," J. Fluid Mech., July 1956.

11. Alber, I., and Coats, D., "Analytical Investigations of Equilibrium and Non-Equilibrium Turbulent Boundary Layers," AIAA Paper 69-689, 1969.

12. Mathews, D., Childs, M., and Paynter, G., "Use of Coles Universal Wake Functions for Compressible Turbulent Boundary Layers," J. Aircraft, 7, 2, 1973.

13. Alber, I., Bacon, J., Masson, B., and Collins, D., "An Experimental Investigation of Turbulent Transonic Viscous-Inviscid Interaction," AIAA J., May 1973.

14. Kline, S., Morkovin, M., Sovran, G., and Cockrell, D., "Computation of Turbulent Boundary Layers - 1968 - AFOSR - IFP - Stanford Conference," Stanford Press, 1968.

15. White, F., Viscous Fluid Flow, McGraw-Hill Book Co., 1974.

16. Van Driest, E., "On Turbulent Flow Near a Wall," J. Aero Sci., 23, 11, 1956.

17. Cebeci, T., Smith, A., and Mosinskis, G., "Calculation of Compressible Adiabatic Turbulent Boundary Layers," AIAA J., 8, 11, 1974.

18. "Free Turbulent Shear Flows", NASA SP-321.

19. Alber, I., "Application of an Exact Expression for the Equilibrium Dissipation Integral to the Calculation of Turbulent Nonequilibrium Flows," Computation of Turbulent Boundary Layers, Stanford Press, 1968.

20. Clauser, F., "The Turbulent Boundary Layer," Adv. in Appl. Mech., 4, 1956.

21. Simpson, R., Strickland, J., and Barr, P., "Laser and Hot-Film Anenometer Measurements in a Separating Turbulent Boundary Layer," Report WT-3, Southern Methodist University, 1974. See also J. Fluid Mech., 79, 3, 1977.

22. Goldberg, P., "Upstream History and Apparent Stress in Turbulent Boundary Layers," MIT Gas Turbine Lab Report 85, 1966.

23. Nash, J., and Hicks, J., "An Integral Method Including the Effects of Upstream History on the Turbulent Shear Stress," Computation of Turbulent Boundary Layers, Stanford Press, 1968.

24. Bradshaw, P., Ferris, D., and Atwell, N., "Calculations of Boundary Layer Development Using the Turbulent Energy Equation," J. Fluid Mech., 28, 3.

25. McDonald, H., and Camarata, F., "An Extended Mixing Length Approach for Computing the Turbulent Boundary Layer Development," Computation of Turbulent Boundary Layers, Stanford Press, 1968.

26. McDonald, H., and Fish, R., "Practical Calculations of Transitional Boundary Layers," Int. J. Heat and Mass Transfer, 16, 1973.

27. Collins, M., and Simpson, R., "Flowfield Prediction for Separating Turbulent Boundary Layers," Report WT-4, Southern Methodist University, 1976.

28. Newman, B., "Some Contributions to the Study of the Turbulent Boundary Layer Near Separation," ACA-53, 1951.

29. Townsend, A., The Structure of Turbulent Shear Flow, Cambridge University Press, 1956.

30. McDonald, H., and Stoddart, J., "On the Development of the Incompressible Turbulent Boundary Layer," ARC R&M 3484, 1967.

31. Crocco, L., and Lees, L., "A Mixing Theory for the Interaction Between Dissipative Flows and Nearly Isentropic Streams", J. Aero Sci., October 1952.

32. Cebeci, T., Mosinskis, G., and Smith, A., "Calculation of Separation Points in Incompressible Turbulent Flows," J. Aircraft, 9, 9, 1972.

33. Gerhart, P., and Bober, L., "Comparison of Several Methods for Predicting Separation in a Compressible Turbulent Boundary Layer," NASA TM-X-3102, 1974.

34. Gerhart, P., "On Prediction of Separated Boundary Layers with Pressure Distribution Specified," AIAA J., September 1974.

35. Lees, L., and Reeves, B., "Theory of Laminar Near Wake of Blunt Bodies in Hypersonic Flow," AIAA J., November 1965.

36. Alber, I., "Integral Theory for Turbulent Base Flows at Subsonic and Supersonic Speed," Ph.D. Thesis, Calif. Inst. of Technology, 1967.

37. Todisco, A., and Reeves, B., "Turbulent Boundary Layer Separation and Reattachment at Supersonic and Hypersonic Speeds," Proc. of 1969 Symposium: Viscous Interaction Phenomena in Supersonic and Hypersonic Flow, University of Dayton Press, 1969.

38. Cebeci, T., "An Inverse Boundary-Layer Method for Compressible Laminar and Turbulent Boundary Layers," J. Aircraft, 13, 9, 1976.

39. Sandborn, V., and Kline, S., "Flow Models in Boundary-Layer Stall Inception," J. Basic Engrg., 83, 3, 1961.

40. Shammroth, S., "On Integral Methods for Predicting Shear Layer Behavior," ASME Paper 69-WA/APM-11, 1969.

41. Shammroth, S., and McDonald, H., "A New Solution to the Turbulent Near Wake Recompression Problem," AIAA Paper 70-228, 1970.

42. Green, J.E., "Two-Dimensional Turbulent Reattachment as a Boundary-Layer Problem," AGARD Symposium: Fully Separated Flows, 1965.

43. Tai, T. C., "Transonic Laminar Viscous-Inviscid Interaction over Airfoils," AIAA Paper No. 74-600, 1974.

44. Tai, T. C., "Transonic Turbulent Viscous-Inviscid Interaction over Airfoils," AIAA Paper No. 75-78, 1975.

45. Putnam, L., and Abeyouens, W., "Experimental and Theoretical Study of Flow Fields Surrounding Boattail Nozzles and Subsonic Speeds," Presented at 12th AIAA/SAE Propulsion Conf., 1976.

46. Tranen, T. L., "A Rapid Computer Aided Transonic Airfoil Design Method," AIAA Paper No. 74-501.

47. Carlson, L. A., "Transonic Airfoil Analysis and Design Using Cartesian Coordinates," J. Aircraft, v13, n5, May 1976.

48. Bristow, D., "A Solution to the Inverse Problem for Incompressible Axisymmetric Potential Flow," AIAA Paper 74-520, 1974.

49. Dorodnicyn, A. A., "A Contribution to the Solution of Mixed Problems of Transonic Aerodynamics," International Council of the Aeronautical Sciences, 1st, Madrid, 1958 - Proceedings of the Congress. From Advances in Aeronautical Sciences, v2, Pergamon Press, New York, 1959.

50. Holt, M., and Masson, B. S., "The Calculation of High Subsonic Flow Past Bodies by the Method of Integral Relations," Proceedings of the Second International Conference on Numerical Methods in Fluid Dynamics, v8, Springer-Verlag, New York, 1971, pp 207-214.

51. Melnik, R. E., and Ives, D. C., "Subcritical Flows over Two-Dimensional Airfoils by a Multistrip Method of Integral Relations," Proceedings of the Second International Conference on Numerical Methods in Fluid Dynamics, v8, Springer-Verlag, New York, 1971, pp 243-251.

52. Tai, T. C., "Application of the Method of Integral Relations to Transonic Airfoil Problems: Part I - Inviscid Supercritical Flow Over Symmetric Airfoils at Zero Angle of Attack," Naval Ship Research and Development Center Report 3424-I, September 1970.

53. Tai, T. C., "Application of the Method of Integral Relations to Transonic Airfoil Problems: Part II - Inviscid Supercritical Flow About Lifting Airfoils with Embedded Shock Wave." Naval Ship Research and Development Center Report 3424-II, July 1972.

54. Lien, D. and Tai, T. C., "A Computer Program That Uses Interactive Graphics to Solve Inviscid Transonic Flows Over Lifting Airfoils," Naval Ship Research and Development Center Report 4252, September 1973.

55. Hess, J., and Smith, A., "Calculations of Potential Flow About Arbitrary Bodies," Prog. Aero Sci., Vol. 8, Pergamon, 1966.

56. Hess, J., "Higher Order Numerical Solutions of the Integral Equation for the Two-Dimensional Neumann Problem," Comp. Meth. in Appl. Mech. and Engrg., February 1973.

57. Bristow, D., "A New Surface Singularity Method for Multi-Element Airfoil Analysis and Design," AIAA Paper 76-20, 1976.

58. Bristow, D., "Recent Improvements in Surface Singularity Methods for the Flow Field Analysis About Two-Dimensional Airfoils," AIAA Paper 77-641, 1977.

59. Popinski, Z., and Baker, A. J., "An Implicit Finite Element Algorithm for the Boundary Layer Equations," J. Comp. Physics, accepted.

60. Chow, W. L., Bober, L. J. and Anderson, B. H. "Numerical Calculation of Transonic Boattail Flow," NASA TND-7984, June 1975.

61. Sasman, P. K., and Cresci, R. J., "Compressible Turbulent Boundary Layer with Arbitrary Pressure Gradients and Heat Transfer," ARL-65-65, April 1965.

62. Chung, T. J., "Introduction to Finite Element Analysis in Fluid Dynamics," notes from the short course "Finite Element Analysis in Fluid Dynamics," University of Alabama in Huntsville, July 26-30, 1976.

63. Norrie, D. H., and de Vries, G., "Application of the Finite Element Technique to Potential Flow Problems," Trans. ASME, J. Applied Mech., December 1971.

64. Schmidt, G., "Incompressible Flow in Multiply Connected Regions," from Numerical Methods in Fluid Dynamics, Ed. Brebbia and Connor, 1974.

65. Shen, S. F., "An Aerodynamicist Looks at the Finite Element Method," Finite Elements in Fluids, Ed. J. T. Oden, et al., Wiley, 1975.

66. Street, T. A., "Ideal Flow Over Arbitrary Bodies and Between Parallel Walls by the Finite Element Method and Galerkin's Integral," U.S. Army Missile Command Report No. RD-76-14.

67. Hirsch, C., "The Finite Element Method and Its Applications to Fluid Flow Problems," lecture notes from "Computational Methods for Inviscid and Viscous Two and Three-Dimensional Flows," Dartmouth College, July 1975.

68. Huebner, K. H., The Finite Element Method for Engineers, John Wiley and Sons, N.Y., 1975.

69. Chung, T. J., and Hooks, C. G., "Discontinuous Functions for Calculations in Transonic Flow," AIAA Paper No. 76-329.

70. Chung. T. J., and Chiou, J. N., "Analysis of Unsteady Compressible Boundary Layer Flow via Finite Elements," Computers and Fluids, v. 4, p 1-12, 1976.

71. Carey, G. F., "Perturbation-Variational Solution of Compressible Flows," Finite Element Methods in Flow Problems, Swansea, England Conference, U. Alabama Press, 1974.

72. Carey, G. F., "A Dual Perturbation Expansion and Variational Solution for Compressible Flows Using Finite Elements," Finite Elements in Fluids, Ed. Oden, et al., Wiley Pub., 1975.

73. Leonard, J. W., "Finite Element Analysis of Perturbed Compressible Flow," International J. for Numerical Methods in Engineering, v. 4, 1972, pp 123-132.

74. Habashi, W. G., "A Study of the Finite Element Method for Aerodynamic Problems," Ph.D. Thesis, Cornell Univ., June 1975.

75. Gartling, D., "Finite Element Analysis of Viscous, Incompressible Fluid Flow," Ph.D. Thesis, U. Texas at Austin, January 1975.

76. Oden, J. T., "Finite Element Analogue of the Navier-Stokes Equations," J. of the Engr. Mech. div. ASCE, v. 96, EM4, 1970, pp 529-534.

77. Gartling, D., and Becker, E. B., "Computationally Efficient Finite Element Analysis of Viscous Flow Problems," Computational Methods in Non-Linear Mechanics, Ed. J. T. Oden et al., pub. Texas Institute for Computational Mechanics.

78. Kuhn, G., "Computer Program for Calculation of Separated Turbulent Flows on Axisymmetric Afterbodies," AEDC-TR-77-72, 1977.